

# Sediment mixing processes and accumulation patterns in the south-western Baltic Sea

## **I n a u g u r a l d i s s e r t a t i o n**

zur

Erlangung des akademischen Grades eines

Doktors der Naturwissenschaften  
(Dr. rer. nat.)

der

Mathematisch-Naturwissenschaftlichen Fakultät

der

Ernst-Moritz-Arndt-Universität Greifswald

vorgelegt von

Dennis Bunke

geboren am 29.12.1984

in Bad Saarow-Pieskow

Greifswald, 27.09.2017

Dekan: Prof. Dr. Werner Weitschies

1. Gutachter: Prof. Dr. Helge W. Arz

2. Gutachter: Prof. Dr. Aarno T. Kotilainen

Tag der Promotion: 25.01.2018

“But more wonderful than the lore of old men and the lore of books  
is the secret lore of ocean.”      Howard Phillips Lovecraft



## Contents

List of figures .....	7
List of tables .....	13
List of abbreviations .....	15
1 Introduction .....	19
1.1 Motivation .....	19
1.2 Regional setting .....	19
1.3 Anthropogenic contamination .....	23
2 Materials and methods .....	27
2.1 Sediment coring and subsampling .....	27
2.2 Water content and dry bulk density .....	28
2.3 Particle size analysis .....	29
2.4 Gamma-ray spectrometry .....	29
2.5 Geochemical analyses .....	30
2.5.1 Mercury .....	30
2.5.2 Carbon, nitrogen and sulphur .....	30
2.5.3 Inorganic and organic carbon .....	31
2.5.4 Phosphorus .....	32
2.5.5 Biogenic silica .....	33
2.5.6 Major and trace elements .....	33
2.5.7 Persistent organic pollutants .....	34
2.5.8 Organotin compounds .....	35
2.5.9 Salinity correction .....	35
2.6 Geochemical mapping .....	35
2.7 Inventory calculations .....	36
2.8 Scanning electron microscopy .....	37
2.9 X-ray radiography .....	37



3	Results.....	39
3.1	Sedimentological parameters.....	39
3.2	Geochemical parameters and radionuclide activity.....	39
3.2.1	Mercury and caesium-137 .....	39
3.2.2	Carbon and nitrogen .....	43
3.2.3	Sulphur .....	47
3.2.4	Phosphorus.....	47
3.2.5	Biogenic silica .....	50
3.2.6	Aluminium, iron and heavy metals .....	51
3.2.7	Organic pollutants .....	55
3.3	Sedimentary fabric .....	56
4	Discussion.....	59
4.1	Sediment mixing .....	59
4.1.1	Bioturbation: biogenic mixing .....	61
4.1.2	Hydroturbation: hydrodynamic mixing.....	65
4.1.3	Anthroturbation: anthropogenic mixing.....	70
4.1.4	Interactions .....	74
4.2	Accumulation patterns .....	77
5	Conclusions and outlook.....	79
	References.....	81
	Acknowledgements.....	91

## List of figures

- Figure 1.1.** Map of the Baltic Sea and its catchment area ([HELCOM, 2006](#); [UNEP, 2005](#)). ..... 20
- Figure 1.2.** Distribution map of the major sediment types in the German Baltic Sea area. AB: Arkona Basin, FB: Fehmarn Belt, FRS: Falster-Rügen sand plain, LB: Lübeck Bay, MB: Mecklenburg Bight, OB: Oder Bank, SC: Sassnitz Channel, STOL: Stoltera, TW: Tromper Wiek. Modified after [Leipe et al. \(2017\)](#). ..... 22
- Figure 1.3.** Pollutant (Hg,  $\Sigma$ PCB) and radionuclide ( $^{137}\text{Cs}$ ,  $^{241}\text{Am}$  and  $^{210}\text{Pb}$ ) profiles of an undisturbed short core from the Eastern Gotland Basin at a water depth of 175 m. Modified after [Moros et al. \(2017\)](#). ..... 26
- Figure 2.1.** Map of the south-western Baltic Sea with coring locations (coloured circles). FRS: Falster-Rügen sand plain. Bathymetry data from [Seifert et al. \(2001\)](#). ..... 27
- Figure 2.2.** Map of the south-western Baltic Sea with sampling locations (red circles) for the geochemical mapping of the surface sediments in the German Baltic Sea area and the Arkona Basin. FRS: Falster-Rügen sand plain. Modified after [Leipe et al. \(2017\)](#), bathymetry data from [Seifert et al. \(2001\)](#). ..... 36
- Figure 3.1.** TOC normalised Hg and  $^{137}\text{Cs}$  profiles of the studied cores from the Mecklenburg Bight (A), the Arkona Basin (B) and the adjacent sandy areas (C), arranged from west (left) to east (right). AB: Arkona Basin, FRS: Falster-Rügen sand plain, LB: Lübeck Bay, MB: Mecklenburg Bight, OB: Oder Bank, SC: Sassnitz Channel, STOL: Stoltera, TW: Tromper Wiek. Stations in close vicinity to the local hot spots are marked with an asterisk. Notice the decreasing surface and maximum Hg values with increasing distance to them as well as the different types of profile shapes. .... 41
- Figure 3.2.** Hg content in the surface sediments (0-2 cm) of the German Baltic Sea area and the Arkona Basin. FRS: Falster-Rügen sand plain. Notice the hot spots of high contents in both basins as well as in the Oder Lagoon. Modified after [Leipe et al. \(2017\)](#). ..... 42

<b>Figure 3.3.</b> Hg content in the fine fraction ( $\leq 63 \mu\text{m}$ ) of the surface sediments (0-2 cm) in the German Baltic Sea area and the Arkona Basin. FRS: Falster-Rügen sand plain. Notice the hot spots of high contents in the basins as well as at the Oder mouth and near Kiel. Modified after <a href="#">Leipe et al. (2017)</a> . ....	42
<b>Figure 3.4.</b> TS, TOC, TN, TOC/N and TIC profiles of the studied cores from the Mecklenburg Bight (A), the Arkona Basin (B) and the adjacent sandy areas (C), arranged from west (left) to east (right). AB: Arkona Basin, FRS: Falster-Rügen sand plain, LB: Lübeck Bay, MB: Mecklenburg Bight, OB: Oder Bank, SC: Sassnitz Channel, STOL: Stoltera, TW: Tromper Wiek. Notice the high correlation of TOC and TN as well as the strong increase of TIC in core AL434/364-2 below 15 cm sediment depth. ..	43
<b>Figure 3.5.</b> TOC content in the fine fraction ( $\leq 63 \mu\text{m}$ ) of the surface sediments (0-2 cm) in the German Baltic Sea area and the Arkona Basin. FRS: Falster-Rügen sand plain. Notice the high values on the Oder Bank and in the Oder Lagoon. Modified after <a href="#">Leipe et al. (2017)</a> . ....	46
<b>Figure 3.6.</b> TN content in the fine fraction ( $\leq 63 \mu\text{m}$ ) of the surface sediments (0-2 cm) in the German Baltic Sea area and the Arkona Basin. FRS: Falster-Rügen sand plain. Notice the high values on the Oder Bank and in the Oder Lagoon. Published in the <a href="#">Baltic Sea Atlas (2014)</a> . ....	46
<b>Figure 3.7.</b> TOC/N ratio in the surface sediments (0-2 cm) of the German Baltic Sea area and the Arkona Basin. FRS: Falster-Rügen sand plain. Published in the <a href="#">Baltic Sea Atlas (2014)</a> . ....	47
<b>Figure 3.8.</b> $\text{TP}_{\text{Digest}}$ and $\text{TP}_{\text{Ash}}$ profiles of the studied cores from the Mecklenburg Bight (A) and the Arkona Basin (B, C), arranged from west (left) to east (right). Notice the strong variation between the surface and the maximum at 20 cm sediment depth in core EMB058/15-2. ....	48
<b>Figure 3.9.</b> $\text{TP}_{\text{Ash}}$ content in the surface sediments (0-2 cm) of the German Baltic Sea area and the Arkona Basin. FRS: Falster-Rügen sand plain. Notice the high values in the basin muds as well as in the Oder Lagoon. Modified after <a href="#">Leipe et al. (2017)</a> . ....	49



<b>Figure 3.10.</b> TP <sub>Ash</sub> content in the fine fraction ( $\leq 63 \mu\text{m}$ ) of the surface sediments (0-2 cm) in the German Baltic Sea area and the Arkona Basin. FRS: Falster-Rügen sand plain. Notice the high values on the Oder Bank. Modified after <a href="#">Leipe et al. (2017)</a> . .....	49
<b>Figure 3.11.</b> bioSiO <sub>2</sub> and TOC profiles of the studied cores from the Mecklenburg Bight (A), the Arkona Basin (B) and the Sassnitz Channel (SC). .....	50
<b>Figure 3.12.</b> bioSiO <sub>2</sub> content in the fine fraction ( $\leq 63 \mu\text{m}$ ) of the surface sediments (0-2 cm) in the German Baltic Sea area and the Arkona Basin. FRS: Falster-Rügen sand plain. Notice the high values on the Oder Bank. Published in the <a href="#">Baltic Sea Atlas (2014)</a> . .....	51
<b>Figure 3.13.</b> Al, Fe as well as TOC normalised Hg, Cd, Cu, Pb and Zn profiles of the EMB058 cores 2-2 from the Mecklenburg Bight (A) and 15-2 from the Arkona Basin (B)..	53
<b>Figure 3.14.</b> Cu content in the fine fraction ( $\leq 63 \mu\text{m}$ ) of the surface sediments (0-2 cm) in the German Baltic Sea area and the Arkona Basin. FRS: Falster-Rügen sand plain. Notice the high values on the Oder Bank. Published in the <a href="#">Baltic Sea Atlas (2014)</a> . .....	53
<b>Figure 3.15.</b> Pb content in the fine fraction ( $\leq 63 \mu\text{m}$ ) of the surface sediments (0-2 cm) in the German Baltic Sea area and the Arkona Basin. FRS: Falster-Rügen sand plain. Notice the hot spots of high contents in both basins as well as at the Oder mouth. Published in the <a href="#">Baltic Sea Atlas (2014)</a> . .....	54
<b>Figure 3.16.</b> Zn content in the fine fraction ( $\leq 63 \mu\text{m}$ ) of the surface sediments (0-2 cm) in the German Baltic Sea area and the Arkona Basin. FRS: Falster-Rügen sand plain. Notice the hot spots of high contents in the Lübeck Bay as well as at the Oder mouth. Published in the <a href="#">Baltic Sea Atlas (2014)</a> . .....	54
<b>Figure 3.17.</b> TOC normalised Hg, $\Sigma$ PCB and $\Sigma$ PAH profiles of core EMB058/1-4 from the Lübeck Bay (A) and of core EMB058/6-2 from the south-western edge of the Arkona Basin (B) compared to TOC normalised organotin compounds in core EMB058/6-2 (B) and in surface sediments (C). Organotin data from <a href="#">Abraham et al. (2017)</a> . .....	56

<b>Figure 4.1.</b> Theoretical tracer profiles of a single, one-year pulse recorded in sediment cores with constant sedimentation rate (0.25 cm/a) and (A) no mixing, (B) a mixing rate of 3 cm <sup>2</sup> /a down to 7 cm and (C) an additional recent mixing event down to 20 cm. Within the first year, the tracer is distributed throughout the mixed layer and after 58 years, the tracer distribution bears little resemblance to the original pulse. The penetration depth in the mixed cores is greater than in the core without mixing, while the peak concentration is much lower. Modified after <a href="#">Johannessen and Macdonald (2012)</a> . ....	60
<b>Figure 4.2.</b> Negative X-radiographs of the cores POS475/54-1 and 57-10 from the Mecklenburg Bight with interpreted sedimentary structures, arranged from west (left) to east (right). The dark ovals are holes in the sample box and the straight vertical lines are gaps in the surrounding tape. ....	62
<b>Figure 4.3.</b> Negative X-radiographs of the cores POS475/17-7, 19-2 and 22-1 from the Arkona Basin with interpreted sedimentary structures, arranged from west (left) to east (right). The dark ovals are holes in the sample box and the straight vertical lines are gaps in the surrounding tape. ....	63
<b>Figure 4.4.</b> Meteorological and hydrographical data of the automated measuring station “Darss Sill” on the Falster-Rügen sand plain during the storm “Xaver” in December 2013. A) Wind velocity at sea surface. B) Salinity in the surface (2 m) and bottom water (19 m). C) Mean horizontal flow velocity component in the bottom water (18 m). D) Turbidity in the surface water (2 m). Notice the higher surface water turbidity and the alignment of surface and bottom water salinity during the wind and flow velocity maxima on 6 Dec 2013. Data from <a href="#">BSH/IOW (2013)</a> .....	66
<b>Figure 4.5.</b> Meteorological and hydrographical data of the automated measuring station in the Arkona Basin during the storm “Xaver” in December 2013. A) Wind velocity at sea surface. B) Salinity in the surface (2 m) and bottom water (43 m). C) Mean horizontal flow velocity component in the bottom water (42 m). D) Turbidity in the surface water (2 m). Notice the higher surface water turbidity and the alignment of surface and bottom water salinity after the wind and flow velocity maxima on 6 Dec 2013. Data from <a href="#">BSH/IOW (2013)</a> .....	67

- Figure 4.6.** Flow velocities at which the first particles of a specific mean grain size (red circles) were separated from the sediment of different locations during *SECOS* research cruises in June/July (light green) and October (dark green) 2014. AB: Arkona Basin, LB: Lübeck Bay, MB: Mecklenburg Bight, OB: Oder Bank, STOL: Stoltera, TW: Tromper Wiek. Unpublished data from [Claudia Morys, University of Rostock](#).... 68
- Figure 4.7.** Map of the south-western Baltic Sea showing the fishing effort with mobile bottom-contacting gear in the first quarter of 2013 and coring locations (coloured circles). FRS: Falster-Rügen sand plain. Dataset from [ICES \(2015\)](#) based on vessel monitoring system (VMS) and logbook data..... 70
- Figure 4.8.** Side scan sonar images of the sea floor around coring sites EMB058/3-2 in the Mecklenburg Bight from 2005 (left) and EMB058/15-2 in the Arkona Basin from 2009 (right) reveal multiple generations of bottom trawl, dredge and/or construction tracks ([Franz Tauber, 2015, IOW, personal communication](#))..... 72
- Figure 4.9.** Side scan sonar images of the *DYNAS* dumping test site in the Mecklenburg Bight off Nienhagen one week (A) and 13 years (B) after the dumping of glacial till and mixed sediment at a water depth of 19 m in 2001. Image C shows a super-elevated profile between the points X and Y on image B from 2014. Notice the old furrow (red ellipses) and the main features that are still clearly recognisable in 2014. Image A modified after [Tauber \(2009\)](#), images B and C from [Jörn Kurth \(2014, IOW, personal communication\)](#). ..... 73
- Figure 4.10.** Prime examples for geochemical profiles that are mainly affected by pure sediment mixing without deposition (A), continuous bioturbation (B), continuous bioturbation together with episodic hydroturbation (C), and in-depth disturbance by anthroturbation (D). The mixing intensity and depth increases from A to D. AB: Arkona Basin, FRS: Falster-Rügen sand plain, MB: Mecklenburg Bight. .... 76



## List of tables

<b>Table 2.1.</b> Meta data of the studied cores, retrieved by multi-corer. AL: R/V ALKOR, EMB: R/V ELISABETH MANN BORGESE, POS: R/V POSEDION, AB: Arkona Basin, FRS: Falster-Rügen sand plain, LB: Lübeck Bay, MB: Mecklenburg Bight, OB: Oder Bank, SC: Sassnitz Channel, STOL: Stoltera, TW: Tromper Wiek. ....	28
<b>Table 2.2.</b> Precision and accuracy of TC, TN and TS measurements. AB: Arkona Basin, MB: Mecklenburg Bight, RM: Reference Material.....	31
<b>Table 2.3.</b> Precision and accuracy of TP measurements. CRM: Certified Reference Material. ....	32
<b>Table 2.4.</b> Precision and accuracy of Al, Cd, Cu, Fe, Pb and Zn measurments. CRM: Certified Reference Material, MS: mass spectrometrie, OES: optical emission spectrometry. ....	34
<b>Table 3.1.</b> Total anthropogenic induced inventories (per square metre) of $^{137}\text{Cs}$ and Hg as well as the inventories of TOC, TN, TS and $\text{bioSiO}_2$ in the upper 15 cm of sediment at stations in the Mecklenburg Bight (upper rows), the Arkona Basin (middle rows) and the adjacent sandy areas (lower rows), arranged from west (left) to east (right). FRS: Falster-Rügen sand plain, OB: Oder Bank, SC: Sassnitz Channel, STOL: Stoltera, TW: Tromper Wiek. Stations in close vicinity to the local hot spots are marked with an asterisk. ....	45
<b>Table 3.2.</b> Total anthropogenic induced inventories (per square metre) of Cd, Cu, Pb, $\Sigma\text{PCB}$ and Zn as well as the inventories down to 15 cm sediment depth of $\text{TP}_{\text{Ash}}$ and $\Sigma\text{PAH}$ at stations in the Mecklenburg Bight and the Arkona Basin, arranged from west (left) to east (right). ....	52
<b>Table 4.1.</b> Ichnogenera and other bioturbation structures identified in the studied cores. Modified after <a href="#">Virtasalo et al. (2011)</a> . ....	64



## List of abbreviations

AB	Arkona Basin
ABSS	Arkona Basin Standard Sediment [reference material]
AL	German research vessel ALKOR
ASE	Accelerated Solvent Extractor
BBOT	2,5-Bis(5-tert-butyl-benzoxazol-2-yl)thiophene [certified reference material]
bioSiO <sub>2</sub>	Biogenic silicate
BMBF	Federal Ministry of Education and Research, Germany
BSH	Federal Maritime and Hydrographic Agency, Germany
COMBINE	Cooperative Monitoring in the Baltic Marine Environment
CRM	Certified reference material
CTD	Conductivity, Temperature, Depth
DBD	Dry bulk density
DBT	Dibutyltin
DCE	Danish Centre for Environment and Energy
DMA	Direct mercury analyser
DYNAS	Dynamics of Natural and Anthropogenic Sedimentation [project]
EDX	Energy dispersive X-ray spectroscopy
EMB	German research vessel ELISABETH MANN BORGESE
EPA	United States Environmental Protection Agency
FONA	Research for Sustainable Developments
FRS	Falster-Rügen sand plain
GC	Gas chromatography
GTK	Geological Survey of Finland
HELCOM	Helsinki Commission (Baltic Marine Environment Protection Commission)
HPLC	High-performance liquid chromatography
IAEA	International Atomic Energy Agency
ICES	International Council for the Exploration of the Sea
ICP	Inductively coupled plasma
IOW	Leibniz Institute for Baltic Sea Research Warnemünde, Germany
LB	Lübeck Bay, south-western Mecklenburg Bight
MARNET	Marine Environmental Monitoring Network, Germany

MB	Mecklenburg Bight
MBI	Major Baltic Inflow (of saline water)
MBSS	Mecklenburg Bight Standard Sediment [reference material]
MBT	Monobutyltin
MS	Mass spectrometry
MUC	Multi-corer
NERI	National Environmental Research Institute, Denmark
NDIR	Nondispersive infrared
NIOZ	Royal Netherlands Institute for Sea Research
OB	Oder Bank, Pomeranian Bight
OBSS	Baltic Sea Basin Standard Sediment (Landsort Deep, Gotland Basin) [reference material]
OES	Optical emission spectroscopy
PACS-1	Esquimalt Harbour Sediment [certified reference material]
$\Sigma$ PAH	Polycyclic aromatic hydrocarbons (sum)
$\Sigma$ PCB	Polychlorinated biphenyls (sum)
PDS	Pressure digestion system
POP	Persistent organic pollutant
POS	German research vessel POSEIDON
PTJ	Project Management Jülich, Germany
RM	Reference material
R/V	Research vessel
SC	Sassnitz Channel, east of Rügen Island
SEC	Size exclusion chromatography
SECOS	The Service of Sediments in German Coastal Seas [project]
SEM	Scanning electron microscopy
SGR-1	Green River Shale [certified reference material]
SIBER	Silicate and Baltic Sea Ecosystem Response [project]
STOL	Stoltera, eastern Mecklenburg Bight
TBT	Tributyltin
TC	Total carbon
TH-2	Toronto Harbour Sediment [certified reference material]



TIC	Total inorganic carbon
TN	Total nitrogen
TOC	Total organic carbon
TP <sub>Ash</sub>	Total phosphorus (via ash)
TP <sub>Digest</sub>	Total phosphorus (via total digestion)
TS	Total sulphur
TW	Tromper Wiek, north-east of Rügen Island
VMS	Vessel monitoring system
W <sub>a</sub>	Absolute water content



# 1 Introduction

## 1.1 Motivation

Coastal and marginal seas – like the Baltic Sea – serve as natural reaction sites for the turnover and accumulation of land-derived inputs. The main location for the modification and deposition of the introduced material is, in most cases, not the water mass, but the sediment. Its key function as central reactor in the interaction between land and sea has so far been insufficiently studied and assessed. This study was part of the interdisciplinary *SECOS* project that aimed to identify and evaluate *the service functions of sediments in German coastal seas* in the context of human use with a focus on the Baltic Sea. One of its goals was to assess sediment functions related to the intermediate storage or final sink of imported material like nutrients and contaminants, and quantify their inventory as well as their mass accumulation rates on multi-decadal to multi-centennial time scales. For that, a detailed examination of the natural and anthropogenic processes that interfere with sediment accumulation in the south-western Baltic Sea basins is essential. In this context, the following research questions will be examined and discussed within this study:

1. Which natural and anthropogenic mixing processes take place and what are their effects on the sediments in the south-western Baltic Sea basins?
2. What are the resulting sediment accumulation patterns and inventories?
3. What are the timescales, on which the basins act as sinks for imported material?

## 1.2 Regional setting

The semi-enclosed Baltic Sea is an inner continental shelf sea that lies in the temperate latitudes of the prevailing Northern Hemisphere westerlies (between 10-30°E and 54-66°N). It consists of several basins of different depth, separated by shallower submarine sills that restrict the horizontal water exchange between the basins as well as with the North Sea. The Baltic Sea is connected to the North Sea via the three narrow Danish Straits (Little Belt, Great Belt, Sound) and the Kattegat as transition zone. The Little Belt and the Great Belt merge via the Fehmarn Belt into the Mecklenburg Bight that has a maximum depth of about 25 m. The Mecklenburg Bight and the Sound adjoin the 18 m deep Darss Sill and the 8 m deep Drogden Sill, respectively, where they open into the Arkona Basin with a maximum depth of about 50 m. The Arkona Basin is connected to the up to 100 m deep Bornholm Basin by the Bornholmsgat without a substantial sill. The other main basins are the Eastern and Western

Gotland Basin with maximum depths of about 250 m and 460 m (Landsort Deep), respectively, the Gulf of Finland with a maximum depth of about 120 m, the Bothnian Sea, and the Bothnian Bay with characteristic depths of 120 m and 80 m, respectively (HELCOM, 2002; Lass and Matthäus, 2008).

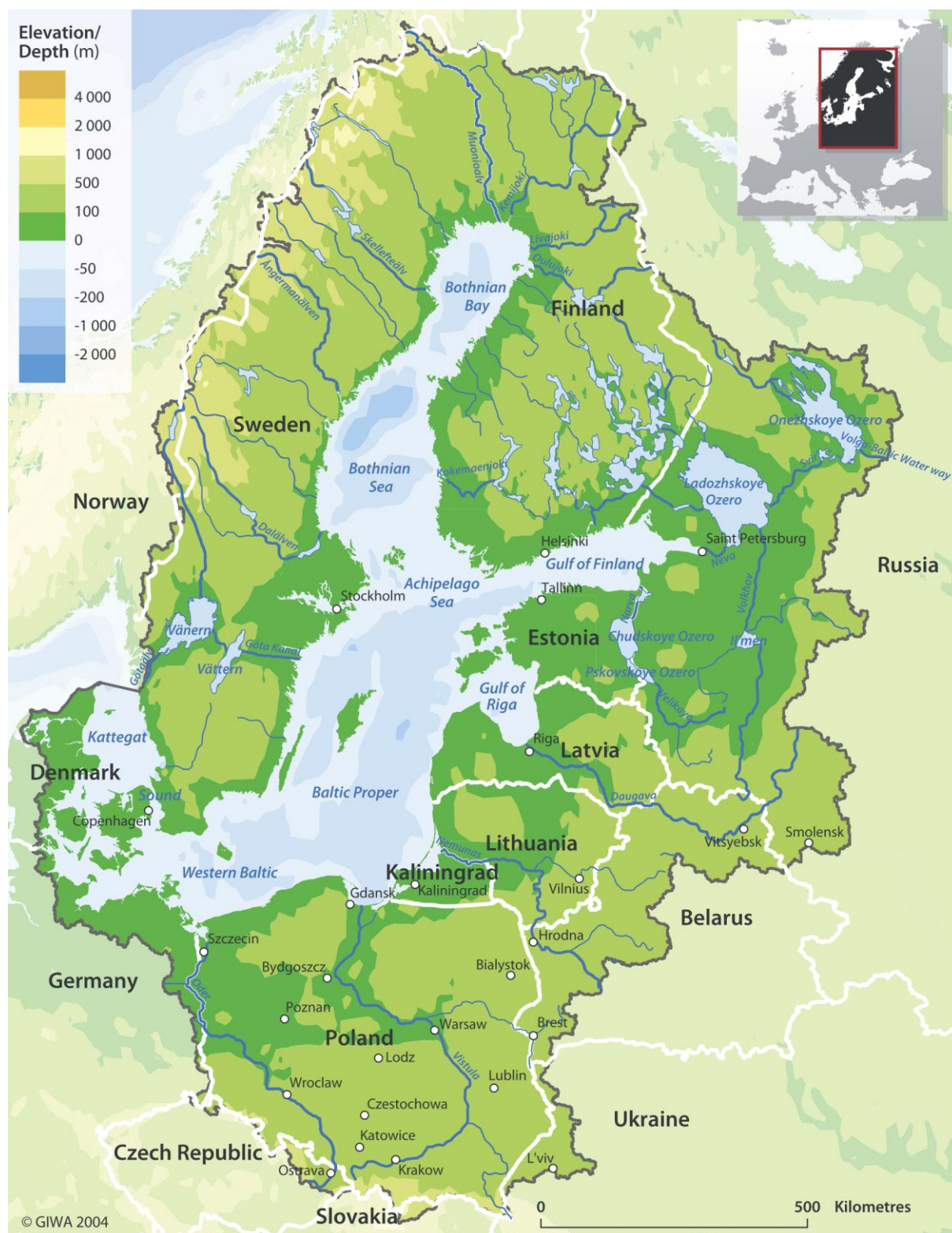


**Figure 1.1.** Map of the Baltic Sea and its catchment area (HELCOM, 2006; UNEP, 2005).

The Baltic Sea has a water volume of 21,721 km<sup>3</sup> and covers an area of 415,266 km<sup>2</sup> with an associated catchment area of 1,720,270 km<sup>2</sup> that is spread over 14 countries (Fig. 1.1). The total long-term mean run-off from all Baltic rivers is 479 km<sup>3</sup>/a, of which nearly 50% drain into the Baltic Sea via the seven largest rivers, i.e., Neva, Vistula, Nemunas, Daugava, Oder, Göta Älv and Kemijoki. This freshwater surplus together with the restricted water exchange with the North Sea leads to brackish water conditions, a residence time of the water within the Baltic Sea of 25-35 years and a permanent density stratification of the water column that hampers the vertical water exchange. In general, there is a surface layer of low saline water (6-8 PSU) flowing out into the North Sea and a compensation current in the deep layer that transports higher saline water (10-14 PSU) into the Baltic Sea, producing a pycnocline. Because these inflows of saline water are restricted by the narrow and shallow transition area to the North Sea, the deep water in the central basins tends to stagnate for periods of several years, thereby creating anoxic conditions and leading to the formation of high concentrations of hydrogen sulphide. The lack of oxygen is accompanied by the impoverishment of the benthic community, followed by the disappearance of higher organisms. Occasionally, larger volumes (100-250 km<sup>3</sup>) of highly saline (17-25 PSU) and oxygenated water – so called Major Baltic Inflows (MBIs) – enter the Baltic Sea under certain meteorological and oceanographic conditions and ventilate the basins for some time (HELCOM, 2002; Lass and Matthäus, 2008).

The Baltic Sea is situated between the Fennoscandian Shield in the north-west and the European Plain in the south-east. The morphology of that region was primarily created by the quaternary glaciations. Glacial erosion shaped the crystalline Precambrian rocks of the Fennoscandian Shield and excavated the Baltic Sea basin, while the lowlands of the European Plain were covered by the resulting glacial sediments. When the Scandinavian Ice Sheet finally retreated some 12,600 years ago, a proglacial lake developed from the melting waters before the ice – the Baltic Ice Lake. On the lake floor, varved clays accumulated due to the seasonal differences in the sediment load from the melting ice. About 10,300 years ago, the Baltic Ice Lake was connected to the world ocean and the brackish Yoldia Sea formed, named after the marine bivalve *Yoldia arctica* (renamed to *Portlandia arctica*) that inhabited it. Eventually, the postglacial isostatic uplift exceeded the eustatic sea level rise and closed the strait in central Sweden again about 9,500 years ago. The sea quickly turned into a fresh-water lake and was populated, among others, by the gastropod *Ancylus fluviatilis*. In the period from 9,000 to 8,000 years, the Ancylus Lake was increasingly affected by salt water ingressions from the

Kattegat and became more and more brackish. Erosion and the eustatic sea level rise finally submerged the Danish Straits permanently and led to a quick rise of the “Baltic” sea level by about 20 m within a few centuries – the Littorina Transgression. The evolved Littorina Sea became so salty that it was populated by the marine gastropod *Littorina litorea* about 7,500 years ago. Due to continued isostatic uplift, the water exchange with the North Sea and thus the salinity of the Baltic Sea decreased about 4,000 years ago. Today, the postglacial isostatic adjustment of the earth’s crust still causes a relative uplift of up to 9 mm/a in the northern parts, resulting in regression and coastal advance. The southern Baltic Sea shows a slow subsiding effect that is exceeded by the eustatic sea level rise of 1 mm/a leading to transgression and coastal erosion (Björck, 1995; Leipe et al., 2008; Lemke, 1998).

Figure 1.2 shows the recent distribution of surface sediments in the south-western Baltic Sea that reflects the integrated effects of hydrodynamics, the initial glacial sediment distribution, and the post-glacial morphological development. There are areas of erosion with glacial till outcrops and partly gravelly, so-called lag sediments (brown) that can be found where fine-grained material is removed by waves and currents, e.g. in the Fehmarn Belt. This fine material is passing through transitional areas with sandy sediments (yellow, green, light blue) – the Oder Bank in the Pomeranian Bight, Stoltera, and the Tromper Wiek – to be deposited at greater depths in the form of organic-rich mud (blue; Leipe et al., 2017). Since the Littorina-Transgression, an up to 9 m thick layer ( $3.7 \text{ km}^3$ ) of mud accumulated in the Mecklenburg Bight (including the Bay of Lübeck) and an up to 11 m thick layer ( $20.4 \text{ km}^3$ ) in the Arkona Basin (Bonacker, 1996).

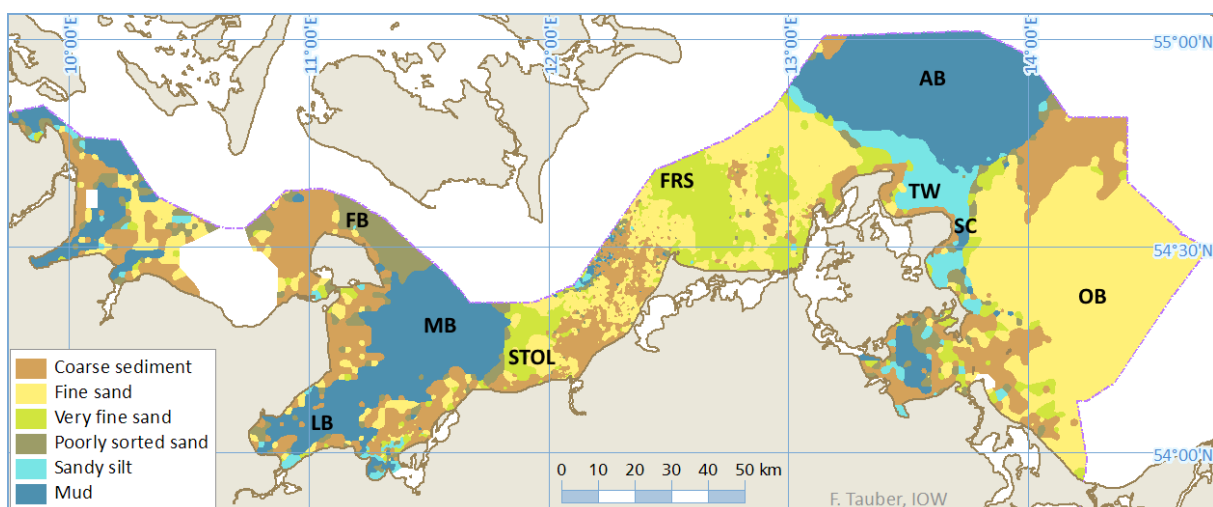


**Figure 1.2.** Distribution map of the major sediment types in the German Baltic Sea area. AB: Arkona Basin, FB: Fehmarn Belt, FRS: Falster-Rügen sand plain, LB: Lübeck Bay, MB: Mecklenburg Bight, OB: Oder Bank, SC: Sassnitz Channel, STOL: Stoltera, TW: Tromper Wiek. Modified after Leipe et al. (2017).



Besides coastal erosion and atmospheric deposition, most land-derived material enters the south-western Baltic Sea via the Oder River after passing the Oder Lagoon in the south-east. Furthermore, bottom inflows of saline water also deliver suspended matter from the North Sea. The Sassnitz Channel is a former riverbed from the Oder that drained further north, when the sea level was lower, and is still a pathway for river discharge into the Arkona Sea during easterly winds (Christiansen et al., 2002; Emeis et al., 2002; Gingele and Leipe, 2001; Leipe and Gingele, 2003; Pohl et al., 1998; Siegel et al., 2005).

### 1.3 Anthropogenic contamination

The Baltic Sea is surrounded by nine highly industrialised countries (Fig. 1.1) and is therefore under strong anthropogenic pressure. Apart from direct impact by commercial use (fishery, maritime traffic and constructions), industry and agriculture are still the main sources of contamination through river discharge and air pollution. The Baltic Sea is particularly sensitive to contamination of different kinds due to the restricted water exchange with the North Sea, the resulting residence time of water within the Baltic Sea and the vertical stratification of the water column (HELCOM, 2011, 2010a; Nausch et al., 2008).

Mercury is a good example for the widespread pollution during the industrial times (last circa 150 years). It has the highest enrichment factor in anthropogenic contaminated sediments (compared to other heavy metals) and is one of the most sensitive elements for environmental studies. It has a high affinity to organic material and thus enriches in the natural food chain, while being highly toxic to organisms. The natural occurrence of Hg is limited to local Hg-rich ores and volatile outcrops of active volcanic zones, which results in a very low natural geogenic background. In Baltic Sea sediments, this pre-industrial background persisted until around 1900, even though industrialisation started around 1850 (Hylander and Meili, 2003; Leipe et al., 2013, 2005). Anthropogenic sources include (i) fossil fuel combustion, (ii) the production of steel and other metals, as well as cement, (iii) mercury, gold and silver mines, smelters and chemical industries, (iv) agriculture and wood industries (e.g. pesticides, paper mills), and (v) batteries, thermometers and lamps. The commercial use peaked in 1970 and has declined sharply since due to environmental measures (Horowitz et al., 2014; Leipe et al., 2013). However, Hg has a long residence time in the environment and its recent contents in the sediments are still much higher than the natural background levels. The main pathways into the Baltic Sea are via (i) atmospheric deposition, (ii) riverine input, (iii) coastal industrial point

sources and (iv) historical dumping sites as local pollution hot spots. In the Lübeck Bight, industrial waste from a smelter was dumped in the 1960s and presumably military waste from World War II was dumped in the western Arkona Basin (Hallberg, 1991; Leipe et al., 2013, 2005).

Another contaminant is the artificial radionuclide  $^{137}\text{Cs}$  that is formed by nuclear fission and has a half-life of 30.17 years. 82.61% of the  $^{137}\text{Cs}$  in the Baltic Sea originates from the Chernobyl accident on 26<sup>th</sup> April 1986, which started a worldwide tracer experiment and affected the Baltic and Black Seas the most (HELCOM, 2013; Povinec et al., 1996). Due to the meteorological conditions at the time, the Chernobyl fallout was unevenly distributed over the drainage area of the Baltic Sea, with highest contamination in the land areas around the Bothnian Sea and the eastern Gulf of Finland. 13.22% originates from atmospheric nuclear weapons tests in the 1950-1980s. The first widespread dispersal and fallout of  $^{137}\text{Cs}$  occurred in November 1952 and was first detected in the atmosphere in 1954, while the maximum deposition in the Northern Hemisphere prior to Chernobyl was in 1963 (Appleby et al., 1991; HELCOM, 2013; Pennington et al., 1973). The Baltic Sea lies within the zone of most intense global fallout between 40° to 60°N (Nies et al., 1995). 4.13% originates from discharges by nuclear reprocessing plants outside the Baltic Sea (mostly U.K. and France) and only 0.04% from nuclear discharges directly into the Baltic Sea. The impact of non-nuclear facilities is negligible and the fallout from the Fukushima accident in March 2011 is not detectable in the Baltic Sea (HELCOM, 2013; Ilus and Ilus, 2000).  $^{137}\text{Cs}$  has a tendency to bind to fine and organic particles, thus 70% of  $^{137}\text{Cs}$  in the Baltic Sea is found in sediments (Ikäheimonen et al., 2009). Its total activity in 2010 was still eight to nine times higher than the pre-Chernobyl level in 1980 and the downwards diffusion of Chernobyl  $^{137}\text{Cs}$  has often obliterated the weapons-testing  $^{137}\text{Cs}$  signal (Appleby et al., 1991; HELCOM, 2013).

Persistent organic pollutants (POPs) like polychlorinated biphenyls (PCBs) and polycyclic aromatic hydrocarbons (PAHs) are also entering the Baltic Sea via atmospheric deposition and river discharge. Because of their hydrophobic character and high persistence, large amounts of POPs accumulate in sediments (Hedman et al., 2009; Witt and Trost, 1999). PCBs are synthetic chemicals that were used as plasticisers, insulators as well as flame retardants and were widely distributed through inappropriate waste handling or leakage from large condensers and hydraulic systems (HELCOM, 2010b). PCBs were produced in large quantities since around 1935 and the commercial use peaked in 1970, similar to Hg and some other



heavy metals. Nowadays, the main sources are of secondary nature, e.g. PCB-containing waste (Breivik et al., 2002a, 2002b). PAHs are mainly formed by incomplete combustion due to a lack of oxygen, but they are also synthesised by some organisms like bacteria, algae and fungi, resulting in low natural geogenic background values. The primary anthropogenic source is fossil fuel combustion, followed by atmospheric deposition and other sources such as domestic and industrial wastewater, continental run-off and spillage of petroleum products by ships. PAHs have a low solubility in water and are easily associated with fine particulate and organic matter. They are slowly decomposed by microbial degradation as well as photo- and chemical oxidation (Witt, 1995). PAH concentrations increased from the late 19<sup>th</sup> century until around 1960 due to the industrialisation, followed by a decrease due to the change of fuels from coal to oil and gas, which emit less PAHs during combustion (Witt and Trost, 1999).

Organotin compounds are another type of organic pollutants and are almost exclusively of anthropogenic origin. Mono- (MBT) and dibutyltin (DBT) were mainly used as stabilising additive in PVC since the 1940s and tributyltin (TBT) was used in antifouling paints for marine vessels to avoid an attachment of organisms onto the hull since the late 1950s. Because of its lipophilic nature, TBT accumulates in marine organisms, where it causes endocrine disorders, e.g. in molluscs. As a consequence, it was banned for boats < 25 m in 1989 and totally in 2008. TBT is degraded to DBT and MBT by UV photolysis and microbial activity with half-lives of six days up to four months in seawater, one year in aerobic and up to ten years in anaerobic sediments (Abraham et al., 2017).

Moreover, the anthropogenic input of nitrogen and phosphorus can also be regarded as a form of contamination that fosters the eutrophication of the Baltic Sea. The additional nutrients increase the production, sedimentation and decomposition of organic matter, thus increasing the oxygen consumption. This often leads to an oxygen depletion of the bottom waters and the sediments. The oxygen depletion further promotes eutrophication because the reduced sediments release significant amounts of P to the overlying water under anoxic conditions. Most of the nutrients (75% of N and 95% of P) originate from waterborne sources, predominantly from agriculture and municipal wastewater treatment plants, but also from industry and aquaculture. The remaining 5-25% enter the Baltic Sea directly via atmospheric deposition and only about 16% of the total nutrient inputs are of natural origin. The nutrient inputs have been reduced significantly since the late 1980s. From 1990 to 2000, the waterborne N and P inputs have declined by 30% and 45%, respectively. The atmospheric N

deposition has also declined since mid-1990s, but increased again from 2003-2007, probably due to the increasing ship traffic in the Baltic Sea (HELCOM, 2011, 2010a, 2010c, 2009).

Measured profiles of some of these contaminants from undisturbed short sediment cores can be used for event stratigraphic purposes to reconstruct environmental changes at a sub-decadal to decadal resolution. In the muds of the Baltic Sea, the main time markers are (i) the exceedance of Hg over natural background levels at around 1900, (ii) the first detectable presence of PCBs at around 1935, (iii) the radionuclide production (e.g.  $^{241}\text{Am}$ ) due to nuclear weapons testing from 1954 to 1975, with a peak in 1963, (iv) the maximum of heavy metal and PCB concentrations at around 1970, and (v) the sharp  $^{137}\text{Cs}$  increase due to the Chernobyl nuclear accident in 1986 (Fig. 1.3). However, this event stratigraphy is only reasonable in areas with continuous sedimentation and limited post-depositional disturbance like the Gotland Basin, where it is also possible to date the sediments via unsupported  $^{210}\text{Pb}$ . The influx of old re-worked sediment dilutes the artificial signals and decreases the  $^{210}\text{Pb}_{\text{unsupp.}}$  activity. In this context, parallel Hg and  $^{137}\text{Cs}$  measurements are useful to assess the suitability of sediment cores for event stratigraphy and dating (Moros et al., 2017).

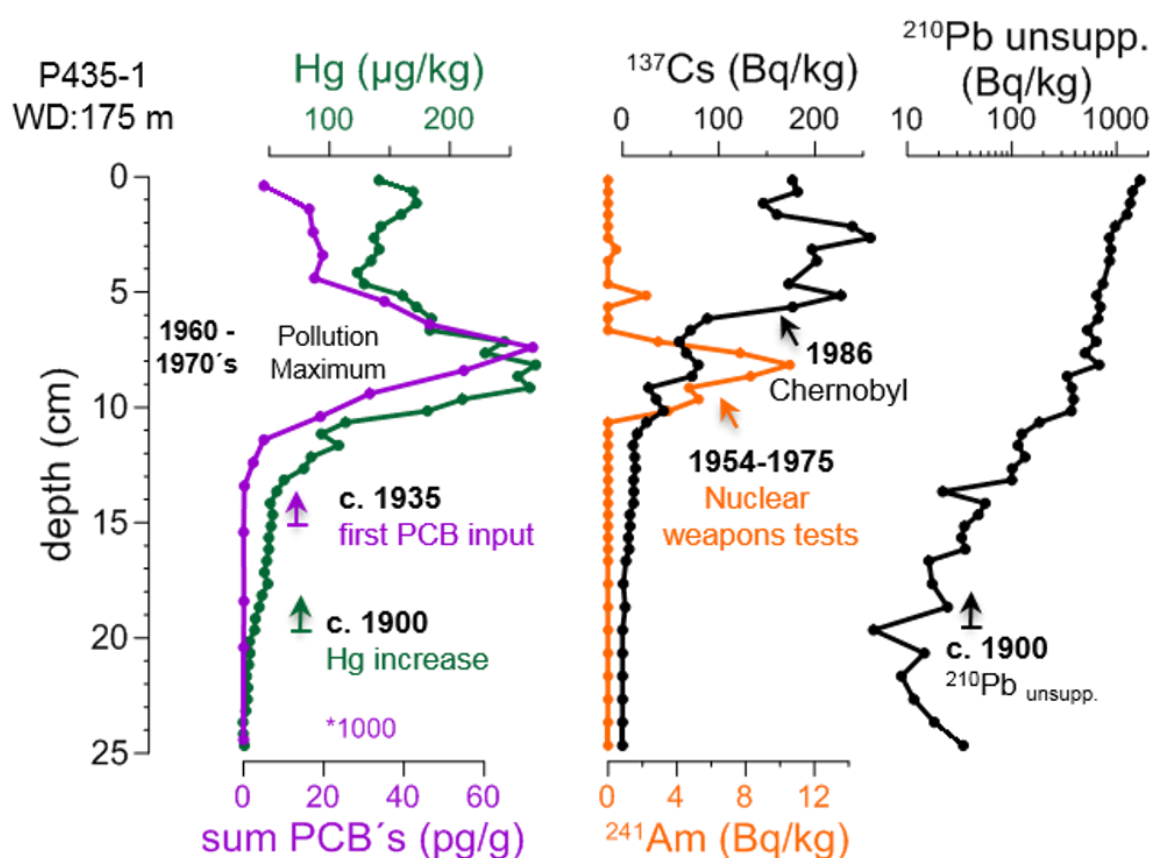


**Figure 1.3.** Pollutant (Hg,  $\Sigma\text{PCB}$ ) and radionuclide ( $^{137}\text{Cs}$ ,  $^{241}\text{Am}$  and  $^{210}\text{Pb}$ ) profiles of an undisturbed short core from the Eastern Gotland Basin at a water depth of 175 m. Modified after Moros et al. (2017).

## 2 Materials and methods

### 2.1 Sediment coring and subsampling

Sediment sampling was performed in the mud areas of the Mecklenburg Bight and the Arkona Basin as well as in selected sandy areas (Stoltera, Falster-Rügen sand plain, Tromper Wiek, Sassnitz Channel, Oder Bank) during cruises with R/V ELISABETH MANN BORGESE (EMB058, EMB076) in 2013 and 2014, R/V ALKOR (AL434) and R/V POSEIDON (POS475) in 2014 (Fig. 2.1, Tab. 2.1). Up to 47 cm long sediment cores were retrieved with a four- (EMB058) or eight-tube multi-corer from *Oktopus GmbH*, equipped with two to eight 61 cm long and 10 cm wide polycarbonate tubes. Most of the gained cores were immediately cut to 1 cm thick slices, which were then transferred to 100 ml plastic jars (EMB058) or 50 ml polypropylene tubes and frozen on board. Back at the *Leibniz Institute for Baltic Sea Research Warnemünde (IOW)*, these samples were freeze-dried under vacuum and homogenised afterwards for particle size analysis. A proportion of each sample was ground with a ball mill for geochemical analyses. For X-ray radiography, some of the POS475 cores were split lengthwise on board and their work halves were further processed at the *Geological Survey of Finland (GTK)* in Espoo. For radiograph samples served plastic boxes (50 x 5 x 2 cm) that were pushed into the half-cores, cut out with a steel string, and sealed with tape (Virtasalo et al., 2011).

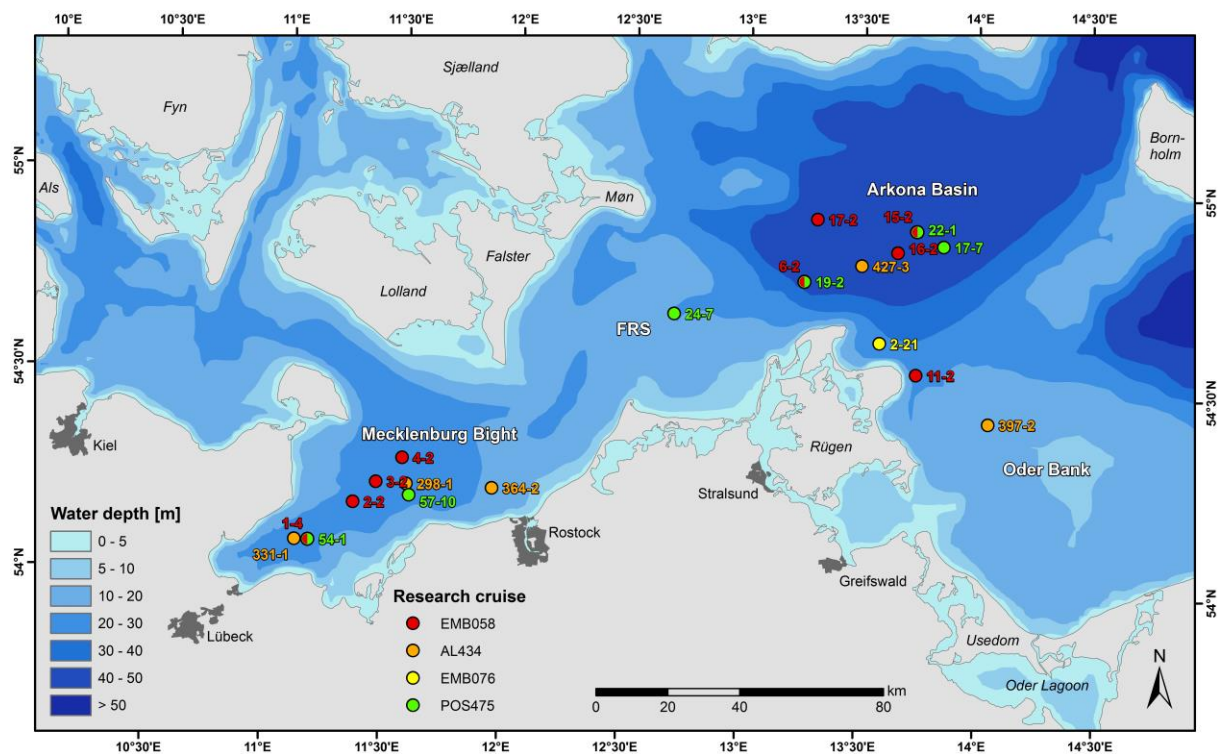


**Figure 2.1.** Map of the south-western Baltic Sea with coring locations (coloured circles). FRS: Falster-Rügen sand plain. Bathymetry data from Seifert et al. (2001).

**Table 2.1.** Meta data of the studied cores, retrieved by multi-corer. AL: R/V ALKOR, EMB: R/V ELISABETH MANN BORGESE, POS: R/V POSEDION, AB: Arkona Basin, FRS: Falster-Rügen sand plain, LB: Lübeck Bay, MB: Mecklenburg Bight, OB: Oder Bank, SC: Sassnitz Channel, STOL: Stoltera, TW: Tromper Wiek.

Core ID	Sampling date	Region	Latitude (WGS 1984)	Longitude (WGS 1984)	Water depth [m]	Recovery [cm]
EMB058/1-4	2 Oct 2013	LB	54°06.07'N	11°09.98'E	22.8	45
EMB058/2-2	2 Oct 2013	MB	54°12.02'N	11°21.00'E	21.8	34
EMB058/3-2	2 Oct 2013	MB	54°15.20'N	11°26.62'E	22.2	36
EMB058/4-2	2 Oct 2013	MB	54°18.97'N	11°33.07'E	24.5	34
EMB058/6-2	3 Oct 2013	AB	54°47.52'N	13°15.13'E	42.0	42
EMB058/11-2	5 Oct 2013	SC	54°33.78'N	13°44.41'E	23.3	44
EMB058/15-2	6 Oct 2013	AB	54°55.27'N	13°44.08'E	46.1	38
EMB058/16-2	6 Oct 2013	AB	54°52.08'N	13°39.29'E	45.2	39
EMB058/17-2	6 Oct 2013	AB	54°56.85'N	13°18.22'E	44.0	40
AL434/298-1	29 Mar 2014	MB	54°15.10'N	11°34.40'E	24.6	38
AL434/331-1	30 Mar 2014	LB	54°06.02'N	11°06.53'E	23.1	38
AL434/364-2	1 Apr 2014	STOL	54°15.03'N	11°56.34'E	18.5	24
AL434/397-2	3 Apr 2014	OB	54°26.50'N	14°03.21'E	16.4	15
AL434/427-3	5 Apr 2014	AB	54°50.01'N	13°29.99'E	45.5	47
EMB076/2-21	24 June 2014	TW	54°38.44'N	13°34.86'E	28.8	28
POS475/17-7	2 Oct 2014	AB	54°53.05'N	13°51.18'E	50.0	42
POS475/19-2	3 Oct 2014	AB	54°47.48'N	13°15.14'E	43.0	30
POS475/22-1	3 Oct 2014	AB	54°55.27'N	13°44.24'E	47.0	36
POS475/24-7	4 Oct 2014	FRS	54°42.17'N	12°41.62'E	22.0	19
POS475/54-1	10 Oct 2014	LB	54°06.05'N	11°09.96'E	23.9	35
POS475/57-10	11 Oct 2014	MB	54°13.42'N	11°35.21'E	27.1	37

## 2.2 Water content and dry bulk density

The absolute water content ( $W_a$ ) of the freeze-dried samples was calculated by subtraction of dry weight from wet weight values. It was used to calculate the dry bulk density (DBD) with the equation of [Flemming and Delafontaine \(2000\)](#), under the assumption of an average grain density of around 2.65 g/cm<sup>3</sup>:

$$DBD = 2.6596369 - 0.0886164 \cdot W_a + 0.0088041 \cdot W_a^{1.5} - 0.0002594 \cdot W_a^2$$

A comparison with DBD values from samples of the same study area calculated after [Dadey et al. \(1992\)](#) considering the fresh sample volume showed a good agreement ([Marko Lipka, 2017, IOW, personal communication](#)).

## 2.3 Particle size analysis

The particle size was determined by laser diffractometry after Fraunhofer's theory with a *CILAS 1180 Laser Particle Size Analyzer* for particle sizes of 0.4 to 2,500 µm used in wet dispersion mode. Depending on the respective sediment type, 0.07 to 1.21 g of each sample (< 0.1 g for mud, > 0.2 g for coarser sediments) were suspended in 10-20 ml deionised water (carrier liquid), followed by 3 to 10 minutes of ultrasonic treatment. Once the background measurement of the carrier liquid was finished, the suspended sample was introduced to the device after passing a 1 mm sieve to protect the device from possible shell or plant remains. The sample circulated then through a closed circuit past the laser, while it was held in dispersion by ultrasound. 20 measurements were performed for each sample and averaged to one result.

To characterise the sediment in an almost natural state, the organic content was not removed and no dispersing agent was added before measuring. Measurements of the sandy samples required more material in order to keep the number of suspended particles high and to guarantee statistical relevance. The precision (relative standard deviation) was regularly determined by repeated measurements of five subsamples and was better than 12%. The sediment classification was based on the median and its sorting ( $\sigma$ ) was calculated after:

$\sigma = \sqrt{D_{75}/D_{25}}$  where  $D_{25}$  and  $D_{75}$  represent the size at 25% and 75% of the sample by weight, respectively.

## 2.4 Gamma-ray spectrometry

The gamma-ray spectra of the EMB058 samples with focus on the radionuclide  $^{137}\text{Cs}$  were determined using a *Broad Energy High-purity Germanium Detector (BE3830-7500SL-RDC-6-ULB)* or a *Germanium Well Detector (GCW4021-7500SL-RDC-6-ULB)* from *Canberra*. The radionuclide activities were calculated using the decay corrected certified reference materials (CRM) *IAEA-385 (Irish Sea Sediment, International Atomic Energy Agency)* and *IAEA-447 (moss-soil)*. The energy used for quantification of the isotope was ~662 keV (Moros et al., 2017). Because of the tendency of  $^{137}\text{Cs}$  to bind to fine and organic particles (Ikäheimonen et al., 2009) and in order to enhance the comparability between different sedimentological environments, the  $^{137}\text{Cs}$  activity was normalised by the total organic carbon (TOC) content of the respective sample (Sect. 2.5.3).

## 2.5 Geochemical analyses

### 2.5.1 Mercury

The Hg content was measured with a *Direct Mercury Analyzer DMA-80* from *Milestone Microwave Laboratory Systems (MLS GmbH)*. Depending on the sediment type, 40 to 120 mg of each sample were weighed into sample boats and loaded onto the auto-sampler. After thermal decomposition at 750 °C in an oxygen stream, the released gases were derived and mercury selectively trapped through amalgamation with gold. Reheating of the amalgam rapidly released Hg that was then carried by the oxygen stream to the measuring cell of the spectrophotometer, where it was determined by atomic absorption at 253.65 nm.

Calibration was done with the CRMs *BCR-142R (Light Sandy Soil, Institute for Reference Materials and Measurements, European Commission)* and *SRM 2709 (San Joaquin Soil, National Institute of Standards & Technology, USA)* using five concentration steps covering a range from 5 to 500 ng Hg (Leipe et al., 2013). Precision (relative standard deviation) and accuracy (deviation from reference value) were checked with alternate measurements of the in-house reference material (RM) *MBSS-1 (Mecklenburg Bight Standard Sediment)* for EMB058 samples (4.74% and 15.18%) and the CRM *BCR-142R* for all other samples (6.63% and -13.04%).

If the measured down-core Hg profiles showed a relative stable level of low values in the deeper core section, this was assumed as the geogenic background of the respective core location. Because of the high affinity of Hg to organic material (Leipe et al., 2013) and in order to enhance the comparability between different sedimentological environments, the Hg content was normalised by the TOC content of the respective sample (Sect. 2.5.3).

### 2.5.2 Carbon, nitrogen and sulphur

The total carbon (TC) as well as nitrogen (TN) and sulphur (TS) contents were measured with a *CHNS-O Elemental Analyser EuroEA 3052* from *EuroVector*. In small stannic cups, 10 to 25 mg of each sample were enclosed together with a pinch of divanadium pentoxide as catalyst. After combustion at 1000 °C in a helium-containing concentrated oxygen atmosphere, the released gases were derived, reduced and then separated by gas chromatography, before they were analysed with a thermal conductivity detector.



Calibration was done with the CRM *BBOT* (2.5-Bis(5-*tert*-butyl-benzoxazol-2-yl)thiophene). Precision and accuracy were checked with alternate measurements of the in-house RM *MBSS-1* or *ABSS-1* (*Arkona Basin Standard Sediment*), depending on the sample origin (Tab. 2.2).

Due to its affinity to fine particles and in order to enhance the comparability between different sedimentological environments, the TN and TS contents were correlated to the fine fraction ( $\leq 63 \mu\text{m}$ ) of the respective sample.

**Table 2.2.** Precision and accuracy of TC, TN and TS measurements. AB: Arkona Basin, MB: Mecklenburg Bight, RM: Reference Material.

Samples	RM	TC [%]	TN [%]	TS [%]
EMB058 (AB)	ABSS-1	1.25 / -1.97	3.40 / 4.37	2.34 / 0.77
EMB058 (MB)	MBSS-1	0.91 / -2.98	3.78 / 2.06	1.57 / 0.91
Other	MBSS-1	1.70 / -1.54	8.39 / 2.34	8.91 / 0.80

### 2.5.3 Inorganic and organic carbon

The total inorganic carbon (TIC) content of most samples from EMB058 and AL434 was measured with a *Macro-Elemental Analyser multi EA 2000 CS* from *Analytik Jena*. Ca. 100 mg of the samples were weighed into glass flasks, covered with deionised water and then heated and stirred with a magnetic hot plate. Through addition of 6 ml of phosphorus acid in an oxygen stream, the mineral-bound carbonate (e.g.  $\text{CaCO}_3$ ) was released as carbon dioxide and transferred by the carrier gas to the nondispersive infrared (NDIR) detector. For reasons of time, only the top, bottom and every fourth to tenth sample of the cm-wise sliced EMB058 cores were measured.

For samples from all other cruises and from the core AL434/427-3, a *Macro-Elemental Analyser multi EA 4000 CS BU* from *Analytik Jena* was used. Circa 80 mg of the freeze-dried and homogenised sediment samples were weighed into sample boats and loaded onto the auto-sampler. By addition of 800  $\mu\text{l}$  of phosphorus acid in an oxygen stream, the mineral-bound carbonate was released as carbon dioxide and transferred by the carrier gas to the NDIR detector.

Calibration was done with synthetic calcium carbonate; precision and accuracy were checked with alternate measurements of the in-house RMs *MBSS-1*, *ABSS-1* or *OBSS-1* (*Baltic Sea Basin Standard Sediment*), depending on the sample origin and measuring device, respectively. For

the EMB058 samples from the Mecklenburg Bight, precision and accuracy were 2.55% and 4.47% and for the EMB058 samples from the Arkona Basin 2.98% and -24.38%. For most AL434 samples, MBSS-1 was used and precision and accuracy were 8.53% and 1.73%. For the remaining AL434 samples as well as those from EMB076 and POS475, OBSS-1 was used and precision and accuracy were 5.92% and 13.01%.

The total organic carbon (TOC) content was calculated by the subtraction of TIC from TC values (Leipe et al., 2011). Due to its affinity to fine particles and in order to enhance the comparability between different sedimentological environments, the TOC content was correlated to the fine fraction ( $\leq 63 \mu\text{m}$ ) of the respective sample.

#### 2.5.4 Phosphorus

The total phosphorus content ( $\text{TP}_{\text{Ash}}$ ) was determined for the cores EMB058/2-2 from the Mecklenburg Bight as well as 15-2 and 17-2 from the Arkona Basin. A portion of the samples was incinerated for 3 h at 550 °C. 50 mg of the resulting ashes were weighed into glass flasks, treated with 25 ml 1 N hydrochloric acid and covered by aluminium foil before heating for 15 minutes on a hot plate. The extracts were then filtered with 0.45  $\mu\text{m}$  syringe filters into polypropylene tubes, filled up with deionised water to a final dilution factor of 2,000 and stored in a fridge pending analysis by inductively coupled plasma optical emission spectrometry (ICP-OES) with an *iCAP 6300 Duo* from *Thermo Fischer Scientific*.

To verify the accuracy of  $\text{TP}_{\text{Ash}}$ , the total phosphorus ( $\text{TP}_{\text{Digest}}$ ) content in the cores EMB058/2-2 and 15-2 was additionally measured, along with other major and trace elements, by ICP-OES after total digestion of the sediment (Sect. 2.5.6). Precision and accuracy (Tab. 2.3) were checked with alternate measurements of the CRMs *SGR-1* (*Green River Shale, United States Geological Survey*), *TH-2* (*Toronto Harbour Sediment, National Water Research Institute, Canada*) or *PACS-1* (*Esquimalt Harbour Sediment, National Research Council, Canada*).

**Table 2.3.** Precision and accuracy of TP measurements. CRM: Certified Reference Material.

Samples	CRM	$\text{TP}_{\text{Ash}}$ [%]	$\text{TP}_{\text{Digest}}$ [%]
EMB058/2-2, 15-2	SGR-1	6.44 / -15.03	
EMB058/2-2, 15-2	PACS-1		0.81 / -1.97
EMB058/17-2	TH-2	0.98 / -7.05	



### 2.5.5 Biogenic silica

The biogenic silica ( $\text{bioSiO}_2$ ) content of the EMB058 samples was determined by wet chemical leaching modified after Müller and Schneider (1993). 50 mg of each sample were weighed into stainless steel cylinders, treated with 100 ml 1 M sodium hydroxide and heated for 40 minutes at 80 °C in a shaking water bath. After cooling down in a cold-water bath, the suspensions were centrifuged for 15 minutes at 4000 rpm. The supernatants were filtered with 0.45 µm syringe filters, filled into polypropylene tubes and stored in a fridge pending analysis by ICP-OES (*iCAP 6300 Duo*, Thermo Fischer Scientific) at a dilution factor of 20,000. The measured biogenic silicon content was then multiplied with the molecular weight of silicon dioxide and divided by the atomic weight of silicon to obtain the  $\text{bioSiO}_2$  content.

Precision was between 0.7% and 13.4%. It was checked with alternate measurements of the in-house RM *Arkona Basin Sediment* that was produced during the *SiBER* project (*Silicate and Baltic Sea Ecosystem Response*) by Daniel Conley of the former *National Environmental Research Institute (NERI)* in Roskilde, Denmark (now the *Danish Centre for Environment and Energy, DCE*).

### 2.5.6 Major and trace elements

The major and trace element contents including Al, Fe and heavy metals (e.g. Cd, Cu, Pb, Zn) of one core from each mud basin (EMB058/2-2 and 15-2) were measured by ICP-OES with an *iCAP 6300 Duo* or ICP mass spectrometry (ICP-MS) with an *iCAP Q ICP-MS* from Thermo Fischer Scientific after total digestion of the sediment. For that, circa 50 mg of the samples were treated with 1 ml of a 65% nitric acid solution for some hours to remove the organic content. Then, 3 ml of hydrofluoric and 2 ml of perchloric acid were added and the samples were put into a pressure digestion system *PDS-6* from *Loftfields Analytical Solutions* (Heinrichs et al., 1986) for 15 hours at 185 °C. Thereafter, the acids were evaporated at 180 °C, the wet residues were re-dissolved with 2 ml semi-concentrated hydrochloric acid and fumed off three times, before they were diluted in 2% nitric acid to a final dilution factor of 1,000 (OES) to 5,000 (MS). The used acids were purified by sub-boiling distillation, with exception of hydrofluoric acid that was of suprapure quality already (Dellwig et al., 2007).

Precision and accuracy were checked with simultaneous measurements of the CRMs *SGR-1* and *PACS-1* (Tab. 2.4). If the measured down-core element profiles showed a relative stable

level of low values in the deeper core section, this was assumed as the geogenic background of the respective core location.

**Table 2.4.** Precision and accuracy of Al, Cd, Cu, Fe, Pb and Zn measurements. CRM: Certified Reference Material, MS: mass spectrometrie, OES: optical emission spectrometry.

Samples	CRM	Al (OES) [%]	Cd (MS) [%]	Cu (MS) [%]
EMB058/2-2	SGR-1	1.92 / -0.67	1.22 / 18.25	0.46 / -8.31
EMB058/2-2	PACS-1	3.80 / -9.90	0.69 / 10.25	0.03 / -13.88
EMB058/15-2	SGR-1	1.92 / -0.67	1.37 / 17.81	1.66 / -8.38
EMB058/15-2	PACS-1	3.80 / -9.90	0.85 / 18.08	0.65 / -5.18
Samples	CRM	Fe (OES) [%]	Pb (MS) [%]	Zn (MS) [%]
EMB058/2-2	SGR-1	0.65 / -4.55	0.77 / 7.97	0.63 / 5.50
EMB058/2-2	PACS-1	0.33 / -6.77	0.45 / -10.30	0.01 / -8.38
EMB058/15-2	SGR-1	0.65 / -4.55	2.06 / 8.26	1.40 / 8.11
EMB058/15-2	PACS-1	0.33 / -6.77	0.07 / -0.75	0.71 / 3.30

### 2.5.7 Persistent organic pollutants

For one core from each basin (EMB058/1-4 and 6-2), various POPs were determined by the *Organic Trace Substances* group of the *Marine Chemistry* department at *IOW*. 24 PCB congeners were selected to cover the structural diversity of this group of substances including the 7 ICES indicator congeners (*International Council for the Exploration of the Sea*). For PAHs, 15 of the 16 priority EPA congeners (*United States Environmental Protection Agency*; [HELCOM, 2010b](#)) were selected. Naphthalene was excluded due to its volatility and thus inaccurate determinability. The extraction, purification and analysis were basically conducted as described in the “Manual for Marine Monitoring in the COMBINE Programme of HELCOM” ([HELCOM, 2012a, 2012b](#)). The organic pollutants were extracted from 1 g of sample with an *Accelerated Solvent Extractor (ASE) 350* from *Dionex* and desulphurised on activated copper spirals. Then, they were purified through flush column chromatography on silica and aluminium, followed by further purification through size exclusion chromatography (SEC). The final separation and detection was done with a gas chromatography mass spectrometry (GC-MS) system (*Trace GC / DSQ*) from *Thermo Fischer Scientific*.

The individual derivatives were summed up to  $\Sigma$ PCB and  $\Sigma$ PAH, respectively. If the measured down-core profiles showed a relative stable level of low values or zero in the deeper core section, this was assumed as the geogenic background of the respective core location. Because of their high affinity to organic material ([Schulz-Bull et al., 1998](#); [Witt, 1995](#)) and in

order to enhance the comparability between different sedimentological environments, the ΣPCB and ΣPAH contents were normalised by the TOC content of the respective sample.

### 2.5.8 Organotin compounds

The analysis of the organotin compounds MBT, DBT and TBT in core EMB058/6-2 were performed by the *Organic Trace Substances* group of the *Marine Chemistry* department at *IOW* and were basically conducted as described in *DIN EN ISO 23161:2011* with modifications. The organic pollutants were extracted from 1 g of sample in a potassium hydroxide / methanol / hexane solution at 70 °C and then derivatised with sodium tetraethylborate at a pH of 4.5. The products were extracted with hexane and dried on sodium sulphate, followed by desulphurisation on activated copper spirals and purification by flush column chromatography on activated silica. The final separation and detection was done with a GC-MS system (*Trace GC / Automass III Solo*) from *Thermo Fischer Scientific*. For quantification, the internal standard TPT (Tetrapentyltin) was used. Further details can be obtained from and the results were published in [Abraham et al. \(2017\)](#).

Because of the high affinity of organotin compounds to organic material ([Suzdalev et al., 2015](#)) and in order to enhance the comparability between different sedimentological environments, their contents were normalised by the TOC content of the respective sample.

### 2.5.9 Salinity correction

All geochemical parameters, including the radionuclide activity, were corrected for salinity, using the measured bottom water salinity from a CTD (conductivity, temperature, depth) device that was deployed at each station, under the assumption that the pore water salinity in the upper 50 cm of the sediment largely correspond to the salinity of the overlying bottom water.

## 2.6 Geochemical mapping

Another part of the *SECOS* project, led by Thomas Leipe from the *Marine Geology* department at *IOW*, was the mapping of various geochemical parameters in the upper 2 cm of the surface sediments in the German Baltic Sea area and the Arkona Basin. For that, the fine fraction ( $\leq 63 \mu\text{m}$ ) of about 850 samples ([Fig. 2.2](#)) was separated and analysed for Hg, TIC, TOC, TN,  $\text{bioSiO}_2$  ([Sect. 2.5](#)) and ca. 600 of these samples were additionally analysed for Ca, Cr, Cu, Fe, Mn, P, Pb and Zn by ICP-OES after the extraction method described in [Section 2.5.4](#). Moreover,

six samples were taken in the Oder Lagoon and analysed for all of the already mentioned substances.

The bulk sediment contents were then calculated by using the measured grain size distribution of the respective original sample, assuming that the coarse fraction mainly consists of chemically inert grains of quartz and other silicate minerals (Leipe et al., 2017). The transformation and interpolation to geochemical maps was done by Michael Naumann from the *Physical Oceanography and Instrumentation* department at *IOW* by using *ArcGIS* version 10.2 and *Surfer* version 12. These maps were published in the web-based *Baltic Sea Atlas* (2014). For further details see Leipe et al. (2017) and Naumann et al. (2015).

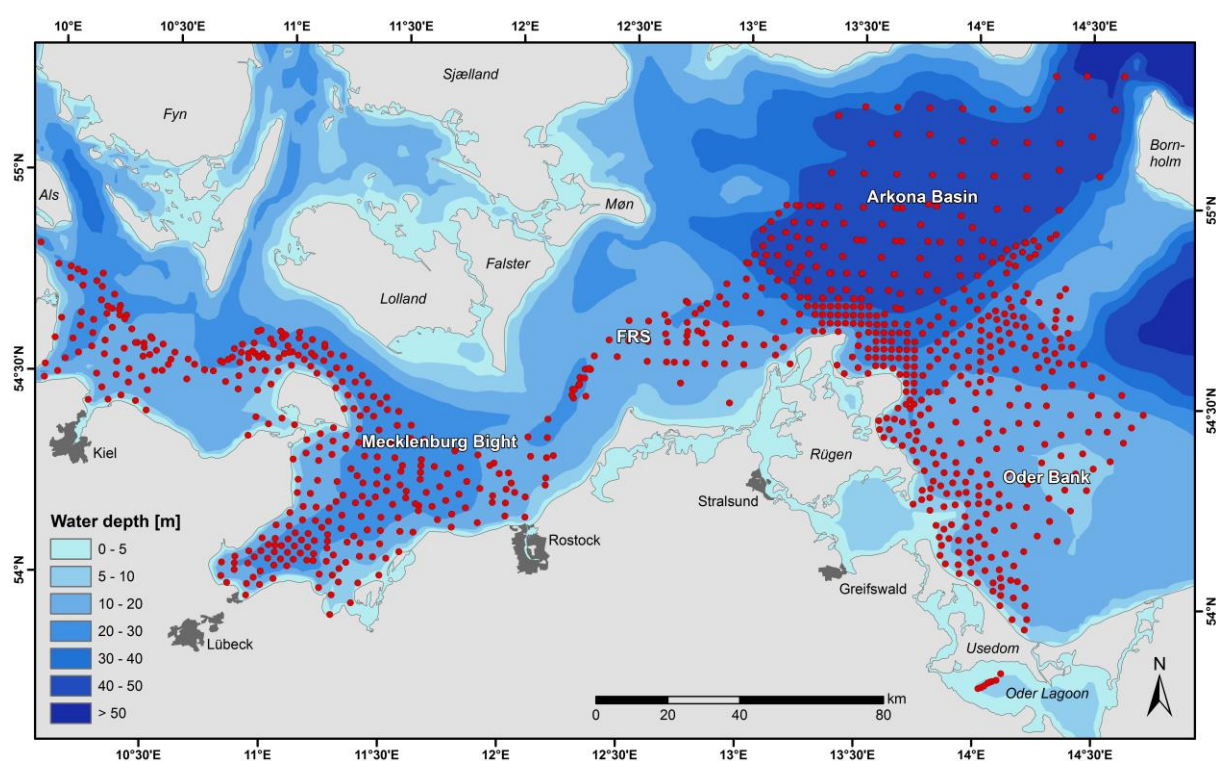


**Figure 2.2.** Map of the south-western Baltic Sea with sampling locations (red circles) for the geochemical mapping of the surface sediments in the German Baltic Sea area and the Arkona Basin. FRS: Falster-Rügen sand plain. Modified after Leipe et al. (2017), bathymetry data from Seifert et al. (2001).

## 2.7 Inventory calculations

The inventory of the salt-corrected geochemical parameters, including  $^{137}\text{Cs}$ , per square metre of sea floor was calculated by multiplication of their content/activity in each 1 cm deep sediment layer with the corresponding DBD after appropriate unit conversions. The inventories of all sediment layers were then added up to the total inventory until a specific depth. For a better comparability between the different stations, a core depth of 15 cm was

generally chosen. For parameters that allowed a separation of the geogenic background like Hg and other heavy metals, the total anthropogenic-induced inventory per square metre was calculated and indicated with the prefix “anth” to the respective chemical symbol, unless the parameters are anyway of artificial origin like  $^{137}\text{Cs}$  and PCBs. Furthermore, the average total anthropogenic-induced inventory/activity in the mud areas of the Mecklenburg Bight (1480 m<sup>2</sup>) and the Arkona Basin (4330 m<sup>2</sup>) were calculated for  $_{\text{anth}}\text{Hg}$  and  $^{137}\text{Cs}$  in tons and megabequerel, respectively.

## 2.8 Scanning electron microscopy

Motivated by an unusual TP profile that raised the question about its form of bonding (Fig. 3.8), the mineral composition of core EMB058/15-2 was analysed with a *MERLIN VP Compact* scanning electron microscope (SEM) from *Carl Zeiss* equipped with an *AZtecEnergy* energy dispersive X-ray spectroscopy (EDX) unit from *Oxford Instruments*. For that, the samples were distributed on *Nucleopore* filters, mounted on aluminium stubs and coated with carbon. Further details on the general procedure can be obtained from [Leipe et al. \(1999\)](#).

## 2.9 X-ray radiography

For sedimentary fabric analysis, high-resolution digital X-radiographs of the prepared POS475 samples were produced by the *Laboratory of Microtomography, University of Helsinki* using a custom-made tungsten-anode *phoenix/x-ray nanotom* micro-computed tomograph from *GE Sensing & Inspection Technologies*. X-ray source power settings were adjusted to 150 kV and 240  $\mu\text{A}$ , and the detector was set to an exposure time of 750 ms and an averaging of 15 images per radiograph ([Virtasalo et al., 2011](#)). The resulting X-radiographs were mirrored, inverted to negatives and combined to one radiograph per core by using the *MosaicJ* plugin ([Thévenaz, 2006; Thévenaz and Unser, 2007](#)) for *ImageJ* version 1.50i ([Rasband, 1997](#)), followed by adjustments of their brightness and contrast.



## 3 Results

### 3.1 Sedimentological parameters

The sediments of the Mecklenburg Bight and the Arkona Basin consist of poorly sorted ( $\sigma$  of around 2) medium to coarse silt with 5% to 10% of clay-sized particles and from 0% up to 3% of fine sand. The sediments become coarser towards the Falster-Rügen sand plain (FRS) and the Oder Bank, respectively, where fine sand predominates (Fig. 1.2). In general, there are only minor variations in the particle size distribution with increasing sediment depth (upper 40-50 cm). In core EMB058/15-2 from the Arkona Basin, there are minor increases of fine sand to up to 1% in 10 and 20 cm sediment depth that coincides with maxima of several geochemical parameters (Sect. 3.2.3, 3.2.4, 3.2.6). In core EMB058/6-2 from the southwestern edge of the Arkona Basin, a coarsening is recognisable below 20 cm with increasing fine sand from 12% up to 30% and decreasing coarse silt from 50% down to 30%. In core EMB058/11-2 from the Sassnitz Channel south of the Arkona Basin, siltier sections (up to 44% coarse silt) alternate with more sandy sections (up to 57% fine sand). In core AL434/364-2 from Stoltera just east of the Mecklenburg Bight basin, the dominating fine and medium sand decreases below 17 cm from 88% down to 24% and the fine fraction ( $\leq 63 \mu\text{m}$ ) increases accordingly from 12% up to 76%.

The water content of the fine-grained basin sediments is very high at the surface ( $\geq 80\%$ ), declining more or less exponentially to 65-70% at about 40 to 50 cm sediment depth due to compaction processes. With increasing sand fraction, the water content decreases to around 35% at stations from the edge of the Arkona Basin and down to 19% at the sandy sites. The DBD is negatively correlated to the water content so that the surface values of the basin sediments are low ( $\leq 0.27 \text{ g/cm}^3$ ), increasing exponentially to 0.35-0.45  $\text{g/cm}^3$  with increasing sediment depth. At the edge of the Arkona Basin, the DBD increases to around 1.0  $\text{g/cm}^3$ , while in the sandy areas it lies at maximal 1.6  $\text{g/cm}^3$ .

### 3.2 Geochemical parameters and radionuclide activity

#### 3.2.1 Mercury and caesium-137

The down-core profiles of Hg and  $^{137}\text{Cs}$  show similarities in both the Arkona Basin and the Mecklenburg Bight (Fig. 3.1A, B). In the lower parts of the short cores, below 20-45 cm, the geogenic background is visible through low values of around 20  $\mu\text{g/kg}$  dry weight Hg (this



study; [Leipe et al., 2013](#)) and no  $^{137}\text{Cs}$  activity, followed by an in general steep increase to a maximum (138.2-755.6  $\mu\text{g/kg}$  dry weight Hg, 41.3-100.0 Bq/kg dry weight  $^{137}\text{Cs}$ ) and a gentler decrease to the sediment surface (104.5-355.8  $\mu\text{g/kg}$  dry weight Hg, 30.9-88.4 Bq/kg dry weight  $^{137}\text{Cs}$ ). While in some cores (e.g. EMB058/3-2 and 6-2), the profiles show a broad “peak” with an offset between Hg (deeper/earlier) and  $^{137}\text{Cs}$  (higher/later), in others (e.g. EMB058/4-2 and 15-2), the maxima form plateaus with little to no decline and both parameters run parallel with nearly no offset. In core EMB058/16-2, the  $^{137}\text{Cs}$  increase takes place in two steps, interrupted by an almost 10 cm wide plateau.

The Hg profiles of the cores from the sandy areas bear a remarkable resemblance to each other and to a few profiles from the mud basins ([Fig. 3.1C](#)). They show low geogenic background values of around 2-11  $\mu\text{g/kg}$  dry weight in the fine fraction below 20 cm, a relative smooth increase to a maximum (87.4-176.9  $\mu\text{g/kg}$  dry weight in the fine fraction) that lies between 5 and 10 cm, and a gentler decrease to the sediment surface with values above the geogenic background (37.1-95.7  $\mu\text{g/kg}$  dry weight in the fine fraction). In core EMB058/11-2 from the Sassnitz Channel are two relatively sharp Hg maxima with  $^{137}\text{Cs}$  activity, one in the lower (122.62  $\mu\text{g/kg}$  dry weight in the fine fraction) and one in the upper part (136.96  $\mu\text{g/kg}$  dry weight in the fine fraction) with geogenic background values in between ( $4.4 \pm 1.0$   $\mu\text{g/kg}$  dry weight in the fine fraction).

The surface and maximum Hg contents are highest near the local pollution hot spots (AL434/331-1 in the Mecklenburg Bight and EMB058/17-2 in the Arkona Basin) and are decreasing with increasing distance to them, especially in coarser sediments ([Fig. 3.1A, B](#)). This is also visible on the geochemical surface sediment maps as aureoles of contaminated material around the hot spots that stretch to the north-east ([Fig. 3.2](#)). The focus on the fine fraction reveals two more hot spots, one being the Oder Lagoon with a big plume stretching north into the open Baltic Sea, the other smaller one lies near the city of Kiel ([Fig. 3.3](#)). The  $_{\text{anth}}\text{Hg}$  inventory is as well highest near the hot spots ([Tab. 3.1](#)), but it is also higher in cores with an Hg plateau of relatively high values down to 25 cm compared to cores with a peak in lower depths ([Fig. 3.1A, B](#)). In total, about 16 t of  $_{\text{anth}}\text{Hg}$  accumulated in the muds of the Mecklenburg Bight, while the muds of the Arkona Basin contain about 93 t.

The surface and maximum  $^{137}\text{Cs}$  activities are slightly higher in the Arkona Basin than in the Mecklenburg Bight and highest in the cores close to pollution hot spots. The total  $^{137}\text{Cs}$



inventories are also higher in the Arkona Basin and here as well, maximum values are close to the local hot spot. The maximum  $^{137}\text{Cs}$  inventory in the Mecklenburg Bight can be found at station EMB058/4-2, where a plateau of relatively high  $^{137}\text{Cs}$  activity reaches down to 25 cm (Fig. 3.1A). In total, about 3 MBq and 20 MBq  $^{137}\text{Cs}$  still exist in the muds of the Mecklenburg Bight and the Arkona Basin, respectively.

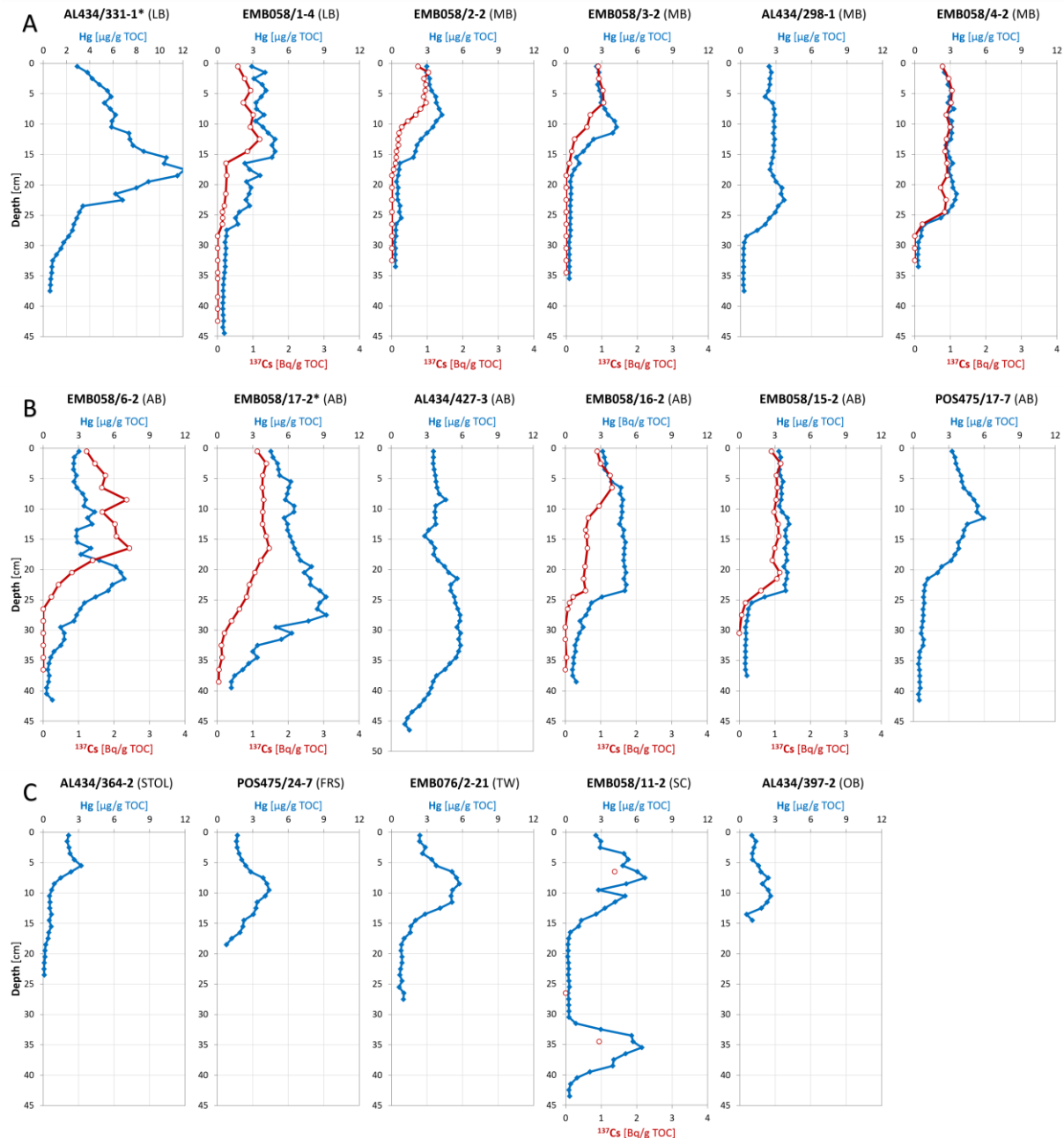


**Figure 3.1.** TOC normalised Hg and  $^{137}\text{Cs}$  profiles of the studied cores from the Mecklenburg Bight (A), the Arkona Basin (B) and the adjacent sandy areas (C), arranged from west (left) to east (right). AB: Arkona Basin, FRS: Falster-Rügen sand plain, LB: Lübeck Bay, MB: Mecklenburg Bight, OB: Oder Bank, SC: Sassnitz Channel, STOL: Stoltera, TW: Tromper Wiek. Stations in close vicinity to the local hot spots are marked with an asterisk. Notice the decreasing surface and maximum Hg values with increasing distance to them as well as the different types of profile shapes.

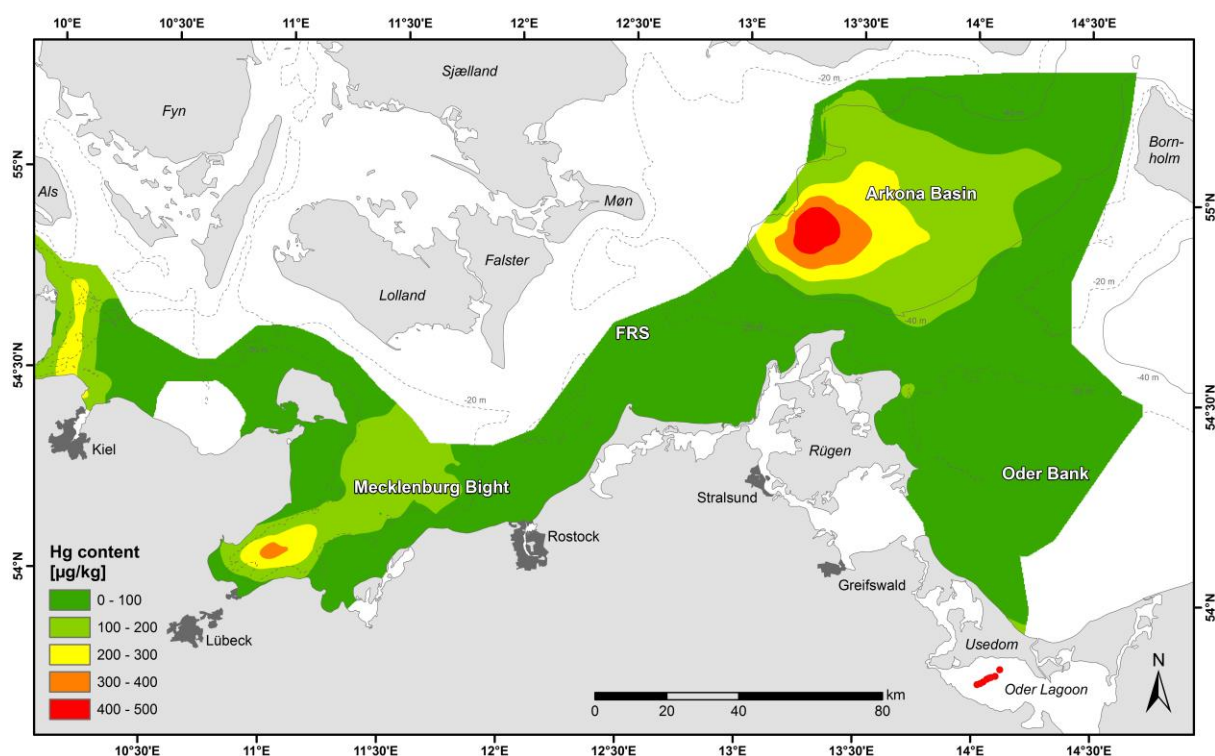


**Figure 3.2.** Hg content in the surface sediments (0-2 cm) of the German Baltic Sea area and the Arkona Basin. FRS: Falster-Rügen sand plain. Notice the hot spots of high contents in both basins as well as in the Oder Lagoon. Modified after [Leipe et al. \(2017\)](#).

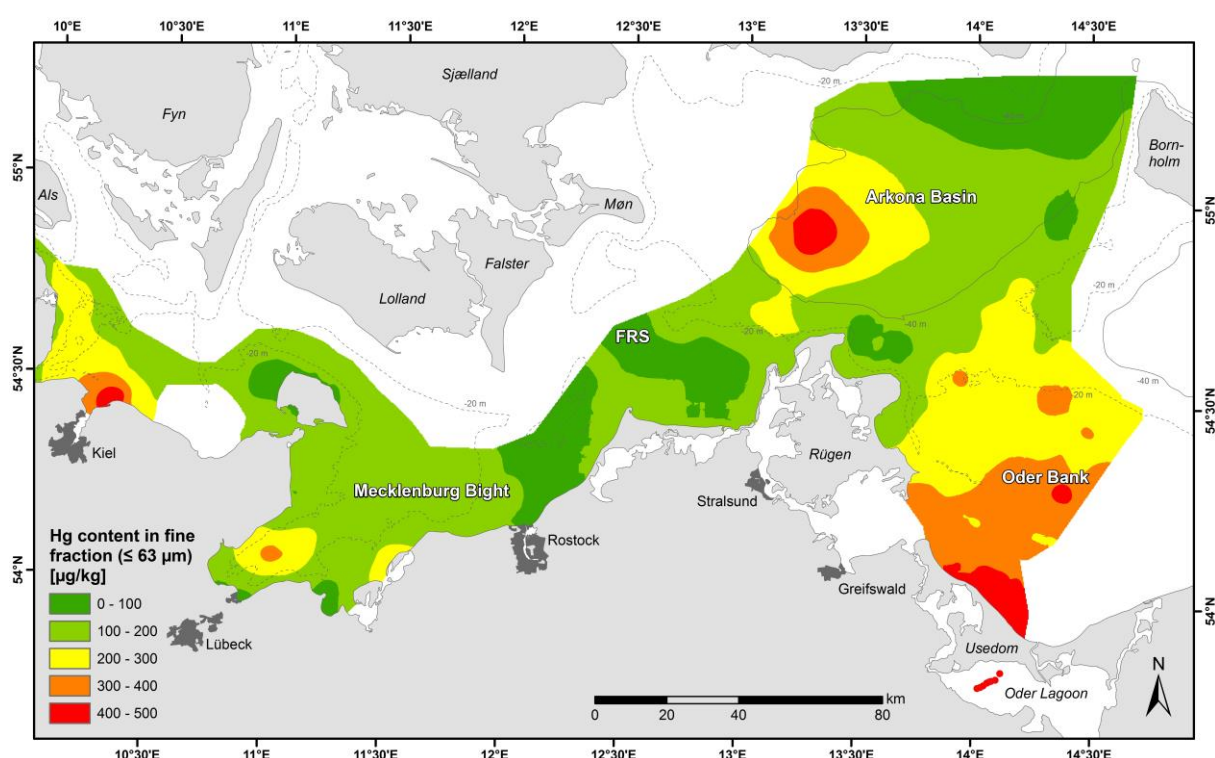


**Figure 3.3.** Hg content in the fine fraction ( $\leq 63 \mu\text{m}$ ) of the surface sediments (0-2 cm) in the German Baltic Sea area and the Arkona Basin. FRS: Falster-Rügen sand plain. Notice the hot spots of high contents in the basins as well as at the Oder mouth and near Kiel. Modified after [Leipe et al. \(2017\)](#).

### 3.2.2 Carbon and nitrogen

The TIC content is generally very low and averages  $0.18 \pm 0.05$  wt.% in the basin muds and  $0.05 \pm 0.04$  wt.% in the fine sands. Only in core AL434/364-2 from Stoltera (Fig. 3.4C), it increases to 6.85 wt.% below 15 cm sediment depth.

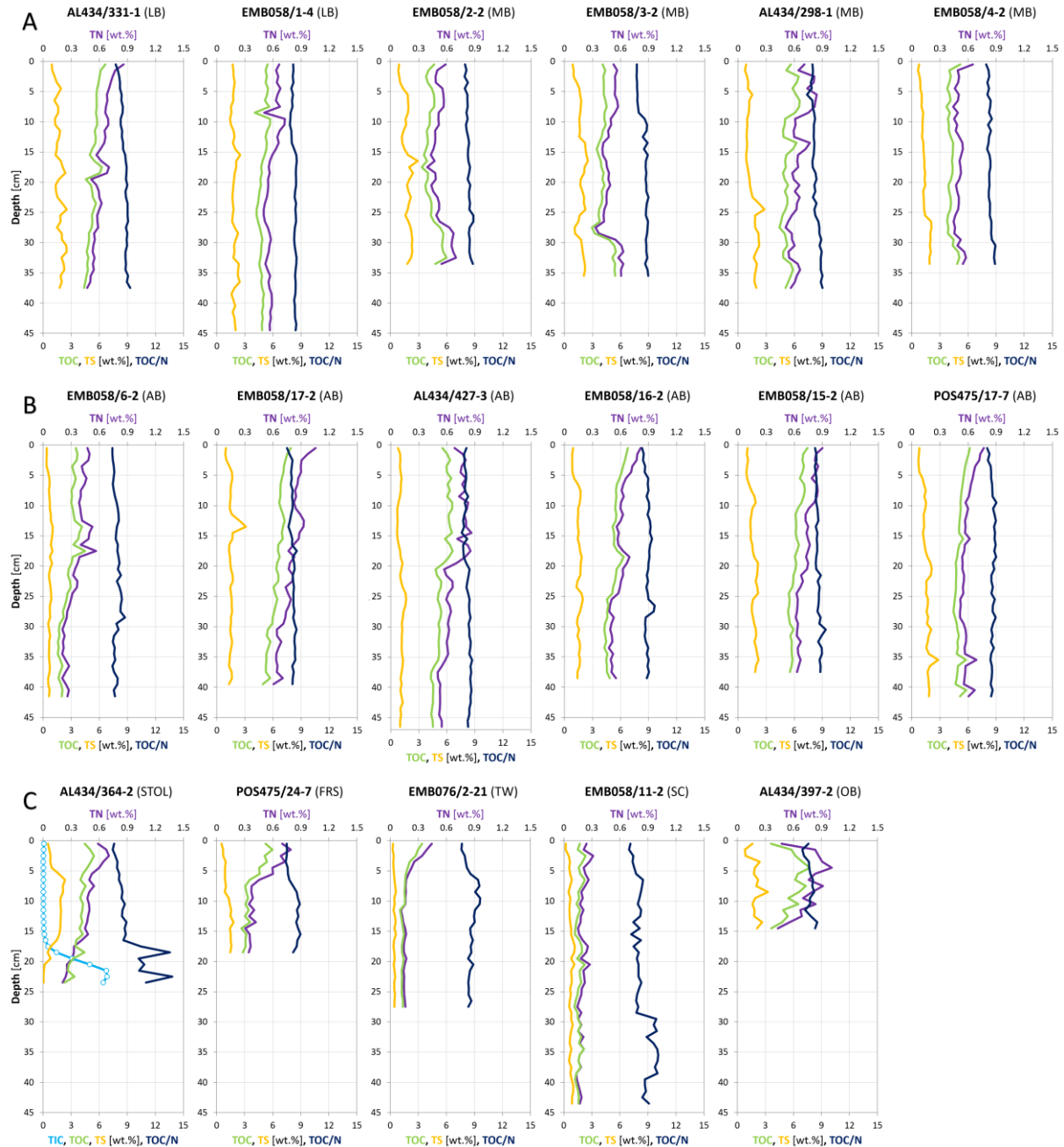


**Figure 3.4.** TS, TOC, TN, TOC/N and TIC profiles of the studied cores from the Mecklenburg Bight (A), the Arkona Basin (B) and the adjacent sandy areas (C), arranged from west (left) to east (right). AB: Arkona Basin, FRS: Falster-Rügen sand plain, LB: Lübeck Bay, MB: Mecklenburg Bight, OB: Oder Bank, SC: Sassnitz Channel, STOL: Stoltera, TW: Tromper Wiek. Notice the high correlation of TOC and TN as well as the strong increase of TIC in core AL434/364-2 below 15 cm sediment depth.

The TOC content, on the other hand, is high with an average surface sediment value of  $5.7 \pm 1.3$  wt.% in the basin muds and  $4.4 \pm 0.7$  wt.% in the fine fraction of the sandy areas (Fig. 3.4, 3.5). Only in the Tromper Wiek (EMB076/2-21), the adjacent Sassnitz Channel (EMB058/11-2) and the south-western edge of the Arkona Basin (EMB058/6-2), the TOC content in the fine fraction is lower with values between 1.73 and 3.49 wt.%. The TOC contents in the Arkona Basin are slightly higher than in the Mecklenburg Bight, but highest in the fine fraction of the fine sands on the Oder Bank. In general, the profiles show a gentle down-core decrease of up to 3 wt.% in the upper 40 cm. However, in the EMB058 cores 2-2, 3-2 and 4-2, the TOC content increases suddenly by 1.5-2.6 wt.% below 28 cm sediment depth. The upper 15 cm of the basin muds contain 2.02-2.38 kg/m<sup>2</sup> TOC, while the sands and silts contain 0.55-1.74 kg/m<sup>2</sup> (Tab. 3.1).

The TN content is highly correlated to TOC and the profiles run nearly parallel (Fig. 3.4). They also follow the sudden TOC increase of the EMB058 cores 2-2, 3-2 and 4-2. The average surface sediment value is  $0.72 \pm 0.16$  wt.% in the basin muds,  $0.59 \pm 0.09$  wt.% in the fine fraction of the sands and 0.24-0.47 wt.% in the fine fraction of the Tromper Wiek, the Sassnitz Channel and the south-western edge of the Arkona Basin (Fig. 3.6). The total TN inventory down to 15 cm sediment depth is 247.73-291.35 g/m<sup>2</sup> in the basin muds and 71.07-200.45 g/m<sup>2</sup> in the sandy areas (Tab. 3.1).

The TOC/N ratio at the surface of the basin muds is  $7.9 \pm 0.3$  and increases gently to maximal 9.6 in the upper 40 cm of sediment (Fig. 3.4, 3.7). The surface of the sands and silts has an average ratio of  $7.5 \pm 0.2$  that increases as well, but in a more irregular manner. In the cores POS475/24-7 from the Falster-Rügen sand plain and EMB076/2-21 from the Tromper Wiek, the TOC/N ratio is highest (9.0-9.6) between 5 and 15 cm and then slightly decreases again. In core AL434/364-2 from Stoltera, the TOC/N ratio increases suddenly from 8.6 to values between 10.2 and 13.8 below 17 cm sediment depth. And a similar sudden increase from 7.8 to values between 8.4 and 10.1 is visible in core EMB058/11-2 from the Sassnitz Channel below 29 cm sediment depth.

**Table 3.1.** Total anthropogenic induced inventories (per square metre) of  $^{137}\text{Cs}$  and Hg as well as the inventories of TOC, TN, TS and  $\text{bioSiO}_2$  in the upper 15 cm of sediment at stations in the Mecklenburg Bight (upper rows), the Arkona Basin (middle rows) and the adjacent sandy areas (lower rows), arranged from west (left) to east (right). FRS: Falster-Rügen sand plain, OB: Oder Bank, SC: Sassnitz Channel, STOL: Stoltera, TW: Tromper Wiek. Stations in close vicinity to the local hot spots are marked with an asterisk.

<b>Mecklenburg Bight</b>	<b>AL434/331-1*</b>	<b>EMB058/1-4</b>	<b>EMB058/2-2</b>	<b>EMB058/3-2</b>	<b>AL434/298-1</b>	<b>EMB058/4-2</b>
$^{137}\text{Cs}$ [kBq/m <sup>2</sup> ]		2.26	1.46	1.66		3.80
$\text{anthHg}$ [mg/m <sup>2</sup> ]	25.89	11.55	7.19	6.32	11.25	11.21
TOC [kg/m <sup>2</sup> /15cm]	2.24	2.10	2.38	2.29	2.02	2.24
TN [g/m <sup>2</sup> /15cm]	269.99	261.86	291.35	282.06	253.06	272.03
TS [kg/m <sup>2</sup> /15cm]	0.56	0.67	0.80	0.89	0.36	0.58
$\text{bioSiO}_2$		1.96	2.74	1.72		1.76
<b>Arkona Basin</b>	<b>EMB058/6-2</b>	<b>EMB058/17-2*</b>	<b>AL434/427-3</b>	<b>EMB058/16-2</b>	<b>EMB058/15-2</b>	<b>POS475/17-7</b>
$^{137}\text{Cs}$ [kBq/m <sup>2</sup> ]	5.59	5.52		2.78	4.36	
$\text{anthHg}$ [mg/m <sup>2</sup> ]	15.99	≥ 35.40	≥ 28.26	16.40	13.43	12.51
TOC [kg/m <sup>2</sup> /15cm]	2.09	2.26	2.20	2.20	2.30	2.29
TN [g/m <sup>2</sup> /15cm]	272.15	284.51	277.01	247.73	274.32	265.44
TS [kg/m <sup>2</sup> /15cm]	0.42	0.51	0.31	0.51	0.44	0.50
$\text{bioSiO}_2$	1.72	1.39		1.56	1.86	
<b>Sandy areas</b>	<b>AL434/364-2 (STOL)</b>	<b>POS475/24-7 (FRS)</b>	<b>EMB076/2-21 (TW)</b>	<b>EMB058/11-2 (SC)</b>	<b>AL434/397-2 (OB)</b>	
$\text{anthHg}$ [mg/m <sup>2</sup> ]	1.39	3.67	5.82	9.79	0.93	
TOC [kg/m <sup>2</sup> /15cm]	1.20	1.35	1.74	1.51	0.55	
TN [g/m <sup>2</sup> /15cm]	145.55	170.84	200.45	192.65	71.07	
TS [kg/m <sup>2</sup> /15cm]	0.45	0.34	0.46	0.55	0.17	
$\text{bioSiO}_2$				1.40		



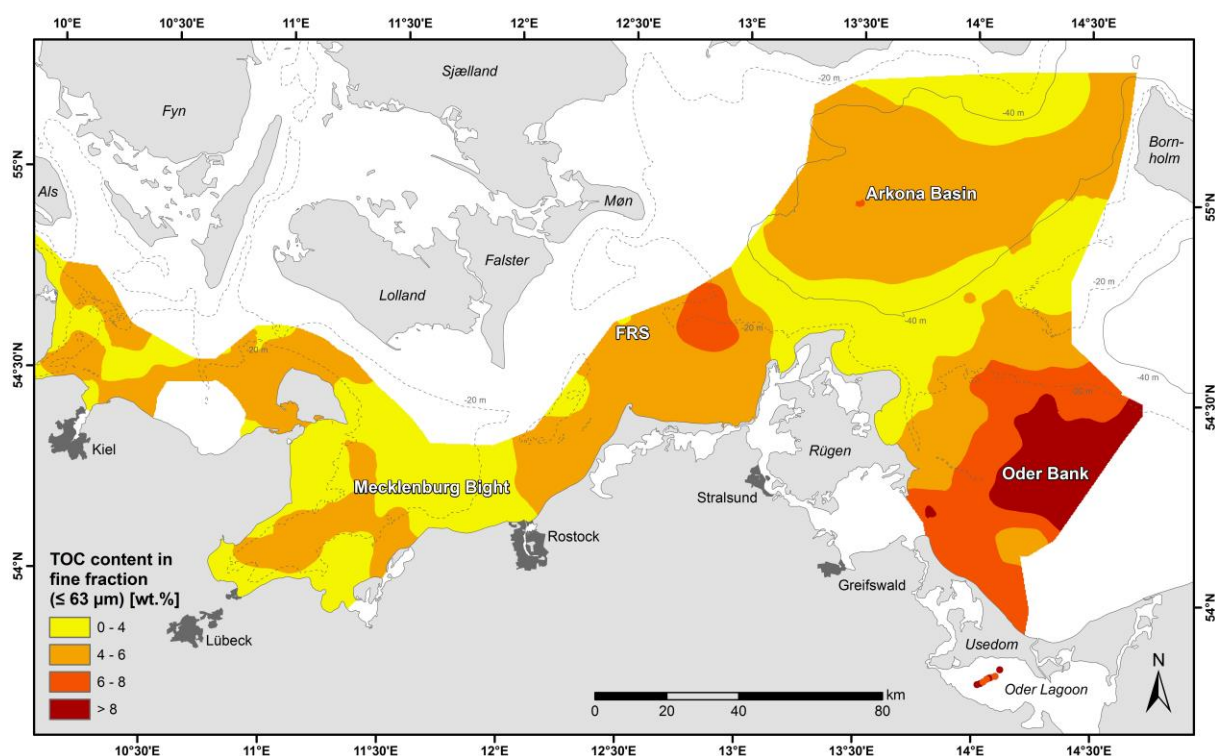


**Figure 3.5.** TOC content in the fine fraction ( $\leq 63 \mu\text{m}$ ) of the surface sediments (0-2 cm) in the German Baltic Sea area and the Arkona Basin. FRS: Falster-Rügen sand plain. Notice the high values on the Oder Bank and in the Oder Lagoon. Modified after [Leipe et al. \(2017\)](#).

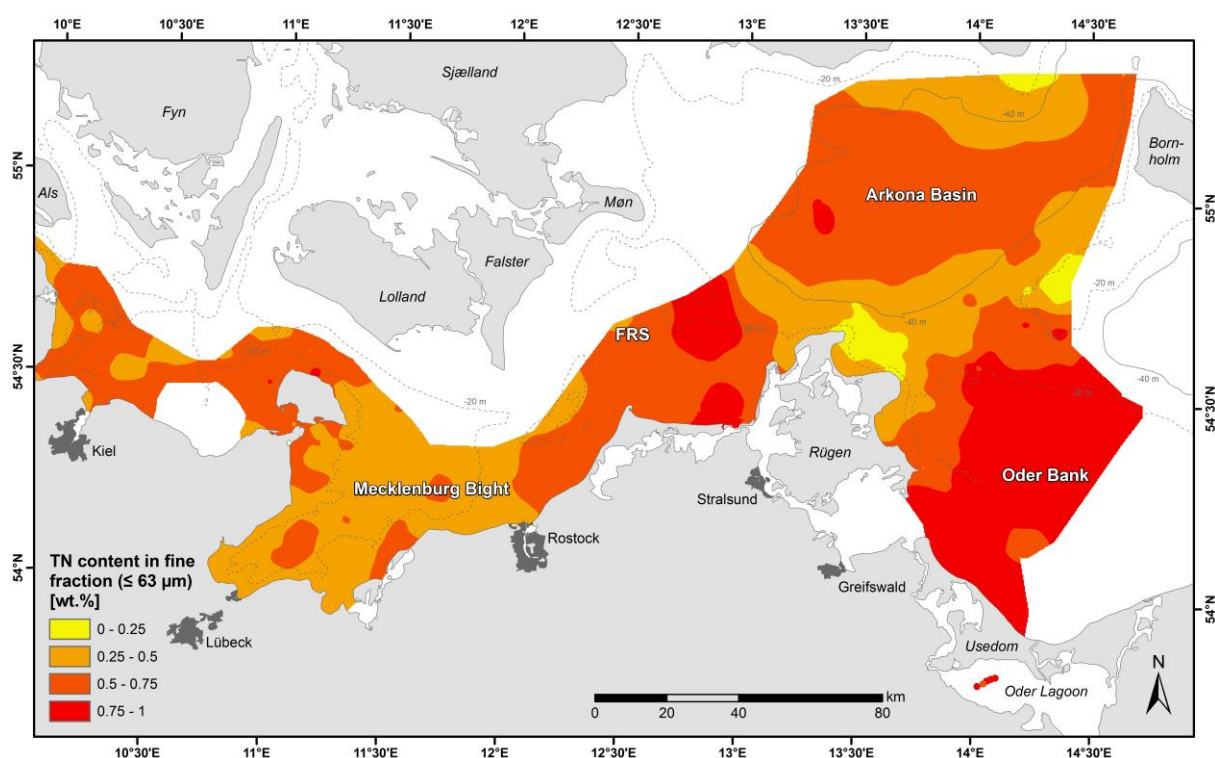


**Figure 3.6.** TN content in the fine fraction ( $\leq 63 \mu\text{m}$ ) of the surface sediments (0-2 cm) in the German Baltic Sea area and the Arkona Basin. FRS: Falster-Rügen sand plain. Notice the high values on the Oder Bank and in the Oder Lagoon. Published in the [Baltic Sea Atlas \(2014\)](#).

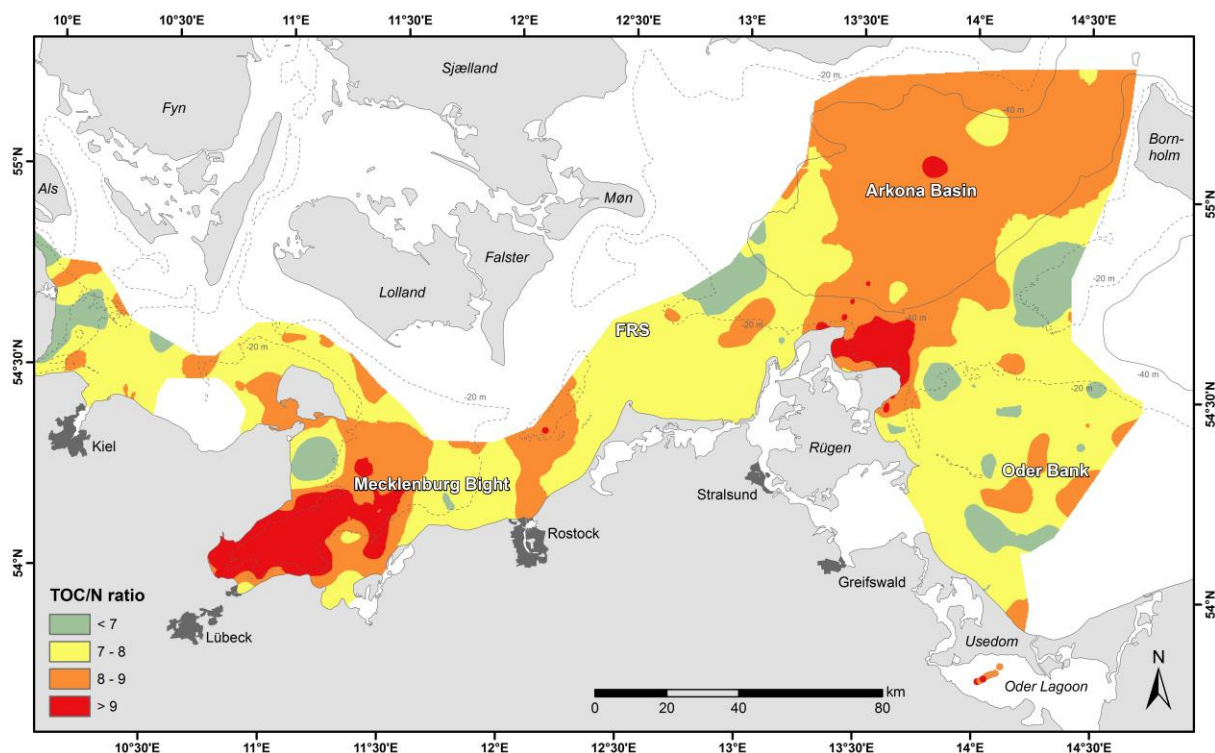


**Figure 3.7.** TOC/N ratio in the surface sediments (0-2 cm) of the German Baltic Sea area and the Arkona Basin. FRS: Falster-Rügen sand plain. Published in the [Baltic Sea Atlas \(2014\)](#).

### 3.2.3 Sulphur

The TS content in the basin muds has an average surface sediment value of  $0.90 \pm 0.28$  wt.% and increases to around 2 wt.% in the upper 40 cm of sediment ([Fig. 3.4](#)). In general, the strongest increase occurs until 5-9 cm, while there are also peaks in deeper sections of some cores. The values in the Arkona Basin are slightly lower than in the Mecklenburg Bight, especially in core EMB058/6-2 from the south-western edge of Arkona Basin with a maximum value of 0.95 wt.% at 14 cm sediment depth. The average surface value of the fine fraction in the fine sands is  $0.88 \pm 0.52$  wt.% and the TS content increases to maximal 3.28 wt.%. In the Sassnitz Channel (EMB05/11-2), the TS content in the fine fraction of the surface sediment is 0.23 wt.% and increases to  $0.75 \pm 0.20$  wt.%. In the Tromper Wiek (EMB076/2-21), the values fluctuate at  $0.44 \pm 0.09$  wt.%. The total TS inventory down to 15 cm sediment depth is 0.36-0.89 kg/m<sup>2</sup> in the muds of the Mecklenburg Bight, 0.31-0.51 kg/m<sup>2</sup> in the Arkona Basin muds and 0.17-0.55 kg/m<sup>2</sup> in the sandy areas ([Tab. 3.1](#)).

### 3.2.4 Phosphorus

The TP<sub>Ash</sub> content in core EMB058/2-2 from the Mecklenburg Bight is highest at the surface with a value of 0.15 wt.% and declines more or less exponentially to  $0.09 \pm 0.01$  wt.% with

increasing sediment depth (Fig. 3.8A). The values of  $TP_{Digest}$  follow the same trend of  $TP_{Ash}$ , but with lesser variation. The total  $TP_{Ash}$  inventory down to 15 cm sediment depth is  $54.70 \text{ g/m}^2$  (Tab. 3.2). In core EMB058/17-2 from the Arkona Basin (Fig. 3.8B), the  $TP_{Ash}$  content at the surface is with 0.29 wt.% higher than in the Mecklenburg Bight, but also decreases exponentially to 0.9 wt.% with increasing depth. The total  $TP_{Ash}$  inventory down to 15 cm sediment depth is  $37.80 \text{ g/m}^2$  (Tab. 3.2). In core EMB058/15-2 from the Arkona Basin (Fig. 3.8C), the  $TP_{Ash}$  content at the surface is with 0.34 wt.% similar to that at site 17-2, but the values strongly fluctuate until 20 cm sediment depth, where a maximum of 0.48 wt.% is reached. The content is also elevated between 6 and 13 cm, before it gently increases towards the maximum. Below that, the content decreases exponentially to 0.10 wt.%. The  $TP_{Digest}$  values follow the same trend and are slightly higher by an average of  $0.007 \pm 0.012 \text{ wt.}\%$ . The total  $TP_{Ash}$  inventory down to 15 cm depth is  $65.45 \text{ g/m}^2$  (Tab. 3.2). The SEM-EDX analysis of this core revealed many small particles of iron oxide rich in phosphorus at the surface, while less but larger particles of reduced iron phosphate (e.g. vivianite) were found in 20 cm depth resulting in the observed peaks of the TP content. Furthermore, a large amount of pyrite crystals as well as inert potash feldspar and titanium minerals were found at the same depth. In line with this is the iron content that has maxima at 9 and 20 cm sediment depth (Fig. 3.13).

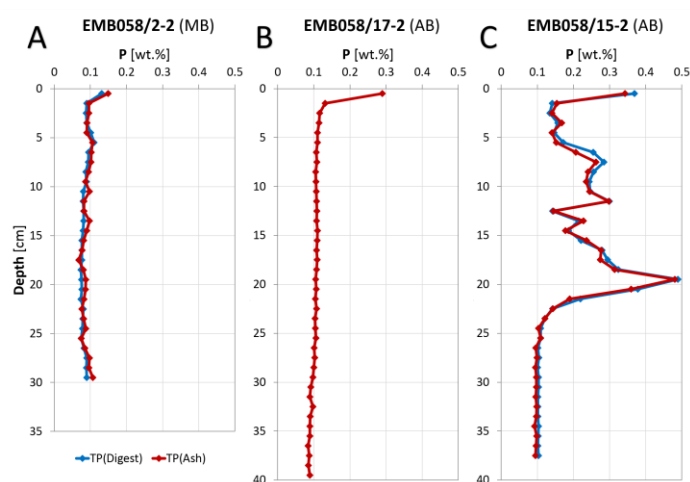


**Figure 3.8.**  $TP_{Digest}$  and  $TP_{Ash}$  profiles of the studied cores from the Mecklenburg Bight (A) and the Arkona Basin (B, C), arranged from west (left) to east (right). Notice the strong variation between the surface and the maximum at 20 cm sediment depth in core EMB058/15-2.

The geochemical maps confirm higher surface TP contents in the muds of the Arkona Basin than in the Mecklenburg Bight (Fig. 3.9), while the coarser sediments in general contain little phosphorus. Only the TP content in the fine fraction of the sands on the Oder Bank indicates a much higher relative proportion compared to the other areas (Fig. 3.10).



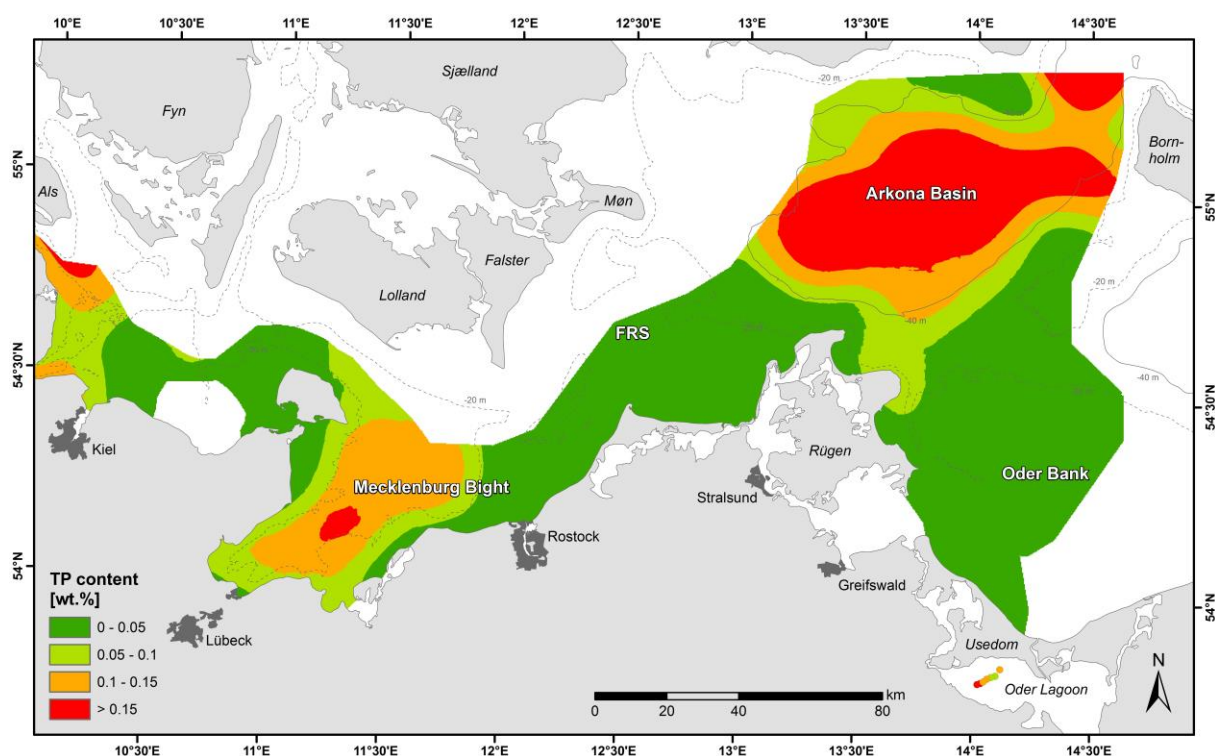


**Figure 3.9.** TP<sub>Ash</sub> content in the surface sediments (0-2 cm) of the German Baltic Sea area and the Arkona Basin. FRS: Falster-Rügen sand plain. Notice the high values in the basin muds as well as in the Oder Lagoon. Modified after [Leipe et al. \(2017\)](#).

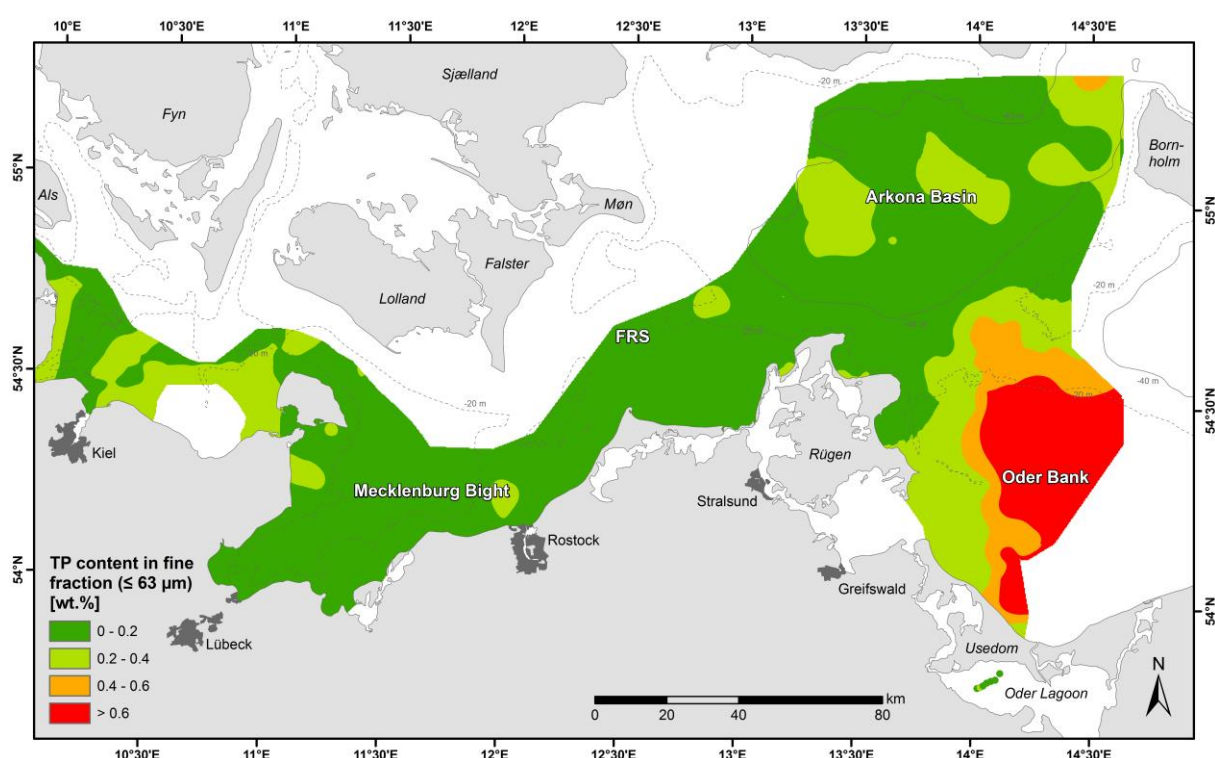


**Figure 3.10.** TP<sub>Ash</sub> content in the fine fraction ( $\leq 63 \mu\text{m}$ ) of the surface sediments (0-2 cm) in the German Baltic Sea area and the Arkona Basin. FRS: Falster-Rügen sand plain. Notice the high values on the Oder Bank. Modified after [Leipe et al. \(2017\)](#).

### 3.2.5 Biogenic silica

The  $\text{bioSiO}_2$  content is generally well correlated to TOC and the profiles run nearly parallel (Fig. 3.11). They also follow the sudden TOC increase of the EMB058 cores 2-2, 3-2 and 4-2. The average surface sediment value is  $3.9 \pm 0.5$  wt.% in the muds of the Mecklenburg Bight and  $5.3 \pm 0.9$  wt.% in the Arkona Basin, while the coarser sediments contain naturally less  $\text{bioSiO}_2$ . But the relative proportions in the fine fraction of the sands on the Oder Bank are again much higher compared to the other areas (Fig. 3.12). Most notable differences to TOC are two  $\text{bioSiO}_2$  peaks in the core EMB058/2-2, one at 11-15 cm sediment depth with up to 10.3 wt.% and a smaller one at 19-21 cm depth with up to 6.1 wt.%. The total  $\text{bioSiO}_2$  inventory down to 15 cm sediment depth is  $1.72\text{--}2.74$  kg/m<sup>2</sup> in the Mecklenburg Bight and  $1.39\text{--}1.86$  kg/m<sup>2</sup> in the Arkona Basin (Tab. 3.1).

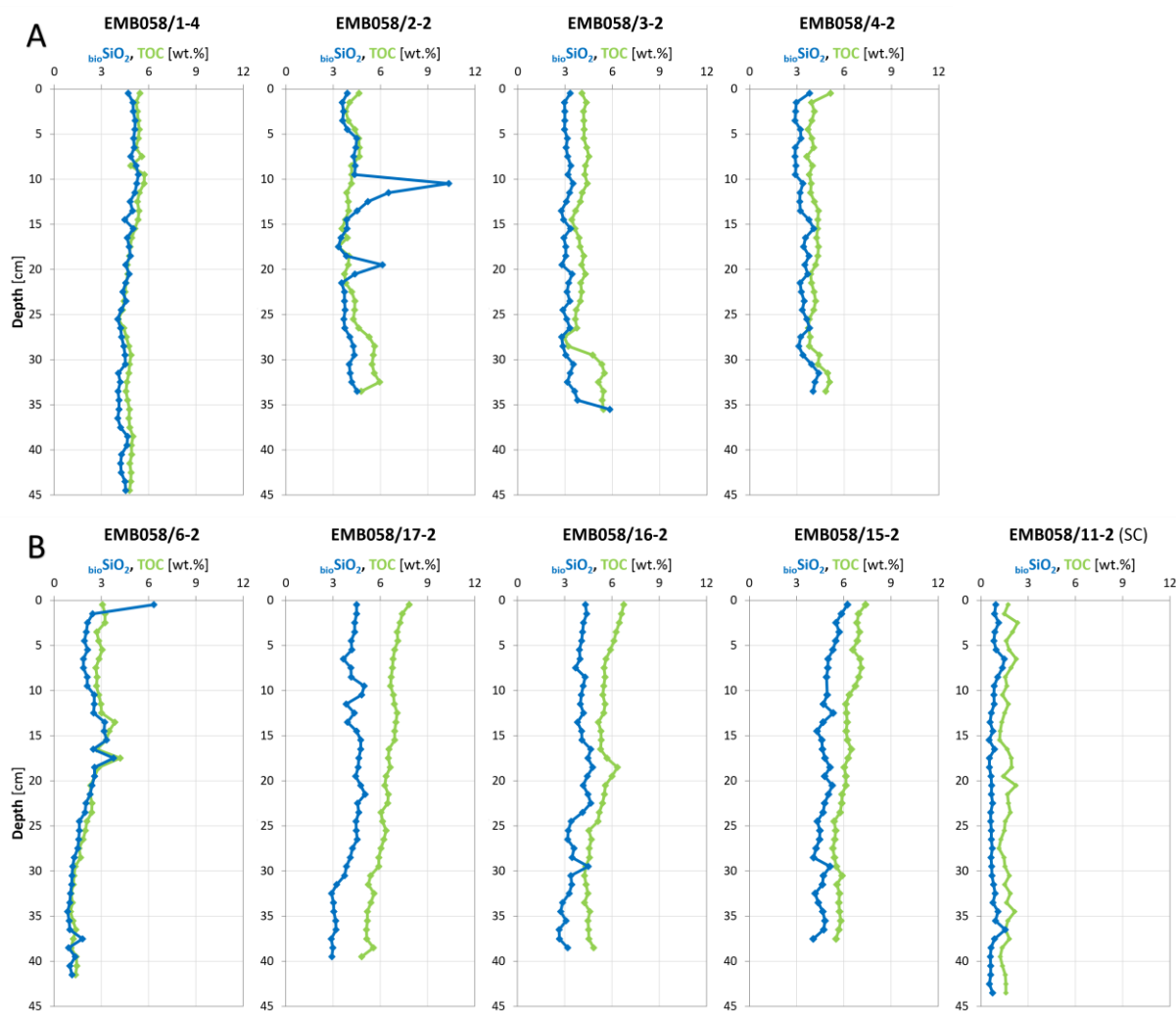


**Figure 3.11.**  $\text{bioSiO}_2$  and TOC profiles of the studied cores from the Mecklenburg Bight (A), the Arkona Basin (B) and the Sassnitz Channel (SC).

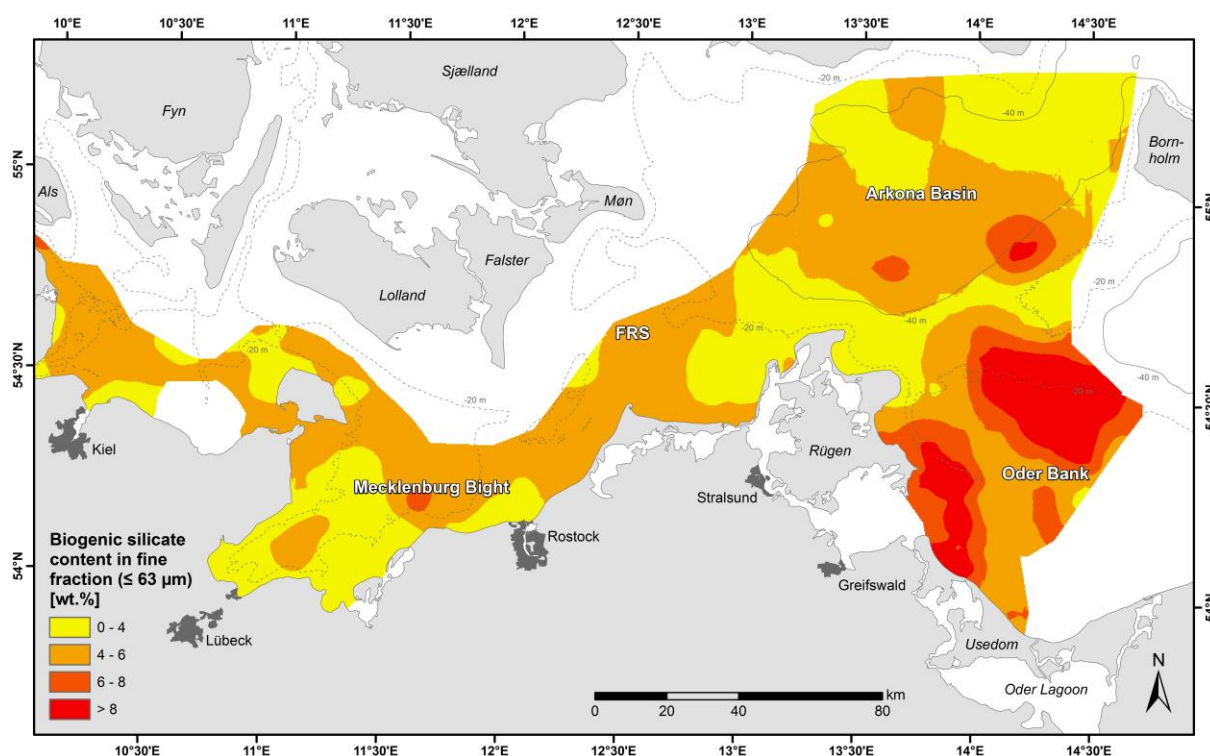


**Figure 3.12.**  $\text{bioSiO}_2$  content in the fine fraction ( $\leq 63 \mu\text{m}$ ) of the surface sediments (0-2 cm) in the German Baltic Sea area and the Arkona Basin. FRS: Falster-Rügen sand plain. Notice the high values on the Oder Bank. Published in the [Baltic Sea Atlas \(2014\)](#).

### 3.2.6 Aluminium, iron and heavy metals

The heavy metals Cd, Cu, Pb and Zn highly correlate with Hg in both analysed cores. In core EMB058/2-2 from the Mecklenburg Bight ([Fig. 3.13A](#)), all profiles show geogenic background values below 17 cm sediment depth (0.26 mg/kg dry weight Cd, 19.48 mg/kg dry weight Cu, 30.33 mg/kg dry weight Pb, 80.97 mg/kg dry weight Zn and 19.56  $\mu\text{g/kg}$  dry weight Hg), followed by a steep increase to the maxima at 6-10 cm (1.18 mg/kg dry weight Cd, 39.62 mg/kg dry weight Cu, 118.31 mg/kg dry weight Pb, 247.23 mg/kg dry weight Zn and 185.58  $\mu\text{g/kg}$  dry weight Hg) and a gentler decrease to the sediment surface (0.65 mg/kg dry weight Cd, 30.15 mg/kg dry weight Cu, 78.47 mg/kg dry weight Pb, 136.04 mg/kg dry weight Zn and 136.15  $\mu\text{g/kg}$  dry weight Hg). The total anthropogenic induced inventories are 29.20  $\text{mg/m}^2$  Cd, 0.65  $\text{g/m}^2$  Cu, 3.28  $\text{g/m}^2$  Pb, 5.67  $\text{g/m}^2$  Zn and 6.69  $\text{mg/m}^2$  Hg ([Tab. 3.1, 3.2](#)).

In core EMB058/15-2 from the Arkona Basin ([Fig. 3.13B](#)), all profiles show geogenic background values below 29 cm (0.24 mg/kg dry weight Cd, 33.47 mg/kg dry weight Cu, 43.54 mg/kg dry weight Pb, 105.79 mg/kg dry weight Zn and 30.74  $\mu\text{g/kg}$  dry weight Hg), followed by a sudden increase to a plateau with little to no decline towards the surface (0.74 mg/kg dry weight Cd, 47.99 mg/kg dry weight Cu, 107.25 mg/kg dry weight Pb,

186.45 mg/kg dry weight Zn and 260.17 µg/kg dry weight Hg). The total anthropogenic induced inventories are 11.90 mg/m<sup>2</sup> Cd, 0.40 g/m<sup>2</sup> Cu, 1.92 g/m<sup>2</sup> Pb, 2.26 g/m<sup>2</sup> Zn and 13.38 mg/m<sup>2</sup> Hg (Tab. 3.1, 3.2). The Al content stays relative stable at 5.25 wt.% in core EMB058/2-2 and 6.04 wt.% in core EMB058/15-2, thus running straight over the mentioned gradients with minor changes only (Fig. 3.13). The Fe content fluctuates a little bit more and lies at around 3.28 wt.% in core EMB058/2-2 and 4.22 wt.% in core EMB058/15-2. In the latter, the Fe profile shows maxima at 9 and 20 cm sediment depth.

Despite the high correlation between Hg and the other investigated heavy metals, there are some differences in their deposition patterns in the south-western Baltic Sea. While Hg, Cu, Pb and Zn naturally show higher contents in the basin muds than in the sandy areas, the hot spots do not always coincide. This is most noticeable with Cu that has a hot spot in the northern rather than in the eastern Arkona Basin, only a little one in the Lübeck Bay, and quite a few others, which are only visible in the fine fraction of the sandy areas (Fig. 3.14). Hot spots of Pb can be found at the same locations as those from Hg in the Lübeck Bay and the Arkona Basin (Fig. 3.15) and for Zn, only the one in the Lübeck Bay is recognisable (Fig. 3.16). Furthermore, all show higher relative proportions in the fine fraction of the fine sands in the Pomeranian Bight, but with different extent.

**Table 3.2.** Total anthropogenic induced inventories (per square metre) of Cd, Cu, Pb, ΣPCB and Zn as well as the inventories down to 15 cm sediment depth of TP<sub>Ash</sub> and ΣPAH at stations in the Mecklenburg Bight and the Arkona Basin, arranged from west (left) to east (right).

Inventory	Station	EMB058/1-4	EMB058/2-2	EMB058/6-2	EMB058/17-2	EMB058/15-2
<sup>anth</sup> Cd [mg/m <sup>2</sup> ]			29.20			11.90
<sup>anth</sup> Cu [g/m <sup>2</sup> ]			0.65			0.40
<sup>anth</sup> Pb [g/m <sup>2</sup> ]			3.28			1.92
<sup>anth</sup> Zn [g/m <sup>2</sup> ]			5.67			2.26
ΣPCB [mg/m <sup>2</sup> ]		1.16		1.08		
TP <sub>Ash</sub> [g/m <sup>2</sup> /15cm]			54.70		37.80	65.45
ΣPAH [mg/m <sup>2</sup> /15cm]		89.37		83.56		



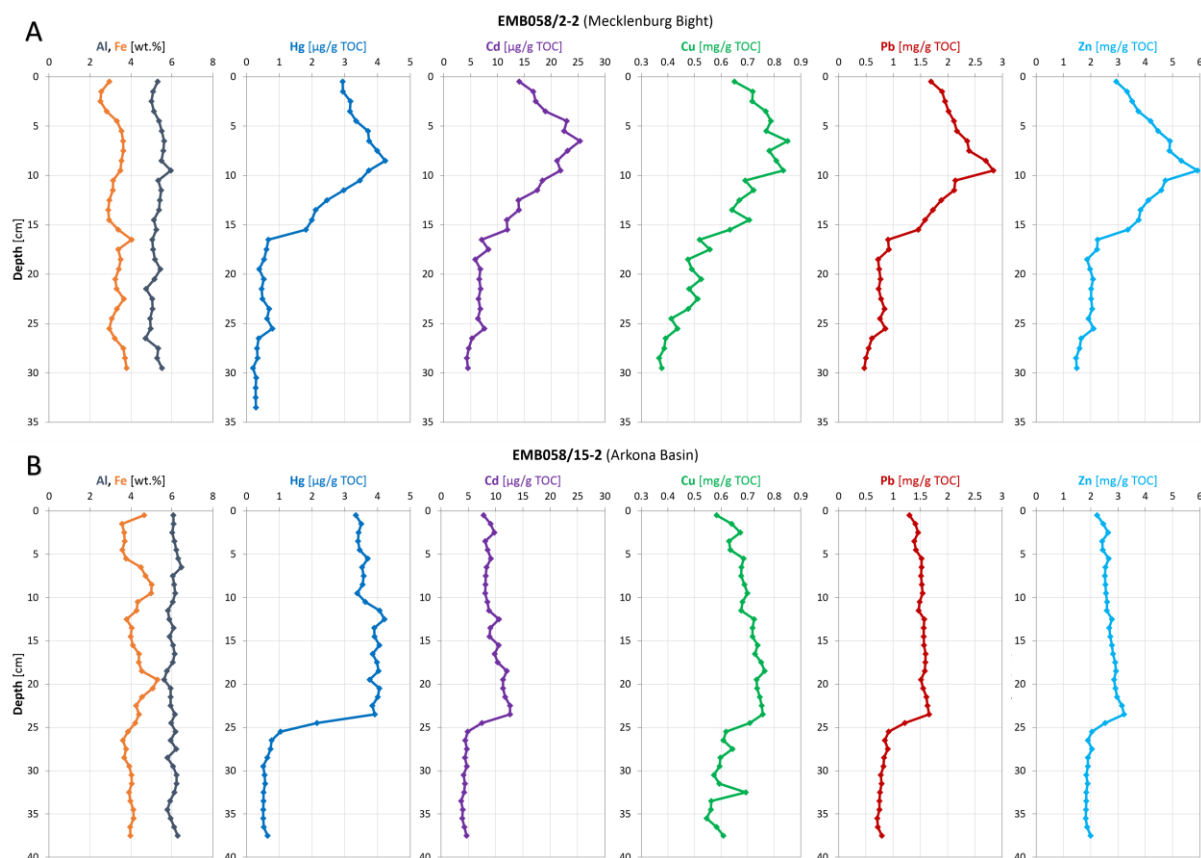


**Figure 3.13.** Al, Fe as well as TOC normalised Hg, Cd, Cu, Pb and Zn profiles of the EMB058 cores 2-2 from the Mecklenburg Bight (A) and 15-2 from the Arkona Basin (B).

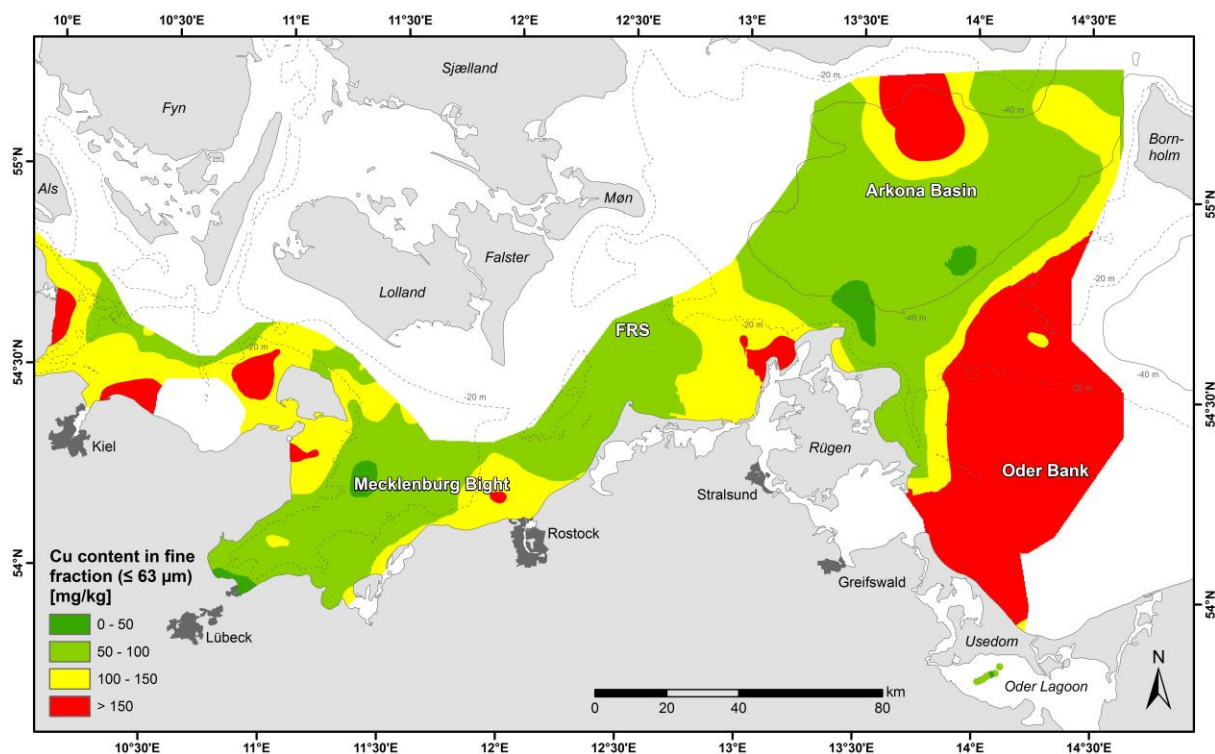


**Figure 3.14.** Cu content in the fine fraction ( $\leq 63 \mu\text{m}$ ) of the surface sediments (0-2 cm) in the German Baltic Sea area and the Arkona Basin. FRS: Falster-Rügen sand plain. Notice the high values on the Oder Bank. Published in the [Baltic Sea Atlas \(2014\)](#).

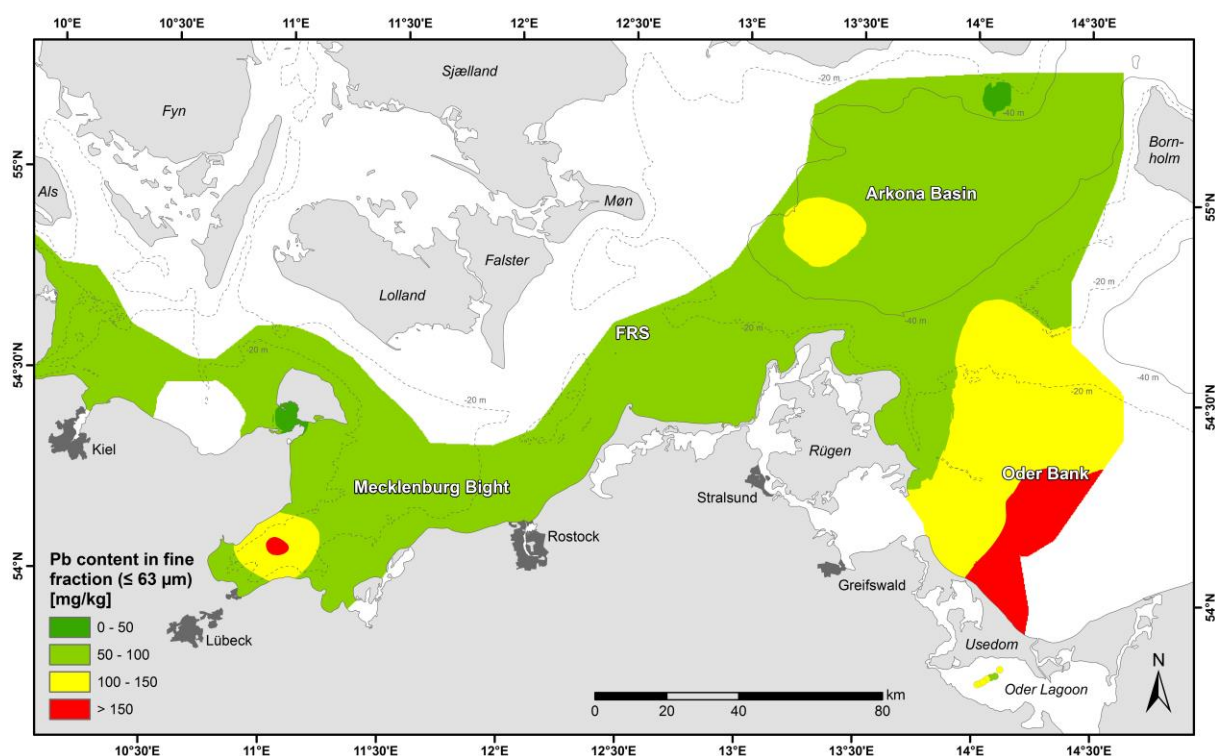


**Figure 3.15.** Pb content in the fine fraction ( $\leq 63 \mu\text{m}$ ) of the surface sediments (0-2 cm) in the German Baltic Sea area and the Arkona Basin. FRS: Falster-Rügen sand plain. Notice the hot spots of high contents in both basins as well as at the Oder mouth. Published in the [Baltic Sea Atlas \(2014\)](#).

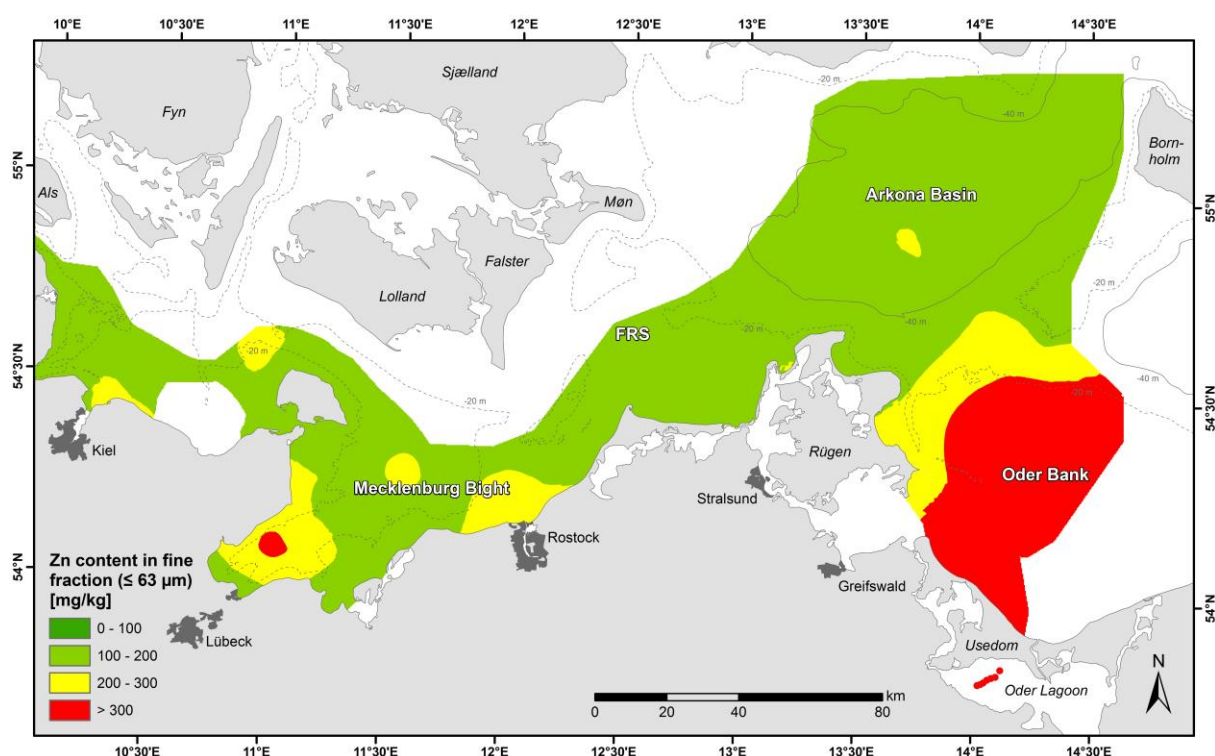


**Figure 3.16.** Zn content in the fine fraction ( $\leq 63 \mu\text{m}$ ) of the surface sediments (0-2 cm) in the German Baltic Sea area and the Arkona Basin. FRS: Falster-Rügen sand plain. Notice the hot spots of high contents in the Lübeck Bay as well as at the Oder mouth. Published in the [Baltic Sea Atlas \(2014\)](#).

### 3.2.7 Organic pollutants

The organic pollutants  $\Sigma$ PCB and  $\Sigma$ PAH also highly correlate with Hg in both analysed cores. In core EMB058/1-4 from the Lübeck Bay (Fig. 3.17A), all profiles show natural background values at around 30 cm sediment depth (no PCBs, 0.23  $\mu\text{g/g}$  dry weight  $\Sigma$ PAH and 27.06  $\mu\text{g/kg}$  dry weight Hg), followed by a varying increase to the maxima at 15 cm (30.16 ng/g dry weight  $\Sigma$ PCB, 2.86  $\mu\text{g/g}$  dry weight  $\Sigma$ PAH and 258.41  $\mu\text{g/kg}$  dry weight Hg) and a similarly varying decrease to the sediment surface (12.66 ng/g dry weight  $\Sigma$ PCB, 1.54  $\mu\text{g/g}$  dry weight  $\Sigma$ PAH and 157.16  $\mu\text{g/kg}$  dry weight Hg). The total anthropogenic induced inventories are 1.16  $\text{mg/m}^2$   $\Sigma$ PCB, 129.84  $\text{mg/m}^2$   $\Sigma$ PAH and 10.98  $\text{mg/m}^2$  Hg (Tab. 3.1, 3.2). The total inventories until 15 cm depth are 0.79  $\text{mg/m}^2$   $\Sigma$ PCB and 80.45  $\text{mg/m}^2$   $\Sigma$ PAH.

In core EMB058/6-2 from the south-western edge of the Arkona Basin, the 30 cm long profiles of  $\Sigma$ PCB and  $\Sigma$ PAH do not reach the natural background that the Hg profile shows below 35 cm (Fig. 3.1B, 3.17A). The maximum lies between 19 and 24 cm (15.74 ng/g dry weight  $\Sigma$ PCB, 2.38  $\mu\text{g/g}$  dry weight  $\Sigma$ PAH and 157.89  $\mu\text{g/kg}$  dry weight Hg) and a second lower one between 9 and 13 cm (13.41 ng/g dry weight  $\Sigma$ PCB, 1.74  $\mu\text{g/g}$  dry weight  $\Sigma$ PAH and 124.32  $\mu\text{g/kg}$  dry weight Hg). The  $\Sigma$ PAH profile shows another peak at 4 cm, while  $\Sigma$ PCB and Hg have a local minimum at that depth. In general, all profiles decrease from the overall maximum to the sediment surface (5.10 ng/g dry weight  $\Sigma$ PCB, 0.83  $\mu\text{g/g}$  dry weight  $\Sigma$ PAH and 92.62  $\mu\text{g/kg}$  dry weight Hg). The total inventories down to 15 cm depth are 0.50  $\text{mg/m}^2$   $\Sigma$ PCB and 94.10  $\text{mg/m}^2$   $\Sigma$ PAH (Tab. 3.2).

Organotin compounds were found in all surface sediment samples (Fig. 3.17C) and down to 20 cm depth in core EMB058/6-2 (Fig. 3.17B). In the Mecklenburg Bight, their content is dominated by DBT and is higher than in the Arkona Basin, where MBT dominates. At 15 cm depth lies the maximum and in general, the values are decreasing towards the surface. Only at the local maximum of  $\Sigma$ PCB and  $\Sigma$ PAH at 9 cm depth, the organotin compounds are slightly higher again.

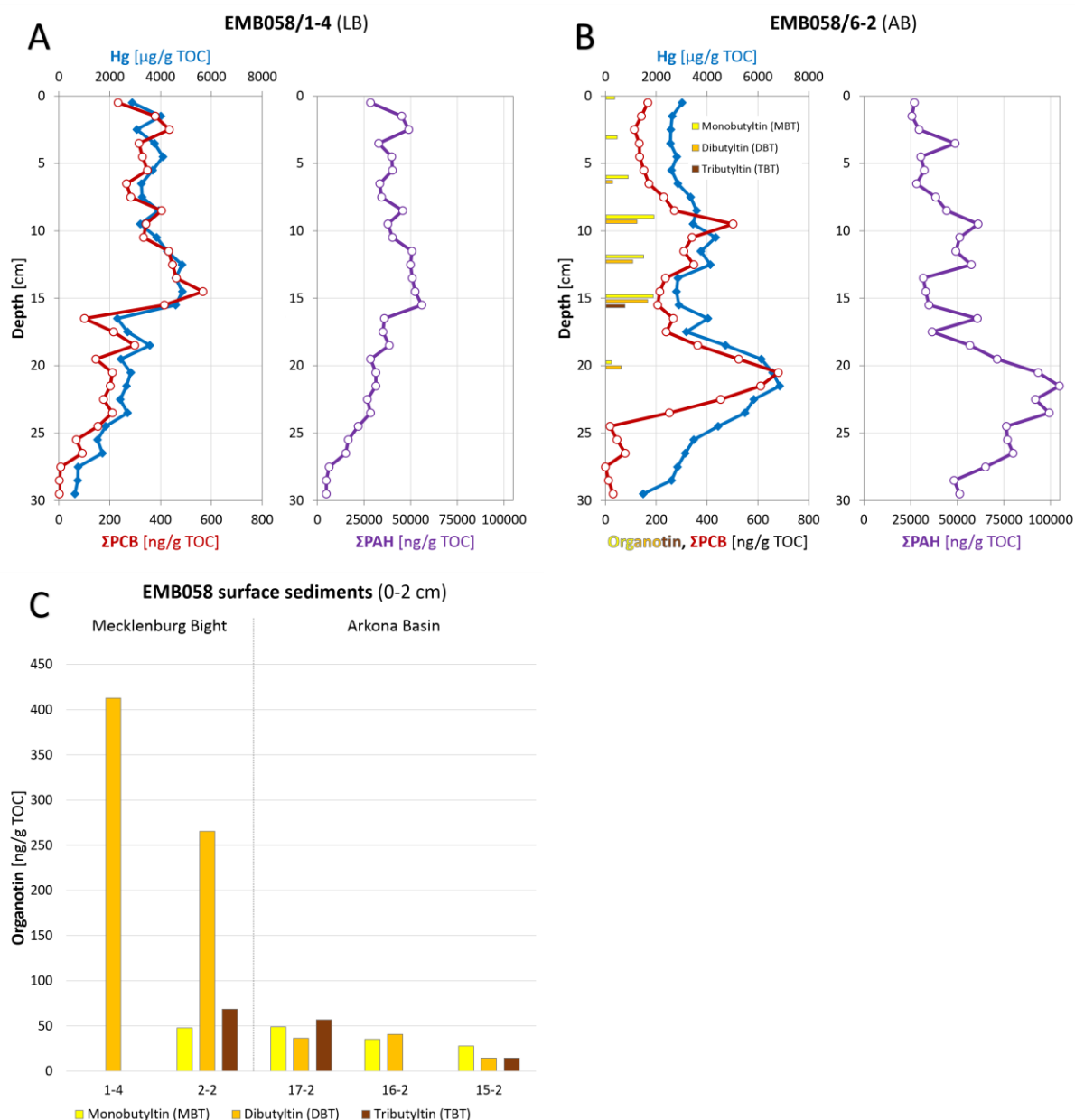


**Figure 3.17.** TOC normalised Hg,  $\Sigma\text{PCB}$  and  $\Sigma\text{PAH}$  profiles of core EMB058/1-4 from the Lübeck Bay (A) and of core EMB058/6-2 from the south-western edge of the Arkona Basin (B) compared to TOC normalised organotin compounds in core EMB058/6-2 (B) and in surface sediments (C). Organotin data from [Abraham et al. \(2017\)](#).

### 3.3 Sedimentary fabric

The negative X-radiographs show density differences within the sediment with brighter parts representing denser material. Deeper buried and thus compacted sediments are generally denser than surface sediments due to smaller contents in water and organic material. Also coarse sediments are denser than fine sediments.

In the cores POS475/54-1 and 57-10 from the Mecklenburg Bight ([Fig. 4.1](#)), areas of laminated to thin-bedded, sometimes bright-to-dark (upward) graded layers alternate with diffuse



mottled areas. The latter are sporadically interspersed with subhorizontal, tubular structures of darker material with or without bright linings (tube wall). Occasionally, discordant surfaces (angular unconformities) are recognisable in both cores.

In contrast, the cores POS475/17-7, 19-2 and 22-1 from the Arkona Basin are nearly entirely mottled with fewer tubular structures ([Fig. 4.2](#)). Sporadically, convex laminated structures up to 3 cm in width are visible. Only in the cores POS475/17-7 and 19-2, a few graded layers and discordant surfaces appear. Moreover, the density suddenly increases at around 16 cm sediment depth in core POS475/19-2 from the south-western edge of the Arkona Basin, indicating a change to coarser material.



## 4 Discussion

### 4.1 Sediment mixing

The profiles of the various pollutants, especially the comparison of Hg and  $^{137}\text{Cs}$ , reveal a strong sediment mixing down to a depth of approx. 25 cm (Fig. 3.1, 3.13, 3.17). Instead of expected sharp  $^{137}\text{Cs}$  peaks and characteristic Hg profiles, the data often show blurred signals that in some cases correlate, indicating a disturbance of these stratigraphic signals. An event pulse, e.g., the  $^{137}\text{Cs}$  fallout succeeding the Chernobyl accident in 1986, deposited at a site with random sedimentation rate and no mixing is buried progressively deeper in the sediment in its original shape and concentration, if no decay processes apply (Fig. 4.1A; Johannessen and Macdonald, 2012). The same pulse, deposited at a site with the same sedimentation rate and additional continuous mixing, is immediately mixed downward and its peak concentration gets reduced, so that the inventory is preserved (decay dependent). After one year, the pulse is unevenly distributed throughout the mixed sediment layer (top profile in Fig. 4.1B). After ten years, the pulse has become more evenly distributed with a slight decline near the sediment surface due to subsequent deposition of less or unpolluted material (centre profile in Fig. 4.1B). With progressing time, the pulse concentration gently increases downwards to a maximum, followed by a strong decrease to pre-depositional values (bottom profile in Fig. 4.1B). An additional recent in-depth mixing event causes an even distribution throughout the affected layer with no decline towards the sediment surface (Fig. 4.1C). The mixing-induced distribution proposes a higher sedimentation rate and prevents a direct relation of a certain depth to a specific time (Johannessen and Macdonald, 2012). Changes over time in the pollution input, the mixing intensity and the sedimentation rate as well as erosional events deform the distribution profile even more. Hence, such profiles are not suitable for a reliable age determination and the calculation of mass accumulation rates. Nevertheless, the general pollution trends and probably the relative timing of different pollution events can be obtained, if there was enough time for an event pulse to pass the mixed layer before another one is deposited. Furthermore, it is still possible to calculate a maximal sedimentation rate along with the actual inventories of natural and artificial material (Johannessen and Macdonald, 2012). In particular, the heavy metal (Fig. 3.1; 3.13), organic pollutant (Fig. 3.17) and artificial radionuclide (Fig. 3.1) profiles down to 30-40 cm allow a distinct separation of geogenic pre-industrial background values from the anthropogenic impact during the last 100-150 years. TOC and sediment-clastic proxies like grain size distribution and Al run straight over the shown

gradients in the core profiles without changes. This indicates no significant change in the basic sedimentation regime over the observed period. Only the mentioned coarsening below 20 cm in core EMB058/6-2 (Sect. 3.1) or below 16 cm in core POS475/19-2 (Sect. 3.3) points to more energetic conditions at the south-western edge of the Arkona Basin in the past. In contrast, the fining below 17 cm in core AL434/364-2 (Sect. 3.1) indicates calmer conditions at Stoltera just east of the Mecklenburg Bight basin in the past.

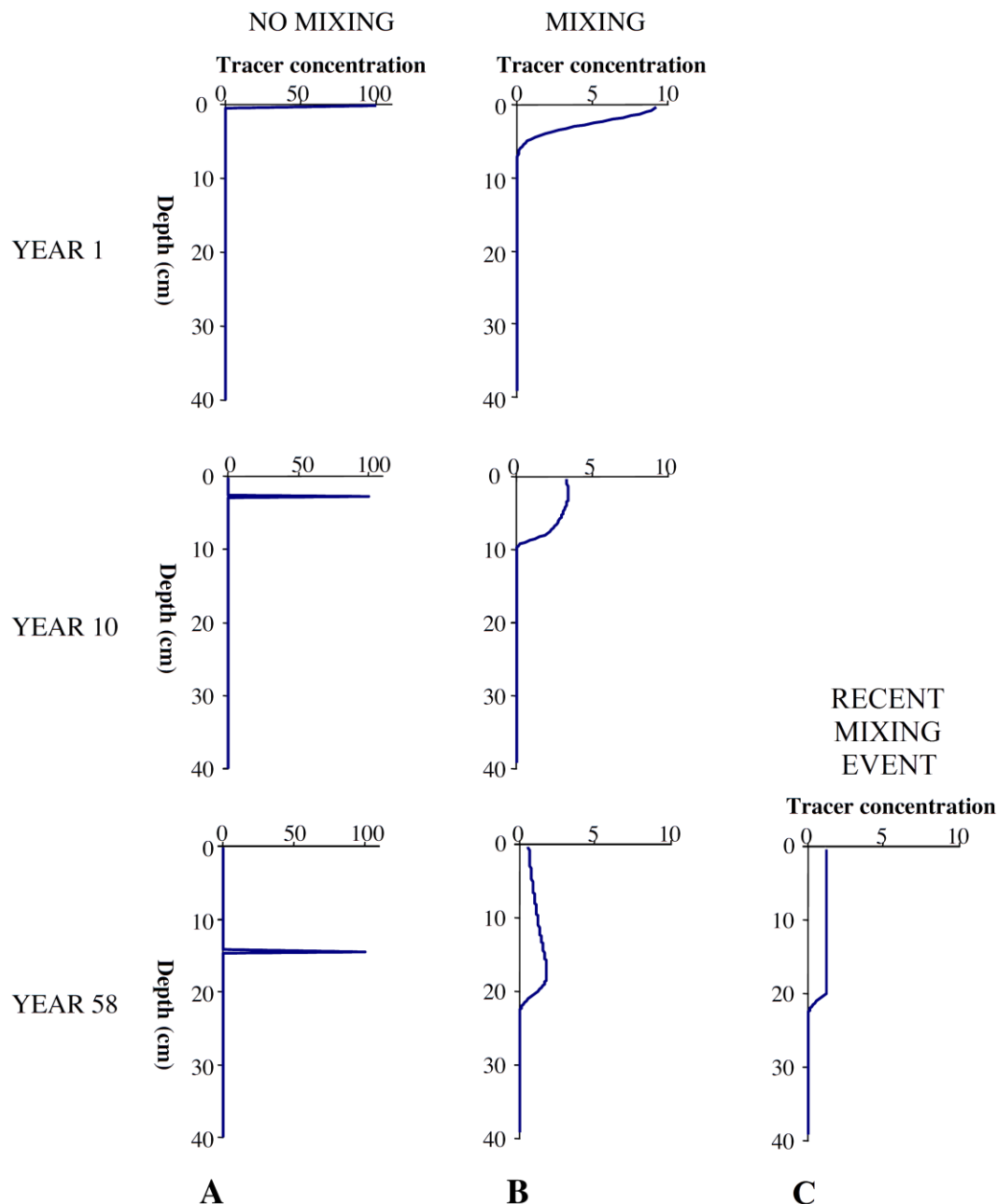


**Figure 4.1.** Theoretical tracer profiles of a single, one-year pulse recorded in sediment cores with constant sedimentation rate (0.25 cm/a) and (A) no mixing, (B) a mixing rate of 3 cm<sup>2</sup>/a down to 7 cm and (C) an additional recent mixing event down to 20 cm. Within the first year, the tracer is distributed throughout the mixed layer and after 58 years, the tracer distribution bears little resemblance to the original pulse. The penetration depth in the mixed cores is greater than in the core without mixing, while the peak concentration is much lower. Modified after Johannessen and Macdonald (2012).

In the following sections, the different mixing processes that are affecting the sediments in the south-western Baltic Sea will be discussed, distinguishing between biogenic, hydrodynamic and anthropogenic impact.

#### 4.1.1 Bioturbation: biogenic mixing

According to [Kristensen et al. \(2012\)](#), faunal bioturbation in aquatic environments is defined as all transport processes carried out by animals that directly or indirectly affect sediment matrices, mainly through foraging and construction of burrows, and including both particle reworking (displacement or biomixing of particles) and burrow ventilation (displacement or bioirrigation of water). Biomixing occurs either locally by frequent and random particle displacements over short distances (analogous to diffusion), or non-locally (advective) over longer distances in discrete steps ([Boudreau, 1986a, 1986b](#); [Boudreau and Imboden, 1987](#)). The same also applies to bioirrigation ([Shull et al., 2009](#)), but is not further investigated within this study, although it is clear that moving water can also move particles and vice versa ([Kristensen et al., 2012](#)). Local biomixing is caused by so called biodiffusors and occurs mainly within the uppermost sediment layer and disturbs or completely erases pre-existing structures. This leads to a more or less homogeneous sedimentary fabric ([Wetzel, 1981](#)). Non-local biomixing is caused by infaunal macro-organisms, e.g. upward and downward conveyors that transport sediment from deeper horizons to the surface or vice versa. This process can leave traces and structures, according to the living and feeding behaviour of macro organisms.

The diffuse mottled areas in the negative X-radiographs ([Fig. 4.2, 4.3](#)) indicate that the basin muds are locally biomixed by indistinct background burrow-mottling of benthic organisms with sporadic discrete tubular structures or burrows ([Virtasalo et al., 2011](#)), probably indicating non-local biomixing. The archetypal *Cruziana* [d'Orbigny, 1842](#) ichnofacies predominates, with various subsurface and/or surface deposit-feeding structures ([Tab. 4.1](#)).

*Arenicolites*, *Palaeophycus*, *Planolites*, *Rhizocorallium* and *Skolithos* are produced by worm-like organisms (e.g. polychaetes), while bivalves produce the observed convex laminated structures (bivalve biodeformation) and plow-sole traces ([Keighley and Pickerill, 1995](#); [Knaust, 2013](#); [Pemberton and Frey, 1982](#); [Schlirf and Uchman, 2005](#); [Virtasalo et al., 2011](#); [Werner, 2002](#); [Werner et al., 1987](#); [Winn, 2006](#)).

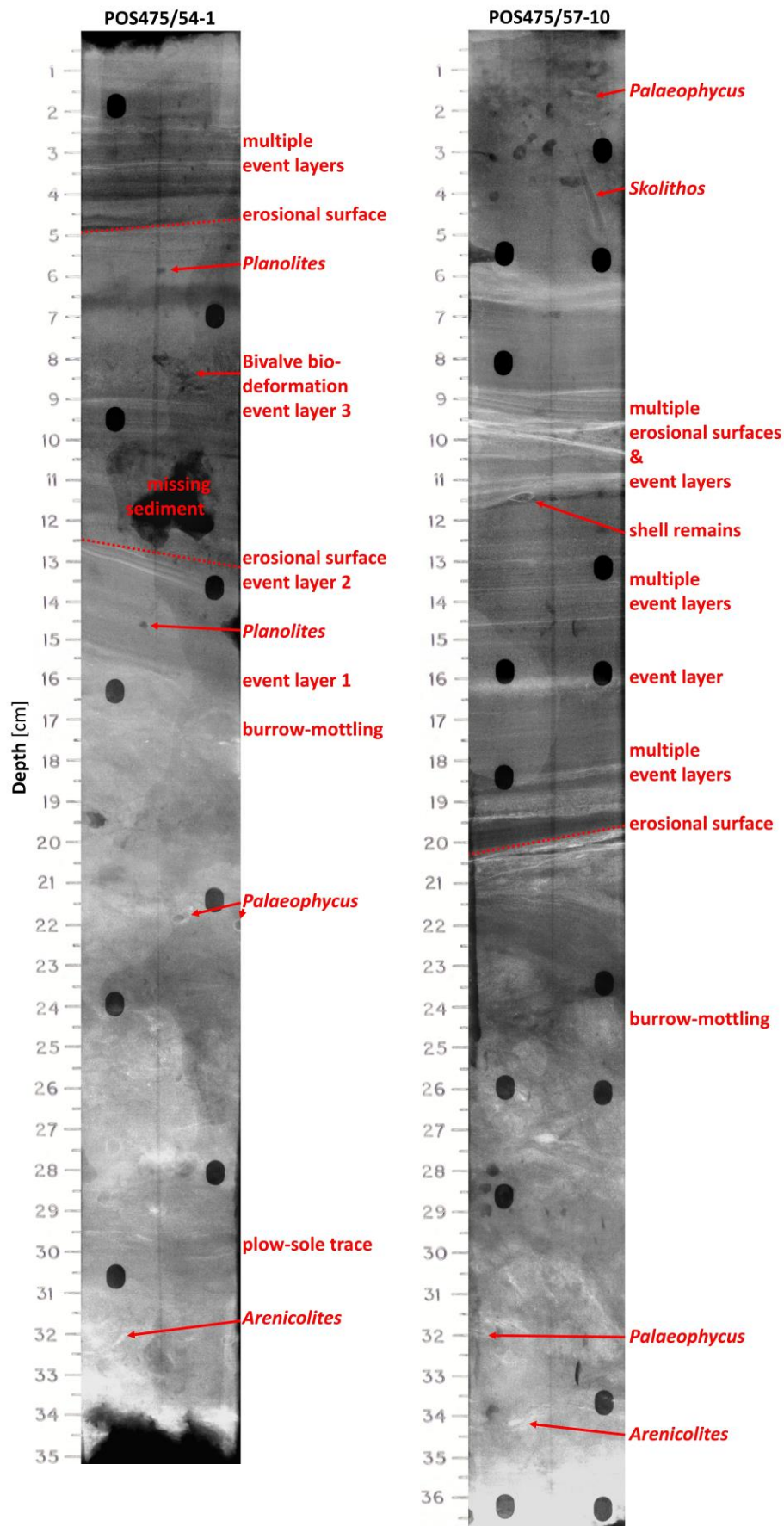


**Figure 4.2.** Negative X-radiographs of the cores POS475/54-1 and 57-10 from the Mecklenburg Bight with interpreted sedimentary structures, arranged from west (left) to east (right). The dark ovals are holes in the sample box and the straight vertical lines are gaps in the surrounding tape.

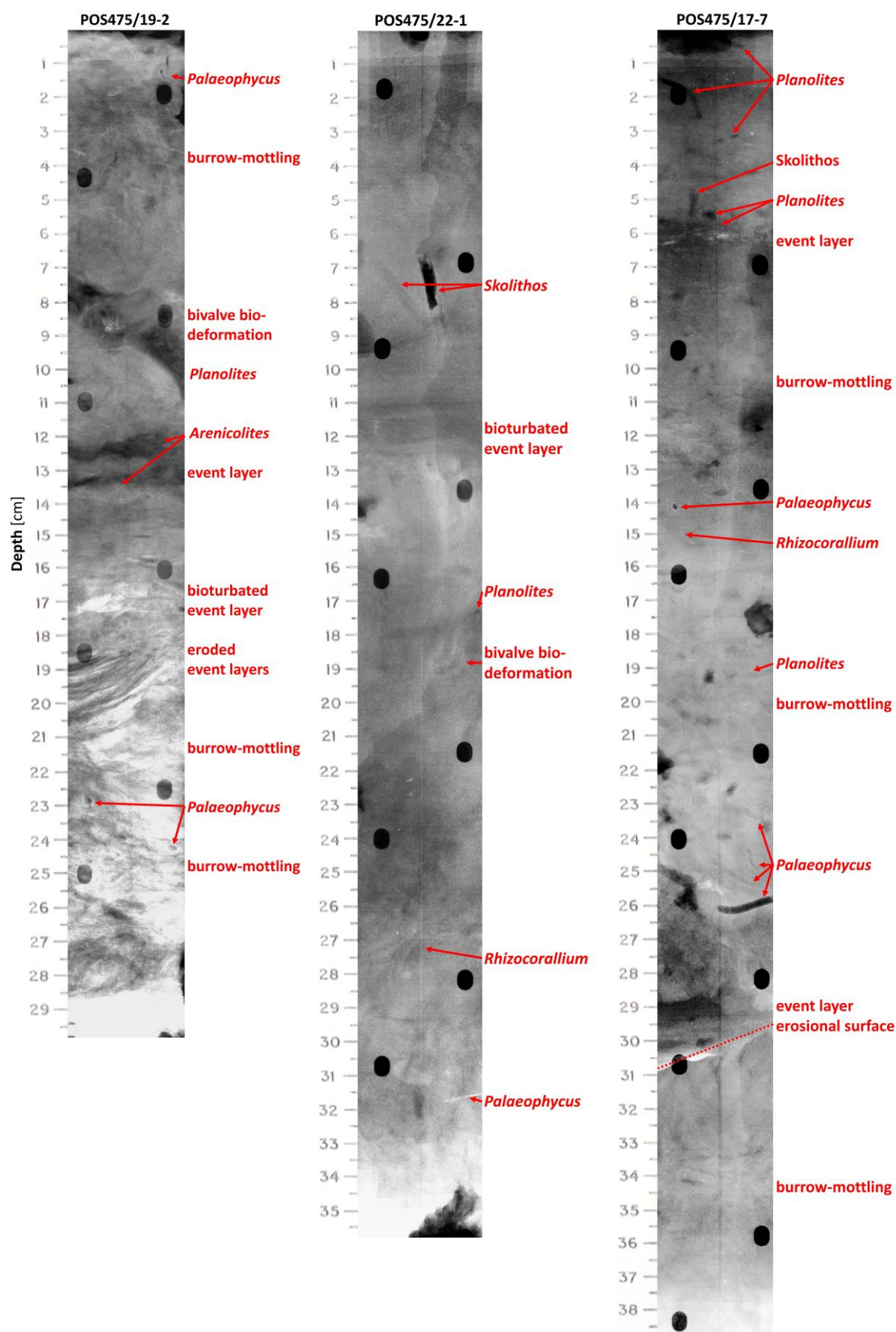


**Figure 4.3.** Negative X-radiographs of the cores POS475/17-7, 19-2 and 22-1 from the Arkona Basin with interpreted sedimentary structures, arranged from west (left) to east (right). The dark ovals are holes in the sample box and the straight vertical lines are gaps in the surrounding tape.



**Table 4.1.** Ichnogenera and other bioturbation structures identified in the studied cores. Modified after Virtasalo et al. (2011).

Bioturbation structure	Description and ethology
<i>Arenicolites</i> Salter, 1857	Weakly lined, flat U-shaped burrows generally less than 3 mm in diameter with less dense (darker) fill than the sediment matrix in the negative X-radiographs. The traces represent reinforced domiciles of surface or subsurface deposit-feeding worm-like organisms (Schlirf and Uchman, 2005).
Bivalve biodeformation	Structures of variably-oriented convex lamination up to 3 cm in width. These structures are formed by bivalves such as <i>Limecola balthica</i> while burrowing, turning and adjusting their position in the sediment (Werner, 2002; Winn, 2006).
<i>Palaeophycus</i> Hall, 1847	Lined, sub-horizontal, straight or gently curved tubular structures < 3 mm in diameter. The burrows occasionally branch. The traces are produced by subsurface or surface deposit-feeding worm-like organisms (Keighley and Pickerill, 1995; Pemberton and Frey, 1982).
<i>Planolites</i> Nicholson, 1872	Sub-horizontal, cylindrical, gently curved, tubular structures < 3 mm in diameter with sharp margins but no distinct wall. The burrows occasionally branch. Their fill is generally less dense (darker) than the sediment matrix in the negative X-radiographs. The traces are produced by deposit-feeding or carnivorous worm-like organisms (Keighley and Pickerill, 1995; Pemberton and Frey, 1982).
Plough-sole trace	A thin, fining upward layer produced by a bivalve burrowing (or “ploughing”) along the sediment surface. The bivalve moves by using its downward protruding foot with the support of pumping motions of its shell, leaving behind a furrow. The movement may lead to a liquefaction of the furrow walls, resulting in a gravitative grain size differentiation and settling, producing a thin, graded layer with a sharp base. Subsequent hydrodynamic events may result in the rapid passive filling of the furrow (Werner, 2002; Werner et al., 1987).
<i>Rhizocorallium commune</i> Schmid, 1876	Sub-horizontal, U-shaped marginal tubes with more or less parallel limbs (or arms) and an actively filled spreite between them. The traces are most likely produced by suspension or deposit-feeding worm-like organisms (Knaust, 2013).
<i>Skolithos</i> Haldeman, 1840	Steeply oriented to inclined, non-branching, straight to slightly curved tubular burrows with a thick wall lining. They are dwelling burrows of suspension or surface deposit-feeding worm-like organisms (Schlirf and Uchman, 2005).

This agrees with recent macrozoobenthic studies in the area (Gogina et al., 2017; Morys et al., 2017; Schiele et al., 2015; Zwicker, 2014), suggesting that the western Baltic Sea basins are mainly populated and bioturbated by infaunal bivalves (e.g. *Abra alba*, *Arctica islandica*, *Kurtiella bidentata*, *Limecola balthica*), the crustacean *Diastylis rathkei* as well as polychaetes like *Capitella capitata*, *Nephtys hombergii* and *Scoloplos armiger*. Furthermore, Morys et al.



(2017, 2016) did parallel photometric measurements of the natural particle tracer chlorophyll  $\alpha$ , which is thought to behave like sediment particles and track the mixing of fresh organic matter (Maire et al., 2008). Based on exponentially decreasing chlorophyll  $\alpha$  concentrations and macrozoobenthos abundances, the authors found a dominance of surficial biodiffusers in the Mecklenburg Bight. In the Arkona Basin, the depth distribution of chlorophyll  $\alpha$  (subsurface maxima) and organisms (most importantly bivalves and polychaetes) indicate a dominance non-local mixing. The resulting mixing depths range between  $5.2 \pm 1.7$  and  $7.1 \pm 1.6$  cm (Morys et al., 2016), matching the strongest increase of TS content in the top 5–9 cm in most cores. This points to decreasing oxygen supply down to this depth, counteracting the diagenetic formation of pyrite (Fig. 3.4).

The ongoing bioturbation is responsible for the slight perturbations of the geochemical profiles described above (blurring of maxima), which still allows a recognition of the relative timing of events (offset between Hg and  $^{137}\text{Cs}$ ) and associated trends in most cores (Fig. 3.1).

#### 4.1.2 Hydroturbation: hydrodynamic mixing

Hydroturbation refers to all sediment mixing and transport processes that are induced by water movements caused by wind, sea currents and other natural triggers. The influence of tides is negligible in the Baltic Sea due to its minor connection to the world ocean. During fair weather conditions, the influence of waves is insignificant at the bottom of the basins, because the wave energy decreases strongly with increasing water depth and is moreover absorbed by internal density boundaries (pycnoclines) of the waterbody (Kirstin Schulz, 2017, NIOZ, personal communication). However, the situation might be different during a major storm event.

In the south-western Baltic Sea, several automated measuring stations collect meteorological and hydrographical data, such as wind velocity and direction, flow velocity, salinity and turbidity of the water. They are part of the German *Marine Environmental Monitoring Network (MARNET)* operated by the *Federal Maritime and Hydrographic Agency (BSH)*. Three of these stations, on the Falster-Rügen sand plain (25 km east of the Darss Sill), in the Arkona Basin (location of the cores POS475/24-2 and POS475/17-7 in Fig. 2.1, respectively) and on the Oder Bank, are maintained by the *Physical Oceanography and Instrumentation* department of *IOW*. They provided data recorded during the storm “Xaver” in early December 2013. During this storm, wind velocities reached up to 25 m/s and led to mean horizontal flow

velocities of over 50 cm/s in the bottom water of both the Falster-Rügen sand plain at 18 m water depth (Fig. 4.4A, C) and the Arkona Basin at 42 m water depth (Fig. 4.5A, C). The linkage between wind and flow velocity is confirmed by the correlation of the lower surface and the higher bottom water salinity with similar values during the time of highest velocities, indicating a homogenisation of the water column (Fig. 4.4B, 4.5B). The higher surface water turbidity during the same time suggests that material was suspended in and transported by the water (Fig. 4.4D, 4.5D). While the turbidity at the Darss Sill station was up to 16 times higher than normal, it was only around three times higher at the station in the Arkona Basin, most likely due to its greater water depth and volume.

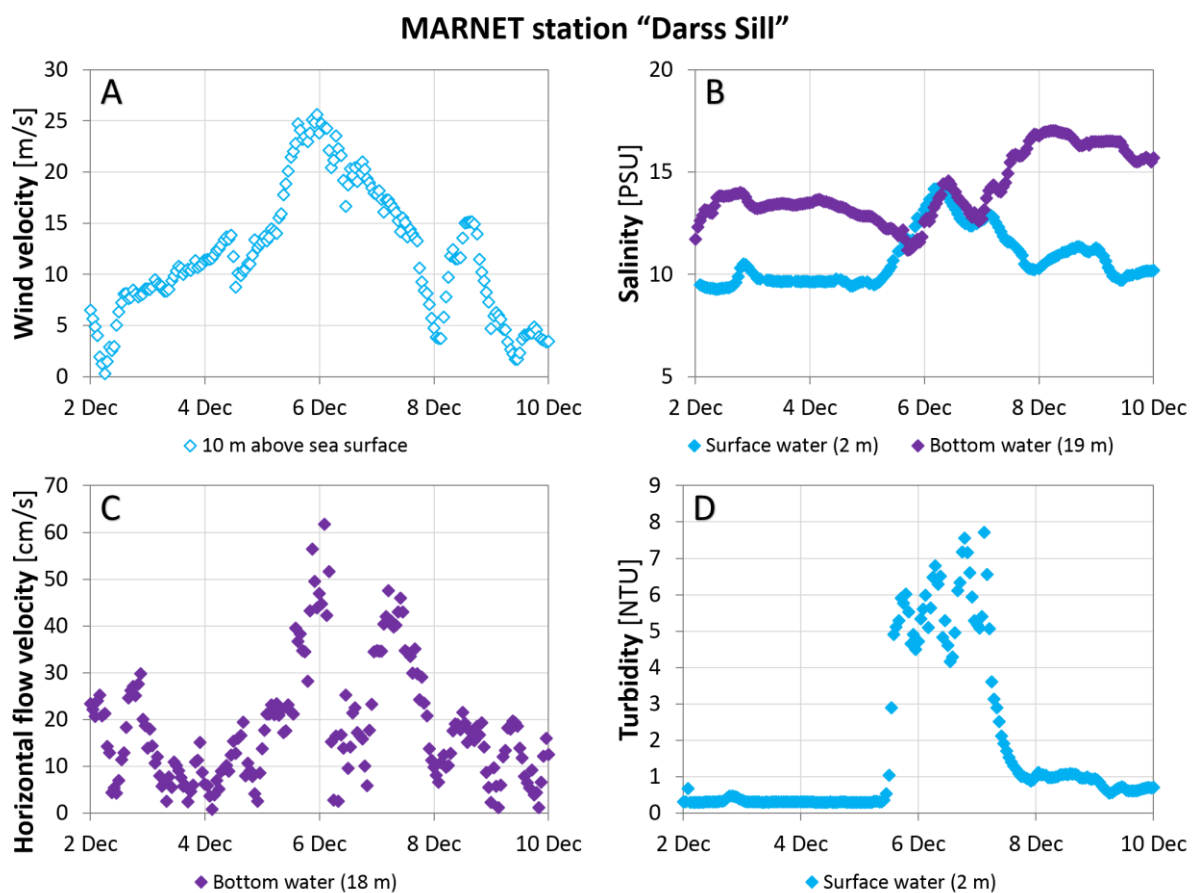


**Figure 4.4.** Meteorological and hydrographical data of the automated measuring station “Darss Sill” on the Falster-Rügen sand plain during the storm “Xaver” in December 2013. A) Wind velocity at sea surface. B) Salinity in the surface (2 m) and bottom water (19 m). C) Mean horizontal flow velocity component in the bottom water (18 m). D) Turbidity in the surface water (2 m). Notice the higher surface water turbidity and the alignment of surface and bottom water salinity during the wind and flow velocity maxima on 6 Dec 2013. Data from [BSH/IOW \(2013\)](#).

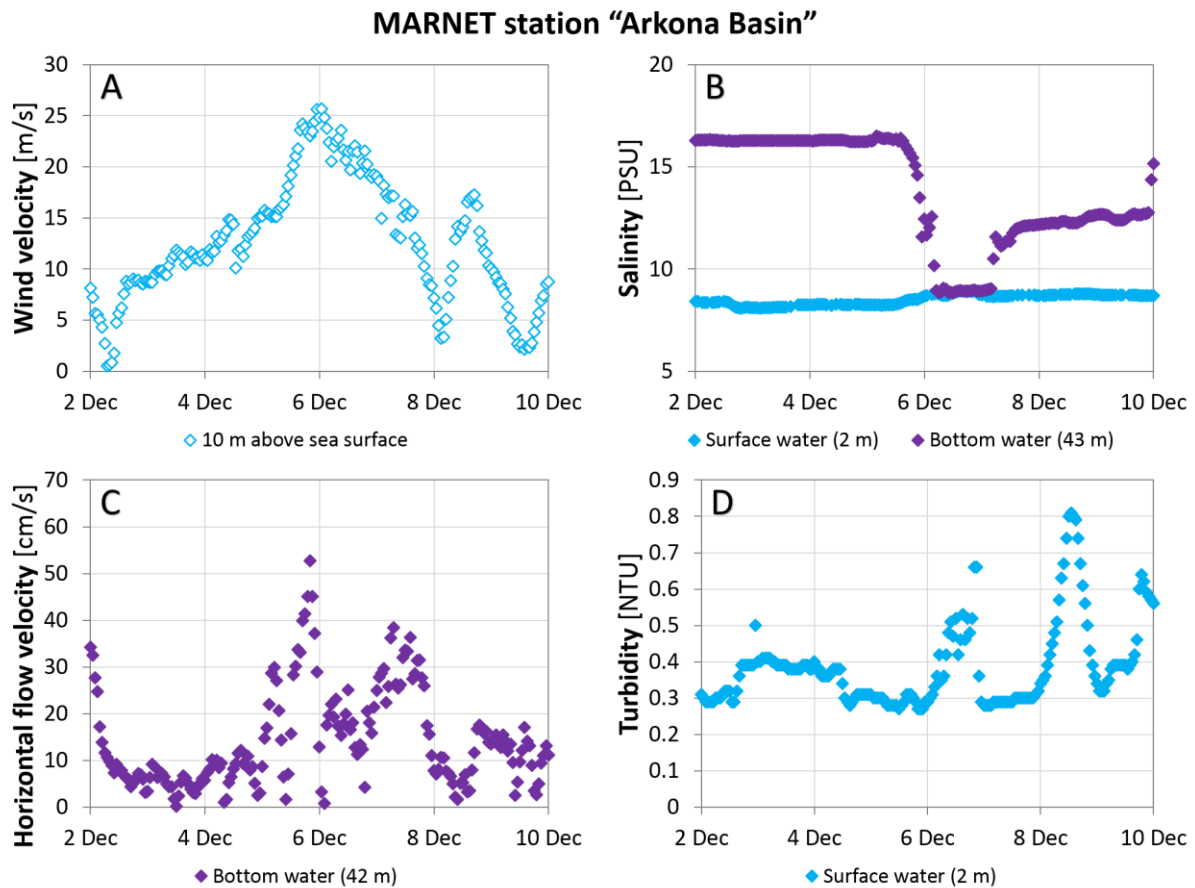


**Figure 4.5.** Meteorological and hydrographical data of the automated measuring station in the Arkona Basin during the storm “Xaver” in December 2013. A) Wind velocity at sea surface. B) Salinity in the surface (2 m) and bottom water (43 m). C) Mean horizontal flow velocity component in the bottom water (42 m). D) Turbidity in the surface water (2 m). Notice the higher surface water turbidity and the alignment of surface and bottom water salinity after the wind and flow velocity maxima on 6 Dec 2013. Data from [BSH/IOW \(2013\)](#).

As part of the *SECOS* project, resuspension experiments with natural sediments using an annular flume were conducted during joint research cruises in June/July (EMB076) and October 2014 (POS475). The flume was similar to that described by [Widdows et al. \(1998\)](#) and modified after [Peine \(2005\)](#). [Figure 4.6](#) shows the results in the form of flow velocities at which the first particles of a specific mean grain size were separated from the sediment at different locations. For the basin muds, the sandy silts of the Tromper Wiek and the fine sands of Stoltera, sediment mobilisation occurred at 7-10 cm/s, while the fine sands on the Oder Bank resuspended at around 20 cm/s ([Claudia Morys, University of Rostock, unpublished](#)). The Hjulström diagram confirms that these flow velocities are sufficient to erode and transport sediment particles of the respective size ([Hjulström, 1935](#)).

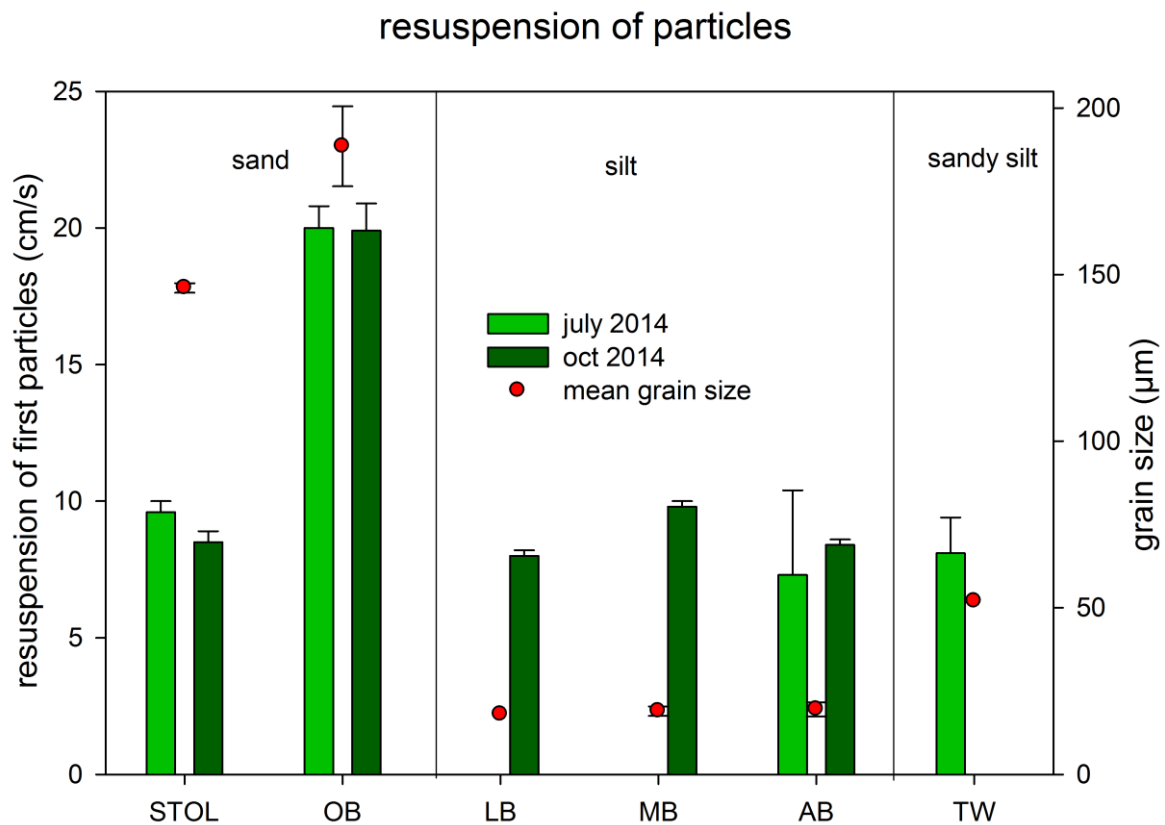


**Figure 4.6.** Flow velocities at which the first particles of a specific mean grain size (red circles) were separated from the sediment of different locations during *SECOS* research cruises in June/July (light green) and October (dark green) 2014. AB: Arkona Basin, LB: Lübeck Bay, MB: Mecklenburg Bight, OB: Oder Bank, STOL: Stoltera, TW: Tromper Wiek. Unpublished data from [Claudia Morys, University of Rostock](#).

In comparison with the averaged bottom flow velocities of up to 50 cm/s at the Darss Sill and Arkona Basin station (Fig. 4.4, 4.5), the data indicate that storms have the potential to resuspend and laterally transport sediments in the western Baltic Sea, even at 50 m water depth. This is also evident from the geochemical aureoles around the pollution hot spots (e.g. in Fig. 3.2) stretching to the north-east. According to [Kersten et al. \(2005\)](#), such storm events occur approximately six times a year (mainly during the winter season), based on wind data obtained at Cape Arkona from 1980 to 2002. Furthermore, this study found storm-generated sediment mixing down to 10 cm in the Mecklenburg Bight (around 23 m water depth) by interpreting activity profiles of the short-lived natural radionuclide  $^{234}\text{Th}$  in sediment cores. [Milkert and Werner \(1996\)](#) reported on a storm event in August 1989 that eroded up to 3.3 cm and deposited about 2 cm of silty clay at the same position at ~24 m water depth in the Eckernförde Bay. They also identified other storm-generated event layers in deeper sediment sections that they associated with major storms in 1954 and 1977/78. The event layer formation depends on the intensity, direction and most importantly the duration of the storm

(Milkert and Werner, 1996). The preservation, however, depends on the depth, intensity, and style of subsequent mixing, as well as on the sedimentation rate (Bentley and Nittrouer, 1999).

The laminated to thin-bedded, bright-to-dark graded layers in the negative X-radiographs (Fig. 4.2, 4.3) represent such event layers. The lamination or bedding is formed by the rapid deposition of sediment layers that are thick enough to bury the pre-existing surface and temporally inhibit the benthic community, thus creating a sharp basal contact (Bentley and Nittrouer, 1999; Nittrouer et al., 1998). An angular unconformity between the pre-existing surface and the newly deposited layer is proof of erosion prior to deposition (e.g. at 30 cm in core POS475/17-7; Fig. 4.3). The gradation represents an upward fining from coarse (bright) to fine silt to mud (dark) due to the decreasing flow velocity of a ceasing event. A dark mud layer indicates a completed event, otherwise the different event layers could also belong to one single event with varying flow velocity (e.g. at 10 cm in core POS475/57-10; Fig. 4.2). After the event, the benthic community re-establishes itself and consequently mixes the event layer to the bioturbation depth, which creates a gradational upper contact (Nittrouer et al., 1998). While the occurrence of multiple event layers in the cores from the Mecklenburg Bight down to around 20 cm (Fig. 4.2) confirms the impact of hydroturbation at that location at least in the last circa 100 years, the lag of such layers in cores from the deeper Arkona Basin (Fig. 4.3) could indicate either no event layer deposition (less hydroturbation) or mixing or total erasure by potentially more intense bioturbation or direct anthropogenic impact (Sect. 4.1.3).

Another important type of hydrodynamic event is the occasional occurring MBIs of highly saline water from the North Sea. *MARNET* data show mean horizontal flow velocities of up to 50 cm/s on the Falster-Rügen sand plain and still up to 38 cm/s in the Arkona Basin during the last MBI in December 2014. This is sufficient enough to resuspend and laterally transport local sediments, probably forming an event layer. Recently, strong MBIs occur only once in a decade (Mohrholz et al., 2015).

This episodic hydroturbation contributes to the slight perturbations of the geochemical profiles by bioturbation and probably further decreases the temporal resolution due to its greater mixing depth. Furthermore, it might be responsible for the local deviations from the general trend of decreasing pollutant contents towards the sediment surface, e.g., at around 10 cm depth in the cores EMB058/6-2, 17-2 and AL434/427-3 (Fig. 3.1B, 3.17), due to reworking of sub-recent, more polluted deposits. In the Sassnitz Channel (core EMB058/11-2),

a hole package of even older unpolluted (pre-industrial) material lies between younger polluted sediments and thus must have been remobilised after the start of industrialisation, possibly due to a submarine landslide (Fig. 3.1C).

### 4.1.3 Anthroturbation: anthropogenic mixing

Anthroturbation in aquatic environments refers to the disturbance of sediments by human activities such as bottom trawling, construction, dredging and anchoring (Soulsby et al., 2007) as well as sediment sampling (Berner, 1976). While the latter four activities have a potentially strong but local impact, bottom trawling affects wide areas of the Baltic Sea floor (HELCOM, 2010a). Figure 4.7 illustrates the bottom trawl effort in the south-western Baltic Sea during the first quarter of 2013, the main fishing season for that gear (ICES, 2015; von Dorrien et al., 2013). In the three months, the complete Arkona Basin and most parts of the Mecklenburg Bight were influenced by bottom trawling for 15-150 hours. Most of the cores studied within this project were taken in these areas.

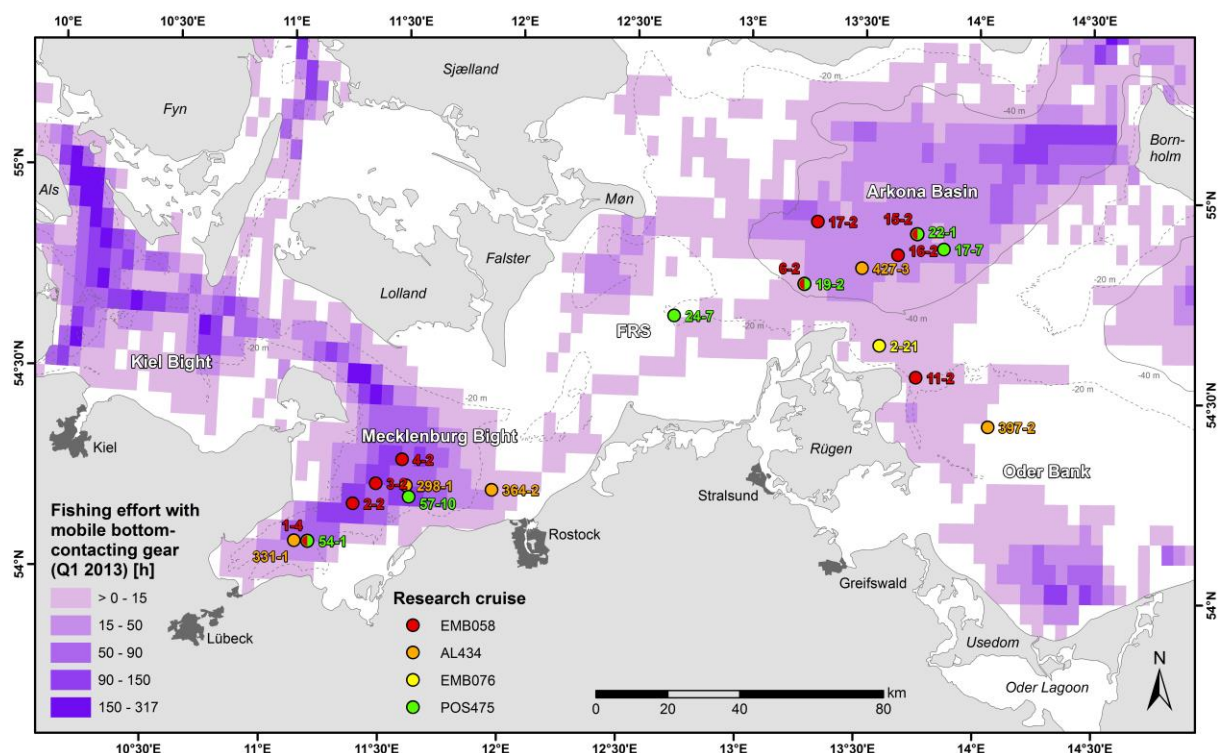


**Figure 4.7.** Map of the south-western Baltic Sea showing the fishing effort with mobile bottom-contacting gear in the first quarter of 2013 and coring locations (coloured circles). FRS: Falster-Rügen sand plain. Dataset from ICES (2015) based on vessel monitoring system (VMS) and logbook data.

Besides the intended and incidental extraction of benthic fauna, bottom trawling has several direct physical effects depending on gear weight (up to several hundred kilogrammes), towing speed, sediment type and strength of currents (Jones, 1992). Especially the otter boards leave



distinct traces by scraping and ploughing. They disturb the benthic communities and resuspend and mix the sediment (Duplisea et al., 2002; Jennings et al., 2001; Krost, 1990; Krost et al., 1990; Rosenberg et al., 2003). The resulting furrows range in width from approximately 0.2 to 2 m and can reach a penetration depth of 30 cm (Krost et al., 1990). The wires cause only a slight scraping, while the ground ropes and nets flatten the sediment surface between the otter boards. Scraping/ploughing and flattening are two opposing actions, with the first having a larger impact on fine sediments and the latter on coarse sediments (Smith et al., 2003). According to Main and Sangster (1981), otter boards cause a strong undertow of 40-80 cm/s, which is sufficient to erode the sediment (Fig. 4.6). Coarser sediments are primarily displaced, while finer sediments rather resuspend and potentially remain in suspension for long time, in particular if they contain high amounts of TOC (Krost, 1990). Werner et al. (1990) calculated that a 0.5 m wide track suspended a layer of mud with a thickness of at least 1 cm. Furthermore, they provided evidence for remobilisation of nutrients, complete perturbation of the age sequences and chemical concentration profiles as well as destruction of the original sedimentary fabric down to the mean penetration depth of 15 cm (maximal 23 cm). Indirect effects of bottom trawling include post-fishing mortality and long-term trawl-induced changes to benthic fauna (Jones, 1992). It can be assumed that dredging and trenching have similar impacts.

In the Kiel Bight west of the Mecklenburg Bight, Krost et al. (1990) mapped bottom trawl tracks by side scan sonar and found patterns stretching over several square kilometres in intensely trawled regions. The track frequency generally increased with water depth and with decreasing mechanical resistance of the sediment. Hence, the track density was highest in mud areas below 20 m. The width of the otter board tracks was usually around 80 cm, sometimes between 1 and 2 m, probably due to jumping otter boards. The penetration depth ranged from circa 2 cm in sand to around 15 cm in mud. Deeper tracks of up to 30 cm in mud were associated with jumping otter boards (Krost, 1990). The roller gear attached to the ground rope of the nets left tracks with a width of 3-8 cm and a penetration depth of 2-5 cm in mud, as observed by video cameras and divers. Krost et al. (1990) concluded that some areas of the Kiel Bight are ploughed at least once a year by otter boards (based on fishing effort data) and that areas with abundant tracks are more or less completely disturbed.

On behalf of the BSH, the Marine Geology department of IOW monitors the Baltic Sea floor with various geophysical methods (e.g. side scan sonar imaging) and has processed a large

amount of respective data. For this study, Franz Tauber provided several side scan sonar images of the sea floor at some of the SECOS coring locations (200 x 200 m) to visualise the morphology of the sediment surface (Fig. 4.8; Franz Tauber, 2015, IOW, personal communication). They reveal a strong anthropurbation of the muds in the Mecklenburg Bight and the Arkona Basin with multiple cross-cutting tracks.

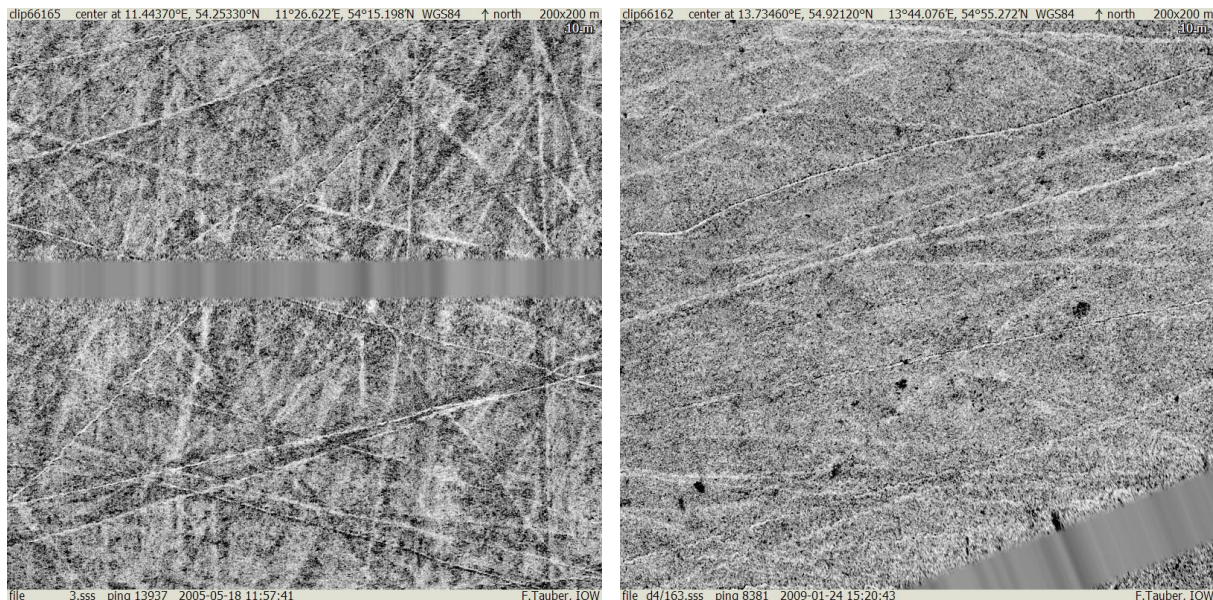


**Figure 4.8.** Side scan sonar images of the sea floor around coring sites EMB058/3-2 in the Mecklenburg Bight from 2005 (left) and EMB058/15-2 in the Arkona Basin from 2009 (right) reveal multiple generations of bottom trawl, dredge and/or construction tracks (Franz Tauber, 2015, IOW, personal communication).

The preservation of such tracks depends on the intensity of subsequent bio-, hydro- and anthropurbation, besides the gear weight, towing speed and sediment type. In shallow sandy areas, they only have a short preservation period due to the low penetration depth as well as stronger rearrangement by waves and currents (Krost, 1990). In deeper muddy areas, they can persist for a much longer time. Ecological investigations in the context of the construction of the *Nord Stream* gas pipeline from the Bornholm Basin to the Greifswald Lagoon had shown that in deep areas (below 20 m water depth) the marks and traces of the workings on the sea floor were freshly recognisable and almost unchanged three years after the construction (Thomas Leipe, 2017, IOW, personal communication). An otter board track in the sandy mud of the Eckernförde Bay (western Kiel Bight) could be identified for almost five years in an area with minor fishing activity (Bernhard, 1989; Krost et al., 1990). An old track in the very fine sand of the eastern Mecklenburg Bight at ~19 m water depth, which existed already before a dumping test during the *DYNAS* project (*Dynamics of Natural and Anthropogenic*



*Sedimentation*) in 2001 (Fig. 4.9A; Tauber, 2009), was clearly recognisable in 2014 and still had a furrow depth of approximately 8 cm (Fig. 4.9B, C; Jörn Kurth, 2014, IOW, personal communication). The main features of the dumping mounds were still visible after 13 years. Erosion, flattening or transportation of the dumped material, e.g. by bottom currents, had not been completed. Since the penetration of otter boards is greater than that of the other gear elements, the latter are not able to erase or flatten these tracks. Moreover, a single track is spatially too localised to produce a total extinction by otter boards. Hence the resulting cross-cutting pattern includes multiple generations of bottom trawl, dredge and/or construction tracks (Fig. 4.8).

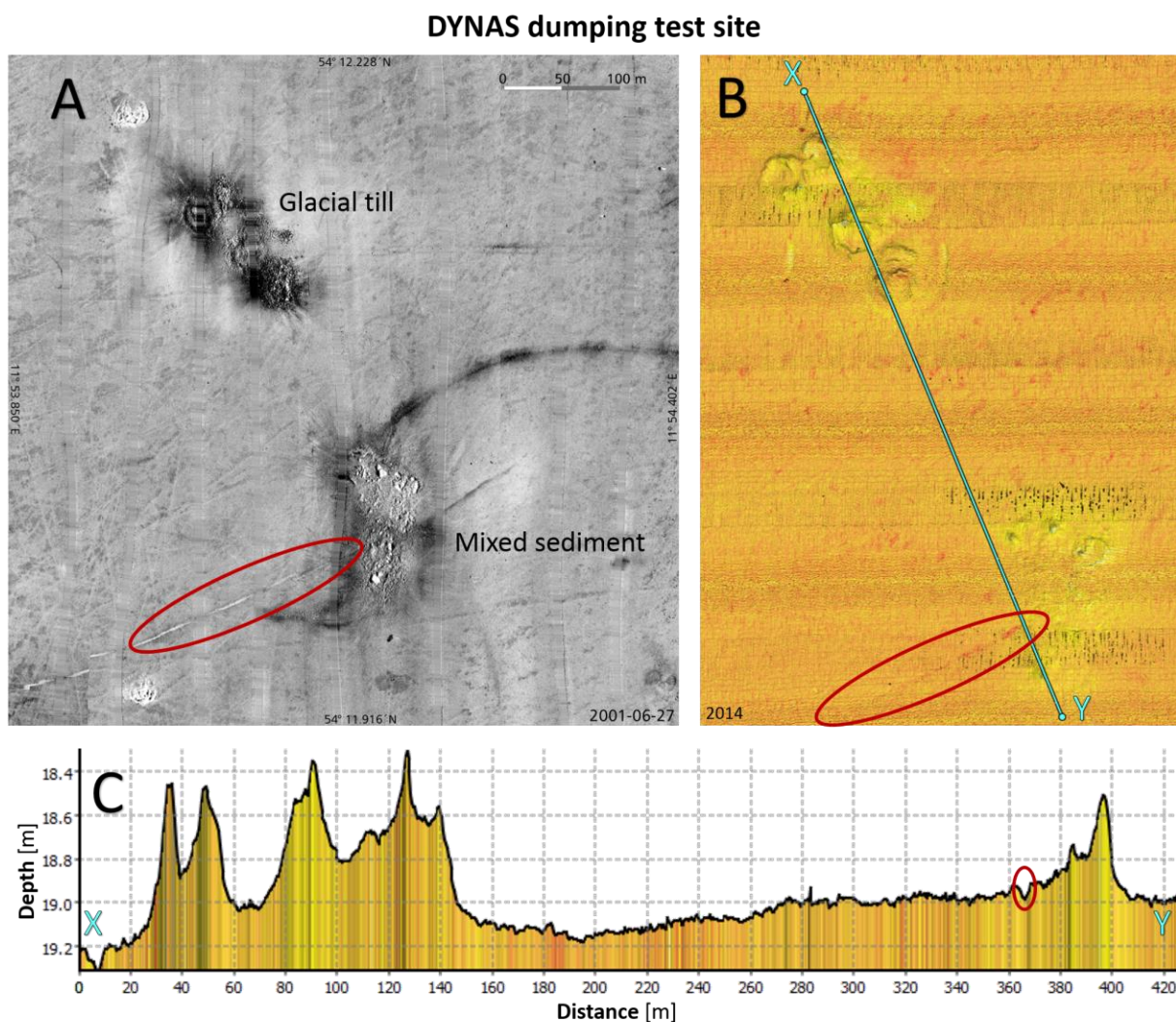


**Figure 4.9.** Side scan sonar images of the *DYNAS* dumping test site in the Mecklenburg Bight off Nienhagen one week (A) and 13 years (B) after the dumping of glacial till and mixed sediment at a water depth of 19 m in 2001. Image C shows a super-elevated profile between the points X and Y on image B from 2014. Notice the old furrow (red ellipses) and the main features that are still clearly recognisable in 2014. Image A modified after Tauber (2009), images B and C from Jörn Kurth (2014, IOW, personal communication).

The regularly occurring anthropurbation by bottom trawling causes the above mentioned in-depth mixing that evenly distributes geochemical signals throughout the affected sediment layer (Fig. 4.1C). The plateaus of more or less stable pollutant contents down to 25 cm core depth in the cores EMB058/4-2, 15-2, 16-2 and probably AI434/298-1 are examples for a strong disturbance that erases any detailed age relationship (Fig. 3.1A, B). The parallelism of Hg and  $^{137}\text{Cs}$  only indicates that the anthropurbation occurred after the Chernobyl accident in 1986, while the reduced Hg contents at the sediment surface show that at least some time has passed. In core EMB058/15-2, the Hg profile shows a small step in 11 cm depth within the plateau, suggesting that another anthropurbation event occurred in more recent times. The same probably happened in core EMB058/16-2 not much after the Chernobyl accident, as indicated by the  $^{137}\text{Cs}$  increase above the plateau.

The increase of the TS content at ~25 cm in these cores also provides evidence for mixing (of oxygen) down to that depth (less at the time of the event), causing an oxidation of pyrite (Fig. 3.4). The unusual fluctuations of the  $\text{TP}_{\text{Ash}}$  content (Fig. 3.8C), the associated peaks of the Fe content (Fig. 3.13B), as well as the occurrence of vivianite, pyrite, potash feldspar and titanium minerals in core EMB058/15-2 might also be associated with at least two anthropurbation events. On the one side, phosphorus and iron oxides, among others, were probably transported down to the anthropurbation depth, thus increasing the authigenic formation of vivianite. On the other side, the resuspension, e.g. by otter boards, might have caused a gravimetric sorting during redeposition, resulting in the input of already existing vivianite and pyrite particles as well as inert potash feldspar and titanium minerals. This might be visible as an event layer similar to those caused by storms, but unfortunately, no x-radiograph was acquired from this core to identify the associated sedimentary fabric. However, the slightly increased amount of fine sand that was found at the same depth could be an indicator for this process (Sect. 3.1).

#### 4.1.4 Interactions

The discussed sediment mixing processes naturally do not occur independently, but are subject to an interplay. Bioturbation influences the shear strength of the sediment and changes its stability and erodibility by bottom currents (Werner, 2002). The intermixture with burrows add a skeleton to the sediment and thus increase its shear strength. Likewise, the biomixing of coarser material, e.g. introduced by storms, into finer sediment has a

strengthening effect. However, the irrigation of the burrows increases the water content and can weaken the shear strength, if bioturbation exceeds a certain intensity. Also the biomixing of finer material into coarser sediment has a weakening effect. Furthermore, the colonisation with macrobenthic fauna increases the roughness of the sediment surface, thus offering more attack points for erosion. The resuspension of sediment due to bottom trawling similarly facilitates erosion and the redistribution by bottom currents (Krost, 1990; Werner et al., 1990). In reverse, Figures 4.8 and 4.9 imply that hydroturbation apparently is not intense enough to fill, flatten or erode the local sedimentary depressions and elevations within a decade. Moreover, anthro- and also hydroturbation can pause or shift the biogenic activity in an affected area.

Concerning the sedimentary fabric, bioturbation can partially or completely erase hydrodynamic event layers shortly after deposition and recolonization. An example for this is the bioturbated event layer at 17 cm in core POS475/19-2 (Fig. 4.3). In reverse, hydroturbation can lead to the erosion of biogenic structures in the surface sediments. Both is true for anthroturbation, only that it also erases pre-existing structures at greater sediment depths.

Besides the input characteristics and the post-depositional degradation, the geochemical profiles, especially those of contaminants, are the result of the combined effects of bio-, hydro- and anthroturbation, which have already been discussed and are summarised in Figure 4.10. A special case are the core profiles in the sandy areas (Fig. 3.1C, 4.10A). They represent the pure sediment mixing signals since there is no net mass accumulation in these highly dynamic areas (Christiansen et al., 2002; Emeis et al., 2002) and since the influence of TOC content and particle size was minimised through normalisation with TOC that is mainly associated with the fine fraction of the sediment. Interestingly, their resemblance indicates a similarly strong mixing influence that seems to be independent from the exact core location. All show a maximal penetration depth of 15-20 cm, an average sediment mixing depth of 5-10 cm and decreasing values towards the sediment surface. This decline is somewhat irritating, as one would expect a more even distribution similar to that of the anthropogenically disturbed cores (Fig. 4.10D). It is possible that less penetrating mixing processes, which predominantly affect only the surficial sediment layer, caused a mixing of younger and thus less polluted material into the sediment, diluting the peak contamination. The profiles therefore also reflect the temporal change to decreasing contamination levels.

Moreover, they imply that the sandy areas are an at least temporary storage for contaminants, which were mixed in, resulting in the calculated inventories (Tab. 3.1).

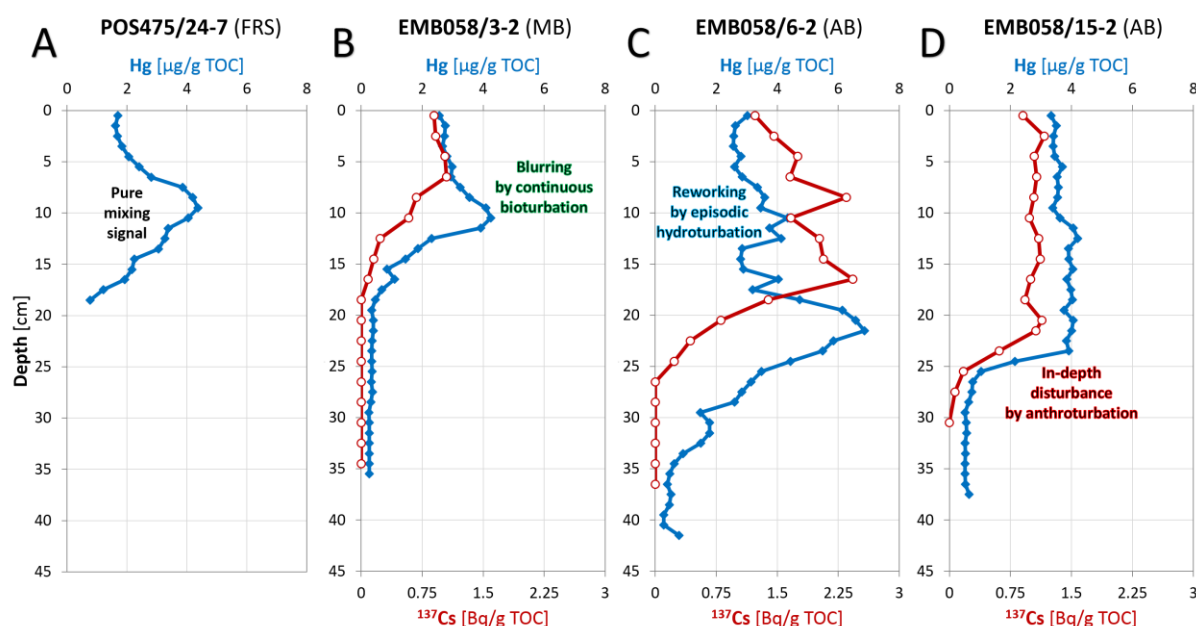


**Figure 4.10.** Prime examples for geochemical profiles that are mainly affected by pure sediment mixing without deposition (A), continuous bioturbation (B), continuous bioturbation together with episodic hydroturbation (C), and in-depth disturbance by anthroturbation (D). The mixing intensity and depth increases from A to D. AB: Arkona Basin, FRS: Falster-Rügen sand plain, MB: Mecklenburg Bight.

The maxima in the basin muds are mostly deeper than in the sandy areas, because of a net mass accumulation and a deeper mixing due to the softer material as well as the bottom trawling effort (Fig. 4.10C, D). However, there is probably less bio- and hydroturbation due to the greater water depth and occasional anoxic conditions. Only in the cores EMB058/2-2 and 3-2 from the Mecklenburg Bight, the maxima of Hg are at shallower depths and indicate a relative low mass accumulation rate compared to the other mud cores, probably due to their location on the way of intruding saline water from the North Sea (Fig. 3.1B, C, 4.10B, C).

The remarkable high  $_{\text{anth}}\text{Hg}$  and  $^{137}\text{Cs}$  inventories of the anthropogenically disturbed cores, which should be similar to nearby less-disturbed cores, might relate to small-scale bathymetric heterogeneities resulting from bottom trawling or bottom current activities (Tab. 3.1). The furrows or depressions that are left by otter boards may act as sediment traps for drifting material (Werner et al., 1990). This causes a local accumulation of fine material enriched in TOC and contaminants, which mixes into the sediment and thus increases the inventory compared to areas with a smoother surface.

## 4.2 Accumulation patterns

As a result of the high affinities between the fine fraction ( $\leq 63 \mu\text{m}$ ) and the contents of TOC, nutrients (N, P),  $\text{bioSiO}_2$ , heavy metals (e.g. Hg),  $^{137}\text{Cs}$  and organic pollutants, similar distribution patterns can be observed. Considering the total sediment, the TOC and N contents increase with the mud content and thus are highest in the western Kiel Bight, the inner Mecklenburg Bight, the central Arkona Basin and the Oder Lagoon. However, their relative proportion in the fine fraction is highest in areas with lower mud content, especially on the Oder Bank. Furthermore, their reduction with increasing sediment depth is stronger and the low TOC/N ratios are indicative for fresh organic matter in those areas. Also the geochemical maps of  $\text{bioSiO}_2$  and  $\text{TP}_{\text{Ash}}$  show similar patterns. While the contents of Hg and other anthropogenic induced heavy metals also increase with mud content, their areas of maximum contents are more confined, corresponding to the pollution hot spots. Their relative proportions in the fine fraction are also very high on the Oder Bank. Because of a strong linear correlation of PAHs and presumably PCBs to heavy metals, a similar spatial distribution can be expected for organic pollutants (Witt and Trost, 1999). The high contamination of the Mecklenburg Bight with DBT thus might be associated with the local dumping site as well as its usage in plastic materials (Fig. 3.17C; Abraham et al., 2017).

Besides the Oder Bank being a highly productive area that is densely colonised by benthic fauna, the whole area is also strongly influenced by the Oder Lagoon, which acts as a stopover of nutrients and contaminants from the former highly “fertilised” and polluted Oder River (Leipe et al., 2017). The Oder Bank is not an area of long-term deposition due to strong hydroturbation, resulting in resident times in the range of weeks to months (Christiansen et al., 2002). As a consequence, there is an ongoing transport of old contaminated and fine material from the Oder Lagoon to the Arkona and Bornholm Basins, where it accumulates despite the discussed strong sediment mixing processes. However, the geochemical aureoles around the pollution hot spots indicate a lateral sediment transport from west to east, caused by near-bottom currents (Leipe et al., 2013).



## 5 Conclusions and outlook

On the way from the sources to the final sinks, the basins of the south-western Baltic Sea act at least intermediately as storage sites for fine-grained particulate matter on a decadal to centennial scale. This sub-recent material contains natural detritic, mostly silicate minerals, autochthonous biogenic material (organic matter, bio-minerals like opal) and anthropogenically sourced contaminants (heavy metals, organic pollutants). The near-surface sediment column is furthermore characterised by early diagenetic effects (redox-cline, sulphate reduction, etc.).

Nevertheless, the near-bottom environmental conditions of the south-western Baltic Sea basins prevent a continuous and undisturbed accumulation, as can be detected in some deep and anoxic basins of the central Baltic Sea. Continuous bioturbation with changing intensity, episodic hydrodynamically driven sediment mixing and in-depth physical anthropogenic impact by fishery, off-shore constructions and other factors disturb or mask the vertical profiles of several measured parameters in the sediment column. Thus, the basin sediments from the south-western Baltic Sea are only partly suitable for dating and a reasonable determination of mass accumulation rates. Furthermore, it seems possible that the south-western Baltic Sea basins may already reached the limit of net sediment accumulation on geological time scales. The aureoles of contaminated material around the pollution hot spots indicate the resuspension and general lateral transport of sediments towards the east.

However, some analysed sediment cores allow a reliable reconstruction of historical changes and events, and the assessable inventories of contaminants clearly reflect the remarkable storage function of the sedimentary deposits. The identified types of geochemical profiles from (non-depositional) shallow-water sandy sediments to the adjacent basin muds is a novel finding of this study, and supports similar investigations in other areas of the Baltic Sea. Moreover, the pervasive anthropogenic impact through bottom trawling and dredging, e.g. on the sedimentary fabric and the distribution of contaminants, is worth further investigation. Here, data from relative “undisturbed” sedimentation areas, e.g. in the vicinity of larger sea floor obstacles, which are avoided by bottom trawlers, could serve as reference.





## References

- Abraham, M., Westphal, L., Hand, I., Lerz, A., Jeschek, J., Bunke, D., Leipe, T., Schulz-Bull, D.E., 2017. *TBT and its metabolites in sediments: Survey at a German coastal site and the central Baltic Sea*. Marine Pollution Bulletin 121, 404–410. doi:10.1016/j.marpolbul.2017.06.020
- Appleby, P.G., Richardson, N., Nolan, P.J., 1991. *<sup>241</sup>Am dating of lake sediments*. Hydrobiologia 214, 35–42. doi:10.1007/BF00050929
- Baltic Sea Atlas, 2014 [WWW map service]. Leibniz Institute for Baltic Sea Research Warnemünde (IOW), Rostock, Germany <http://bio-50.io-warnemuende.de/iowbsa/index.php> (accessed 2017-03-03).
- Bentley, S.J., Nittrouer, C.A., 1999. *Physical and biological influences on the formation of sedimentary fabric in an oxygen-restricted depositional environment: Eckernförde Bay, southwestern Baltic Sea*. PALAIOS 14, 585–600. doi:10.2307/3515315
- Berner, R.A., 1976. *The Benthic Boundary Layer from the Viewpoint of a Geochemist*, in: McCave, I.N. (Ed.), The Benthic Boundary Layer. Springer, New York, pp. 33–55. doi:10.1007/978-1-4615-8747-7\_3
- Bernhard, M., 1989. *Sedimentologische Beeinflussung der Oberflächensedimente durch Grundfischerei in der Kieler Bucht* [Diploma thesis]. Christian-Albrechts-Universität Kiel, Germany.
- Björck, S., 1995. *A Review of the History of the Baltic Sea*. Quaternary International 27, 19–40. doi:10.1016/1040-6182(94)00057-C
- Bonacker, P., 1996. *Mächtigkeiten der marinen Schlicke in den Ostseebecken* [Report]. Leibniz Institut für Ostseeforschung Warnemünde (IOW), Rostock, Germany.
- Boudreau, B.P., 1986a. *Mathematics of tracer mixing in sediments: I. Spatially-dependent, diffusive mixing*. American Journal of Science 286, 161–198. doi:10.2475/ajs.286.3.161
- Boudreau, B.P., 1986b. *Mathematics of tracer mixing in sediments: II. Nonlocal mixing and biological conveyor-belt phenomena*. American Journal of Science 286, 199–238. doi:10.2475/ajs.286.3.199
- Boudreau, B.P., Imboden, D.M., 1987. *Mathematics of tracer mixing in sediments: III. The theory of nonlocal mixing within sediments*. American Journal of Science 287, 693–719. doi:10.2475/ajs.287.7.693
- Breivik, K., Sweetman, A., Pacyna, J.M., Jones, K.C., 2002a. *Towards a global historical emission inventory for selected PCB congeners - A mass balance approach: 1. Global production and consumption*. The Science of the Total Environment 290, 181–198. doi:10.1016/S0048-9697(01)01075-0
- Breivik, K., Sweetman, A., Pacyna, J.M., Jones, K.C., 2002b. *Towards a global historical emission inventory for selected PCB congeners - A mass balance approach: 2. Emissions*. The Science of the Total Environment 290, 199–224. doi:10.1016/S0048-9697(01)01076-2

- Christiansen, C., Edelvang, K., Emeis, K.-C., Graf, G., Jähmlich, S., Kozuch, J., Laima, M., Leipe, T., Löffler, A., Lund-Hansen, L.C., Miltner, A., Pazdro, K., Pempkowiak, J., Shimmield, G., Shimmield, T., Smith, J., Voss, M., Witt, G., 2002. *Material transport from the nearshore to the basinal environment in the southern Baltic Sea I. Processes and mass estimates*. Journal of Marine Systems 35, 133–150. doi:10.1016/S0924-7963(02)00126-4
- d’Orbigny, A.D., 1842. *Voyage dans l’Amerique meridionale*. Tome troisième. 4e partie: Paléontologie. Paris/Strasbourg, p. 30.  
<https://archive.org/stream/voyagedanslamr3341844orbi#page/30/mode/2up>  
(accessed 2017-09-24)
- Dadey, K.A., Janecek, T., Klaus, A., 1992. *Dry-Bulk Density: Its Use and Determination*. Proceedings of the Ocean Drilling Program, Scientific Results 126, 551–554. doi:10.2973/odp.proc.sr.126.157.1992
- Dellwig, O., Bosselmann, K., Kölsch, S., Hentscher, M., Hinrichs, J., Böttcher, M.E., Reuter, R., Brumsack, H.-J., 2007. *Sources and fate of manganese in a tidal basin of the German Wadden Sea*. Journal of Sea Research 57, 1–18. doi:10.1016/j.seares.2006.07.006
- Duplisea, D.E., Jennings, S., Warr, K.J., Dinmore, T.A., 2002. *A size-based model of the impacts of bottom trawling on benthic community structure*. Canadian Journal of Fisheries and Aquatic Sciences 59, 1785–1795. doi:10.1139/f02-148
- Emeis, K.-C., Christiansen, C., Edelvang, K., Jähmlich, S., Kozuch, J., Laima, M., Leipe, T., Löffler, A., Lund-Hansen, L.C., Miltner, A., Pazdro, K., Pempkowiak, J., Pollehne, F., Shimmield, T., Voss, M., Witt, G., 2002. *Material transport from the near shore to the basinal environment in the southern Baltic Sea II: Synthesis of data on origin and properties of material*. Journal of Marine Systems 35, 151–168. doi:10.1016/S0924-7963(02)00127-6
- Flemming, B.W., Delafontaine, M.T., 2000. *Mass physical properties of muddy intertidal sediments: some applications, misapplications and non-applications*. Continental Shelf Research 20, 1179–1197. doi:10.1016/S0278-4343(00)00018-2
- Gingele, F.X., Leipe, T., 2001. *Southwestern Baltic Sea—A sink for suspended matter from the North Sea?* Geology 29, 215–218. doi:10.1130/0091-7613(2001)029<0215:SBSASF>2.0.CO;2
- Gogina, M., Morys, C., Forster, S., Gräwe, U., Friedland, R., Zettler, M.L., 2017. *Towards benthic ecosystem functioning maps: Quantifying bioturbation potential in the German part of the Baltic Sea*. Ecological Indicators 73, 574–588. doi:10.1016/j.ecolind.2016.10.025
- Haldeman, S.S., 1840. *Supplement to Number One of “A Monograph of the Limniades, Or Freshwater Univalve Shells of North America”: Containing Descriptions of Apparently New Animals in Different Classes and the Names and Characters of the Subgenera in Paludina and Anculosa*. J. Dobson, Philadelphia.
- Hall, J., 1847. *Palaeontology of New York. Volume I. Containing Descriptions of the Organic Remains of the Lower Division of the New York System (equivalent to the Lower Silurian rocks of Europe)*. Palaeontology 7, 338 pp.

- Hallberg, R.O., 1991. *Environmental Implications of Metal Distribution in Baltic Sea Sediments*. *Ambio* 20, 309–316. <http://www.jstor.org/stable/4313851> (accessed 2017-09-24)
- Hedman, J.E., Tocca, J.S., Gunnarsson, J.S., 2009. *Remobilization of Polychlorinated Biphenyl from Baltic Sea Sediment: Comparing the Roles of Bioturbation and Physical Resuspension*. *Environmental Toxicology and Chemistry* 28, 2241. doi:10.1897/08-576.1
- Heinrichs, H., Brumsack, H.-J., Loftfield, N.S., König, N., 1986. *Verbessertes Druckaufschlußsystem für biologische und anorganische Materialien*. *Zeitschrift für Pflanzenernährung und Bodenkunde* 149, 350–353. doi:10.1002/jpln.19861490313
- HELCOM, 2013. *Thematic assessment of long-term changes in radioactivity in the Baltic Sea, 2007-2010*. *Baltic Sea Environment Proceedings* 135, 40 pp. <http://helcom.fi/Lists/Publications/BSEP135.pdf> (accessed 2017-03-03)
- HELCOM, 2012a. *Manual for Marine Monitoring in the COMBINE Programme of HELCOM. Part B: General guidelines on quality assurance for monitoring in the Baltic Sea. Annex B-13, Appendix 1: Technical note on the determination of polycyclic aromatic hydrocarbons (PAHs) in sediment*. Helsinki Commission. [http://www.helcom.fi/Documents/Action areas/Monitoring and assessment/Manuals and Guidelines/Manual for Marine Monitoring in the COMBINE Programme of HELCOM\\_PartB\\_AnnexB13\\_Appendix1.pdf](http://www.helcom.fi/Documents/Action%20areas/Monitoring%20and%20assessment/Manuals%20and%20Guidelines/Manual%20for%20Marine%20Monitoring%20in%20the%20COMBINE%20Programme%20of%20HELCOM_PartB_AnnexB13_Appendix1.pdf) (accessed 2017-04-11)
- HELCOM, 2012b. *Manual for Marine Monitoring in the COMBINE Programme of HELCOM. Part B: General guidelines on quality assurance for monitoring in the Baltic Sea. Annex B-13, Appendix 2: Technical note on the determination of chlorinated biphenyls in sediment*. Helsinki Commission. [http://www.helcom.fi/Documents/Action areas/Monitoring and assessment/Manuals and Guidelines/Manual for Marine Monitoring in the COMBINE Programme of HELCOM\\_PartB\\_AnnexB13\\_Appendix2.pdf](http://www.helcom.fi/Documents/Action%20areas/Monitoring%20and%20assessment/Manuals%20and%20Guidelines/Manual%20for%20Marine%20Monitoring%20in%20the%20COMBINE%20Programme%20of%20HELCOM_PartB_AnnexB13_Appendix2.pdf) (accessed 2017-04-11)
- HELCOM, 2011. *Fifth Baltic Sea Pollution Load Compilation (PLC-5)*. *Baltic Sea Environment Proceedings* 128, 217 pp. <http://www.helcom.fi/Lists/Publications/BSEP128.pdf> (accessed 2017-09-24)
- HELCOM, 2010a. *Ecosystem Health of the Baltic Sea 2003-2007: HELCOM Initial Holistic Assessment*. *Baltic Sea Environment Proceedings* 122, 68 pp. <http://helcom.fi/Lists/Publications/BSEP122.pdf> (accessed 2017-07-03)
- HELCOM, 2010b. *Hazardous substances in the Baltic Sea - An integrated thematic assessment of hazardous substances in the Baltic Sea*. *Baltic Sea Environment Proceedings* 120B, 116 pp. <http://helcom.fi/Lists/Publications/BSEP120B.pdf> (accessed 2017-08-14)
- HELCOM, 2010c. *Towards a tool for quantifying anthropogenic pressures and potential impacts on the Baltic Sea marine environment: A background document on the method, data and testing of the Baltic Sea Pressure and Impact Indices*. *Baltic Sea Environment Proceedings* 125, 72 pp. <http://helcom.fi/Lists/Publications/BSEP125.pdf> (accessed 2017-08-16)

- HELCOM, 2009. *Eutrophication in the Baltic Sea - An integrated thematic assessment of the effects of nutrient enrichment and eutrophication in the Baltic Sea region*. Baltic Sea Environment Proceedings 115B, 152 pp. <http://helcom.fi/Lists/Publications/BSEP115B.pdf> (accessed 2017-08-16)
- HELCOM, 2006. *Development of tools for assessment of eutrophication in the Baltic Sea*. Baltic Sea Environment Proceedings 104, 64 pp. <http://www.helcom.fi/Lists/Publications/BSEP104.pdf> (accessed 2017-03-03)
- HELCOM, 2002. *Environment of the Baltic Sea area 1994-1998*. Baltic Sea Environment Proceedings 82B, 218 pp. <http://helcom.fi/Lists/Publications/BSEP82B.pdf> (accessed 2017-08-24)
- Hjulström, F., 1935. *Studies in the morphological activity of rivers as illustrated by the river Fyris* [Dissertation]. Bulletin of the Geological Institution of the University of Upsala 25, 221–527. <http://ci.nii.ac.jp/naid/10006404210/en/> (accessed 2017-07-09)
- Horowitz, H.M., Jacob, D.J., Amos, H.M., Streets, D.G., Sunderland, E.M., 2014. *Historical Mercury Releases from Commercial Products: Global Environmental Implications*. Environmental Science & Technology 48, 10242–10250. doi:10.1021/es501337j
- Hylander, L.D., Meili, M., 2003. 500 years of mercury production: global annual inventory by region until 2000 and associated emissions. Science of The Total Environment 304, 13–27. doi:10.1016/S0048-9697(02)00553-3
- ICES, 2015. *Fishing abrasion pressure maps for mobile bottom-contacting gears in HELCOM area* [WWW document]. International Council for the Exploration of the Sea. [http://ices.dk/sites/pub/Publication Reports/Data outputs/HELCOM\\_mapping\\_fishing\\_intensity\\_and\\_effort\\_data\\_outputs\\_2015.zip](http://ices.dk/sites/pub/Publication%20Reports/Data%20outputs/HELCOM_mapping_fishing_intensity_and_effort_data_outputs_2015.zip) (accessed 2017-07-06)
- Ikäheimonen, T.K., Outola, I., Vartti, V.-P., Kotilainen, P., 2009. *Radioactivity in the Baltic Sea: inventories and temporal trends of 137Cs and 90Sr in water and sediments*. Journal of Radioanalytical and Nuclear Chemistry 282, 419–425. doi:10.1007/s10967-009-0144-1
- Ilus, E., Ilus, T., 2000. *Sources of Radioactivity*. The radiological exposure of the population of the European Community to radioactivity in the Baltic Sea — Marina-Belt project, Radiation Protection 110, 9–76.
- Jennings, S., Pinnegar, J.K., Polunin, N.V.C., Warr, K.J., 2001. *Impacts of trawling disturbance on the trophic structure of benthic invertebrate communities*. Marine Ecology Progress Series 213, 127–142. doi:10.3354/meps213127
- Johannessen, S.C., Macdonald, R.W., 2012. *There is no 1954 in that core! Interpreting sedimentation rates and contaminant trends in marine sediment cores*. Marine Pollution Bulletin 64, 675–678. doi:10.1016/j.marpolbul.2012.01.026
- Jones, J.B., 1992. *Environmental impact of trawling on the seabed: A review*. New Zealand Journal of Marine and Freshwater Research 26, 59–67. doi:10.1080/00288330.1992.9516500

- Keighley, D.G., Pickerill, R.K., 1995. *The ichnotaxa Palaeophycus and Planolites: historical perspectives and recommendations*. *Ichnos* 3, 301–309.  
[doi:10.1080/10420949509386400](https://doi.org/10.1080/10420949509386400)
- Kersten, M., Leipe, T., Tauber, F., 2005. *Storm disturbance of sediment contaminants at a hot-spot in the Baltic sea assessed by <sup>234</sup>Th radionuclide tracer profiles*. *Environmental Science and Technology* 39, 984–990. [doi:10.1021/es049391y](https://doi.org/10.1021/es049391y)
- Knaust, D., 2013. *The ichnogenus Rhizocorallium: Classification, trace makers, palaeoenvironments and evolution*. *Earth-Science Reviews* 126, 1–47.  
[doi:10.1016/j.earscirev.2013.04.007](https://doi.org/10.1016/j.earscirev.2013.04.007)
- Kristensen, E., Penha-Lopes, G., Delefosse, M., Valdemarsen, T., Quintana, C.O., Banta, G.T., 2012. *What is bioturbation? The need for a precise definition for fauna in aquatic sciences*. *Marine Ecology Progress Series* 446, 285–302. [doi:10.3354/meps09506](https://doi.org/10.3354/meps09506)
- Krost, P., 1990. *Der Einfluß der Grundschieppnetzfisherei auf Nährsalz-Freisetzung aus dem Sediment und Makrofauna der Kieler Bucht (Westl. Ostsee)* [Dissertation]. *Berichte aus dem Institut für Meereskunde* 200, 167 pp. [doi:10.3289/IFM\\_BER\\_200](https://doi.org/10.3289/IFM_BER_200)
- Krost, P., Bernhard, M., Werner, F., Hukriede, W., 1990. *Otter trawl tracks in Kiel Bay (Western Baltic) mapped by side-scan sonar*. *Meeresforschung* 32, 344–353.
- Lass, H.-U., Matthäus, W., 2008. *General Oceanography of the Baltic Sea*, in: Feistel, R., Nausch, G., Wasmund, N. (Eds.), *State and Evolution of the Baltic Sea, 1952–2005: A Detailed 50-Year Survey of Meteorology and Climate, Physics, Chemistry, Biology, and Marine Environment*. John Wiley & Sons, Inc., Hoboken, New Jersey, USA, pp. 5–43.  
[doi:10.1002/9780470283134.ch2](https://doi.org/10.1002/9780470283134.ch2)
- Leipe, T., Gingele, F.X., 2003. *The kaolinite/chlorite clay mineral ratio in surface sediments of the southern Baltic Sea as an indicator for long distance transport of fine-grained material*. *Baltica* 16, 31–36.  
[http://www.gamtostyrimai.lt/uploads/publications/docs/211\\_37972ec38c101346e9b8223cb576dc8b.pdf](http://www.gamtostyrimai.lt/uploads/publications/docs/211_37972ec38c101346e9b8223cb576dc8b.pdf) (accessed 2017-09-24)
- Leipe, T., Harff, J., Meyer, M., Hille, S., Pollehne, F., Schneider, R., Kowalski, N., Brüggmann, L., 2008. *Sedimentary Records of Environmental Changes and Anthropogenic Impacts during the Past Decades*, in: Feistel, R., Nausch, G., Wasmund, N. (Eds.), *State and Evolution of the Baltic Sea, 1952–2005: A Detailed 50-Year Survey of Meteorology and Climate, Physics, Chemistry, Biology, and Marine Environment*. John Wiley & Sons, Inc., Hoboken, New Jersey, USA, pp. 395–439. [doi:10.1002/9780470283134.ch14](https://doi.org/10.1002/9780470283134.ch14)
- Leipe, T., Kersten, M., Heise, S., Pohl, C., Witt, G., Liehr, G., Zettler, M.L., Tauber, F., 2005. *Ecotoxicity assessment of natural attenuation effects at a historical dumping site in the western Baltic Sea*. *Marine Pollution Bulletin* 50, 446–459.  
[doi:10.1016/j.marpolbul.2004.11.049](https://doi.org/10.1016/j.marpolbul.2004.11.049)



- Leipe, T., Löffler, A., Bahlo, R., Zahn, W., 1999. *Automatisierte Partikelanalyse von Gewässerproben mittels Raster-Elektronenmikroskopie und Röntgen-Mikroanalytik = Automated particle analysis of water samples by scanning electron microscopy and X-ray microanalysis*. Vom Wasser 93, 21–37.
- Leipe, T., Moros, M., Kotilainen, A.T., Vallius, H., Kabel, K., Endler, M., Kowalski, N., 2013. *Mercury in Baltic Sea sediments—Natural background and anthropogenic impact*. Chemie der Erde - Geochemistry 73, 249–259. doi:10.1016/j.chemer.2013.06.005
- Leipe, T., Naumann, M., Tauber, F., Radtke, H., Friedland, R., Hiller, A., Arz, H.W., 2017. *Regional distribution patterns of chemical parameters in surface sediments of the southwestern Baltic Sea and their possible causes*. Geo-Marine Letters. doi:10.1007/s00367-017-0514-6
- Leipe, T., Tauber, F., Vallius, H., Virtasalo, J.J., Uścińowicz, S., Kowalski, N., Hille, S., Lindgren, S., Myllyvirta, T., 2011. *Particulate organic carbon (POC) in surface sediments of the Baltic Sea*. Geo-Marine Letters 31, 175–188. doi:10.1007/s00367-010-0223-x
- Lemke, W., 1998. *Sedimentation und paläogeographische Entwicklung im westlichen Ostseeraum (Mecklenburger Bucht bis Arkonabecken) vom Ende der Weichselvereisung bis zur Litorinatransgression*. Meereswissenschaftliche Berichte 31, 170 pp.
- Main, J., Sangster, G.I., 1981. *A study of the sand clouds produced by trawl boards and their possible effect on fish capture*. Scottish Fisheries Research Report 20, 20 pp.
- Maire, O., Lecroart, P., Meysman, F.J.R., Rosenberg, R., Duchêne, J., Grémare, A., 2008. *Quantification of sediment reworking rates in bioturbation research: a review*. Aquatic Biology 2, 219–238. doi:10.3354/ab00053
- Milkert, D., Werner, F., 1996. *Formation and Distribution of Storm Layers in Western Baltic Sea Muds*. Baltica 9, 36–50.
- Mohrholz, V., Naumann, M., Nausch, G., Krüger, S., Gräwe, U., 2015. *Fresh oxygen for the Baltic Sea - An exceptional saline inflow after a decade of stagnation*. Journal of Marine Systems 148, 152–166. doi:10.1016/j.jmarsys.2015.03.005
- Moros, M., Andersen, T.J., Schulz-Bull, D.E., Häusler, K., Bunke, D., Snowball, I., Kotilainen, A.T., Zillén, L., Jensen, J.B., Kabel, K., Hand, I., Leipe, T., Loughheed, B.C., Wagner, B., Arz, H.W., 2017. *Towards an event stratigraphy for Baltic Sea sediments deposited since AD 1900: approaches and challenges*. Boreas 46, 129–142. doi:10.1111/bor.12193
- Morys, C., Forster, S., Graf, G., 2016. *Variability of bioturbation in various sediment types and on different spatial scales in the southwestern Baltic Sea*. Marine Ecology Progress Series 557, 31–49. doi:10.3354/meps11837
- Morys, C., Powilleit, M., Forster, S., 2017. *Bioturbation in relation to the depth distribution of macrozoobenthos in the southwestern Baltic Sea*. Marine Ecology Progress Series 579, 19–36. doi:10.3354/meps12236



- Müller, P.J., Schneider, R., 1993. *An automated leaching method for the determination of opal in sediments and particulate matter*. Deep Sea Research Part I: Oceanographic Research Papers 40, 425–444. doi:10.1016/0967-0637(93)90140-X
- Naumann, M., Leipe, T., Tauber, F., Friedland, R., 2015. *Geochemische Karten der Oberflächensedimente der Deutschen Ostsee (GIS-Atlas)* [WWW document]. Baltic Sea Atlas, Leibniz Institute for Baltic Sea Research Warnemünde (IOW), Rostock, Germany. [http://bio-50.io-warnemuende.de/iowbsa/metadata\\_iow/Geochemischer\\_Atlas\\_Kartenanleitung.pdf](http://bio-50.io-warnemuende.de/iowbsa/metadata_iow/Geochemischer_Atlas_Kartenanleitung.pdf) (accessed 2017-03-03)
- Nausch, G., Feistel, R., Wasmund, N., 2008. *Introduction*, in: Feistel, R., Nausch, G., Wasmund, N. (Eds.), *State and Evolution of the Baltic Sea, 1952–2005: A Detailed 50-Year Survey of Meteorology and Climate, Physics, Chemistry, Biology, and Marine Environment*. John Wiley & Sons, Inc., Hoboken, New Jersey, USA, pp. 1–4. doi:10.1002/9780470283134.ch1
- Nicholson, H.A., 1872. *Contributions to the Study of the Errant Annelides of the Older Palaeozoic Rocks*. Proceedings of the Royal Society of London 21, 288–290. doi:10.1098/rspl.1872.0061
- Nies, H., Bojanowski, R., Karlberg, O., Nielsen, S.P., 1995. *Sources of radioactivity in the Baltic Sea*. Baltic Sea Environment Proceedings 61, 6–18. <http://helcom.fi/Lists/Publications/BSEP61.pdf> (accessed 2017-03-03)
- Nittrouer, C.A., Lopez, G.R., Wright, L.D., Bentley, S.J., D’Andrea, A.F., Friedrichs, C.T., Craig, N.I., Sommerfield, C.K., 1998. *Oceanographic processes and the preservation of sedimentary structure in Eckernförde Bay, Baltic Sea*. Continental Shelf Research 18, 1689–1714. doi:10.1016/S0278-4343(98)00054-5
- Peine, F., 2005. *Influence of subtidal macrofauna organisms generating biogenic structures on the near-bottom particle transport in the southwestern Baltic Sea* [Dissertation]. Universität Rostock, Germany. [http://www.biologie.uni-rostock.de/meeresbiologie/download/peine\\_phd\\_thesis.pdf](http://www.biologie.uni-rostock.de/meeresbiologie/download/peine_phd_thesis.pdf) (accessed 2017-03-20)
- Pemberton, S.G., Frey, R.W., 1982. *Trace Fossil Nomenclature and the Planolites-Palaeophycus Dilemma*. Journal of Paleontology 56, 843–881. <http://www.jstor.org/stable/1304706> (accessed 2017-09-24)
- Pennington, W., Tutin, T.G., Cambray, R.S., Fisher, E.M., 1973. *Observations on Lake Sediments using Fallout <sup>137</sup>Cs as a Tracer*. Nature 242, 324–326. doi:10.1038/242324a0
- Pohl, C., Hennings, U., Petersohn, I., Siegel, H., 1998. *Trace metal budget, transport, modification and sink in the transition area between the Oder and Peene rivers and the southern Pomeranian Bight*. Marine Pollution Bulletin 36, 598–616. doi:10.1016/S0025-326X(98)00038-1

- Povinec, P.P., Fowler, S., Baxter, M., 1996. *Chernobyl & the marine environment: The radiological impact in context*. International Atomic Energy Agency Bulletin 38, 18–22. <https://www.iaea.org/sites/default/files/publications/magazines/bulletin/bull38-1/38106081822.pdf> (accessed 2017-03-03)
- Rasband, W., 1997. *ImageJ* 1.50i [Software]. U.S. National Institutes of Health. <https://imagej.nih.gov/ij/>
- Rosenberg, R., Nilsson, H.C., Grémare, A., Amouroux, J.-M., 2003. *Effects of demersal trawling on marine sedimentary habitats analysed by sediment profile imagery*. Journal of Experimental Marine Biology and Ecology 285–286, 465–477. doi:10.1016/S0022-0981(02)00577-4
- Salter, J.W., 1857. *On Annelide-burrows and Surface-markings from the Cambrian Rocks of the Longmynd*. No. 2. Quarterly Journal of the Geological Society 13, 199–206. doi:10.1144/GSL.JGS.1857.013.01-02.29
- Schiele, K.S., Darr, A., Zettler, M.L., Friedland, R., Tauber, F., von Weber, M., Voss, J., 2015. *Biotope map of the German Baltic Sea*. Marine Pollution Bulletin 96, 127–135. doi:10.1016/j.marpolbul.2015.05.038
- Schlirf, M., Uchman, A., 2005. *Revision of the ichnogenus sabellarifex richter, 1921 and its relationship to skolithos haldeman, 1840 and polykladichnus fürsich, 1981*. Journal of Systematic Palaeontology 3, 115–131. doi:10.1017/S1477201905001550
- Schmid, E.E., 1876. *Der Muschelkalk des östlichen Thüringen*. F.J. Frommann, Jena.
- Schulz-Bull, D.E., Petrick, G., Bruhn, R., Duinker, J.C., 1998. *Chlorobiphenyls (PCB) and PAHs in water masses of the northern North Atlantic*. Marine Chemistry 61, 101–114. doi:10.1016/S0304-4203(98)00010-3
- Seifert, T., Tauber, F., Kayser, B., 2001. *A high resolution spherical grid topography of the Baltic Sea — 2nd edition* [WWW dataset]. <https://www.io-warnemuende.de/topography-of-the-baltic-sea.html> (accessed 2017-03-03)
- Shull, D.H., Benoit, J.M., Wojcik, C., Senning, J.R., 2009. *Infaunal burrow ventilation and pore-water transport in muddy sediments*. Estuarine, Coastal and Shelf Science 83, 277–286. doi:10.1016/j.ecss.2009.04.005
- Siegel, H., Seifert, T., Schernewski, G., Gerth, M., Ohde, T., Reißmann, J., Podsetchine, V., 2005. *Discharge and transport processes along the German Baltic Sea Coast*. Ocean Dynamics 55, 47–66. doi:10.1007/s10236-005-0110-6
- Smith, C.J., Rumohr, H., Karakassis, I., Papadopoulou, K.-N., 2003. *Analysing the impact of bottom trawls on sedimentary seabeds with sediment profile imagery*. Journal of Experimental Marine Biology and Ecology 285–286, 479–496. doi:10.1016/S0022-0981(02)00545-2
- Soulsby, R.L., Mead, C.T., Wild, B.R., 2007. *A model for simulating the dispersal tracks of sand grains in coastal areas: “SandTrack”*. Geological Society, London, Special Publications 274, 65–72. doi:10.1144/GSL.SP.2007.274.01.08

- Suzdalev, S., Gulbinskas, S., Blažauskas, N., 2015. *Distribution of tributyltin in surface sediments from transitional marine-lagoon system of the south-eastern Baltic Sea, Lithuania*. Environmental Science and Pollution Research 22, 2634–2642. doi:10.1007/s11356-014-3521-4
- Tauber, F., 2009. *Sidescan sonar survey of a dumping site in the Mecklenburg Bight (south-western Baltic Sea)*. Journal of Marine Systems 75, 421–429. doi:10.1016/j.jmarsys.2008.04.006
- Thévenaz, P., 2006. *MosaicJ* July 6, 2011 [Software]. École polytechnique fédérale de Lausanne (EPFL), Switzerland. <http://bigwww.epfl.ch/thevenaz/mosaicj/> (accessed 2017-09-24)
- Thévenaz, P., Unser, M., 2007. *User-friendly semiautomated assembly of accurate image mosaics in microscopy*. Microscopy Research and Technique 70, 135–146. doi:10.1002/jemt.20393
- UNEP, 2005. Lääne, A., Kraav, E., Titova, G.: *Baltic Sea, GIWA regional assessment 17* [Report]. University of Kalmar, Sweden. 69 pp. <http://projects.inweh.unu.edu/inweh/display.php?ID=931> (accessed 2017-09-24)
- Virtasalo, J.J., Bonsdorff, E., Moros, M., Kabel, K., Kotilainen, A.T., Ryabchuk, D., Kallonen, A., Hämäläinen, K., 2011. *Ichnological trends along an open-water transect across a large marginal-marine epicontinental basin, the modern Baltic Sea*. Sedimentary Geology 241, 40–51. doi:10.1016/j.sedgeo.2011.09.010
- von Dorrien, C., Krumme, U., Grieger, C., Miethe, T., Stötera, S., 2013. *Analyse fischereilicher Daten in den schleswig-holsteinischen Küstengewässern der Ostsee* [Report]. Johann Heinrich von Thünen-Institut, Braunschweig. [http://literatur.thuenen.de/digbib\\_extern/dn055697.pdf](http://literatur.thuenen.de/digbib_extern/dn055697.pdf) (accessed 2017-09-24)
- Werner, F., 2002. *Bioturbation structures in marine Holocene sediments of Kiel Bay (Western Baltic)*. Meyniana 54, 41–72.
- Werner, F., Erlenkeuser, H., von Grafenstein, U., McLean, S., Sarnthein, M., Schauer, U., Unsöld, G., Walger, E., Wittstock, R., 1987. *Sedimentary Records of Benthic Processes*, in: Rumohr, J., Walger, E., Zeitzschel, B. (Eds.), *Seawater-Sediment Interactions in Coastal Waters*. Springer, pp. 162–262. doi:10.1007/978-3-662-02531-4\_6
- Werner, F., Hoffmann, G., Michael, B., Milkert, D., Vikgren, K., 1990. *Sedimentologische Auswirkungen der Grundfischerei in der Kieler Bucht (Westliche Ostsee)*. Meyniana 42, 123–151. doi:10.2312/meyniana.1990.42.123
- Wetzel, A., 1981. *Ökologische und stratigraphische Bedeutung biogener Gefüge in quartären Sedimenten am NW-afrikanischen Kontinentalrand*. Meteor-Forschungs-Ergebnisse C34, 1–47.
- Widdows, J., Brinsley, M.D., Bowley, N., Barrett, C., 1998. *A Benthic Annular Flume for In Situ Measurement of Suspension Feeding/Biodeposition Rates and Erosion Potential of Intertidal Cohesive Sediments*. Estuarine, Coastal and Shelf Science 46, 27–38. doi:10.1006/ecss.1997.0259

- Winn, K., 2006. *Bioturbation structures in marine Holocene sediments of the Great Belt (Western Baltic)*. *Meyniana* 58, 157–178.
- Witt, G., 1995. *Polycyclic Aromatic Hydrocarbons in Water and Sediment of the Baltic Sea*. *Marine Pollution Bulletin* 31, 237–248. doi:[10.1016/0025-326X\(95\)00174-L](https://doi.org/10.1016/0025-326X(95)00174-L)
- Witt, G., Trost, E., 1999. *Polycyclic aromatic hydrocarbons (PAHs) in sediments of the Baltic Sea and of the German coastal waters*. *Chemosphere* 38, 1603–1614. doi:[10.1016/S0045-6535\(98\)00387-7](https://doi.org/10.1016/S0045-6535(98)00387-7)
- Zwicker, A., 2014. *Benthische Fauna und ihre Rolle beim Partikeltransport: eine Untersuchung des Makrozoobenthos im Sublitoral der Mecklenburger Bucht (westliche Ostsee)* [Master's thesis]. Universität Rostock, Germany.

## Acknowledgements

I am deeply grateful to Helge Arz and the other members of my thesis committee, Thomas Leipe, Matthias Moros and Falk Pollehne, for all the constructive discussions and their support in the course of my PhD studies. I would like to thank the Department of *Marine Geology* of *IOW* in general and my office mates in particular as well as many other colleagues from *IOW* and the *University of Rostock* for a wonderful PhD time. Especially my fellow PhD students Claudia Morys, Kirstin Schulz and Marko Lipka as well as the postdocs Jana Wölfel and Mayya Gogina are to be mentioned here, since our bonding went far beyond the project.

Many thanks to Joonas Virtasalo and the marine geology group of *GTK* for introducing me to sedimentary fabric analysis and for the pleasant time during my research stay as well as at conferences. You Finns rock!

I appreciate laboratory, metrological, sampling, technical and/or other support from Adrian Waßmann, Aki Kallonen, Andreas Frahm, Anke Bender, Anne Köhler, Astrid Lerz, Bernd Schlichting, Claudia Morys, Erik Stohr, Frank Janert, Frank Pohl, Franz Tauber, Franziska Thoms, Gerhard Lehnert, Gisela Radloff, Heinz Stark, Henning Kirk, Holger Posselt, Ina Dartsch, Ines Hand, Ines Scherff, Irina Goldschmidt, Jana Wölfel, Jenny Jeschek, Jörg Bengel, Jörn Kurth, Joonas Virtasalo, Julian Schade, Juliane Liebstein, Katrin Bahloul, Kirstin Schulz, Klaus-Peter Wlost, Kristian Rose, Lina Westphal, Marco Juris, Marko Lipka, Matthias Moros, Michael Endler, Michael Pöttsch, Mike Sommer, Olaf Dellwig, Rainer Bahlo, Robert Kostecki, Robert Mars, Sascha Plewe, Sibylle Fink, Siegfried Gust, Steffi Bednarczyk, Thomas Leipe, Tobias Marquardt, Uwe Hehl, Vera Winde, Volker Mohrholz und Wolfgang Roeder. Furthermore, I thank the captains and crews of the research vessels ELISABETH MANN BORGESE, ALKOR and POSEIDON as well as the involved scientific parties for successful and pleasant cruises.

I am much obliged to Friederike Kunz, Joonas Virtasalo, Maike Piepho, Marion Abraham, Michael Endler, Peter Feldens and Sascha Serno for proof-reading and commenting this thesis. I am also thankful to my parents and my sister for their infinite encouragement and support through the years.

This study was embedded in the *KüNO (Coastal Research North Sea / Baltic Sea)* project *SECOS* funded by the German *Federal Ministry of Education and Research (BMBF)* grant 03F0666A) in the frame of their *FONA* call (*Research for Sustainable Developments*) and managed by the *Project Management Jülich (PTJ)*. It was coordinated by Ulrich Bathmann, Eva-Maria Brodte

and Friederike Kunz at *IOW*, which I hereby thank for their work. Additional funds for this study came from the *IOW* budget.